An Investigation of Low Temperature Direct Propane Fuel Cells

Bhavana Parackal

Thesis submitted to the Faculty of Graduate and Postdoctoral Studies in partial fulfillment of the requirements for the degree of

Master of Applied Science

Department of Chemical and Biological Engineering
Faculty of Engineering
University of Ottawa



uOttawa

L'Université canadienne
Canada's university

© Bhavana Parackal, Ottawa, Canada, 2017

Abstract

This research is directed toward the investigation of a low temperature direct propane fuel cell (DPFC). Modeling included a parametric study of a direct propane fuel cell using computational fluid dynamics (CFD), specifically FreeFem++ software. Polarization curves predicted by the CFD model were used to understand fuel cell performance. The predictions obtained from the computational fluid dynamics mathematical model for the fuel cell were compared with experimental results. The computational work identified some critical parameters (exchange current density, pressure, temperature) for improving the overall performance of the fuel cell. The model predictions clearly highlighted the role of catalysts in significantly enhancing the overall performance of a DPFC. Experiments were performed using commercial Nafion-Pt based membrane electrode assemblies (MEAs) to obtain a basis for comparison. It is the first report in the literature that a Pt-Ru (Platinum-Ruthenium) MEA was used in the investigation of a DPFC. Also, it was the first study that fed liquid water continuously to a DPFC by using interdigitated flow field (IDFF) at the anode to humidify the dry propane feed gas. During the experiments oscillations were observed at very low current densities i.e. in nA/cm^2, which is a rare case and not reported in the literature to date. This observation has raised serious concerns about the existence of absolute open-circuit cell potential difference for a DPFC. The cycling behaviour observed with DPFC indicated the presence of a continuous degradation-regeneration process of the catalyst surface near open-circuit potential. The experimental work further evaluated the performance of fuel cell by measurement of polarization curves.

Résumé

Cette recherche porte sur l'étude d'une pile à combustible directe au propane (PCDP) de type basse température. Une partie du travail axée sur la modélisation comprenait une étude paramétrique d'une PCDP en utilisant la dynamique des fluides computationnelle (CFD), mise en œuvre à l'aide du logiciel FreeFem++. Les courbes de polarisation prédites par le modèle CFD ont été utilisées pour analyser la performance de la pile à combustible. Les prédictions obtenues à partir du modèle mathématique ont été comparées aux résultats expérimentaux. Les calculs numériques ont permis d'identifier certains paramètres critiques (densité de courant, pression, température) pour améliorer la performance globale de la pile à combustible. Les prédictions du modèle ont clairement mis en évidence le rôle du catalyseur pour améliorer de manière significative la performance globale d'un PCDP. Des expériences ont été réalisées en utilisant un assemblage électrodes-membrane Nafion-Pt produit commercialement (AEM) afin d'obtenir une base de comparaison. Nous avons produit les premiers résultats rapportés dans la littérature pour un AEM Pt-Ru (Platinum-Ruthénium) utilisé dans une PCDP. En outre, il s'agit de la première étude où une alimentation continue en eau liquide est intégrée à une PCDP en utilisant un champ d'écoulement inter-digitée pour humidifier le gaz d'alimentation (propane) du côté anodique. Au cours des expériences, des oscillations ont été observées pour de très faibles densités de courant, i.e. en nA/cm^2, en soit un cas rare non rapporté dans la littérature jusqu'à ce jour. Ces observations ont soulevé de sérieuses préoccupations au sujet de l'existence d'une différence de potentiel absolue en condition de circuit ouvert pour une PCDP. Le comportement cyclique observé avec les PCDP indique la présence d'un processus de dégradation-régénération continu de la surface du catalyseur pour des conditions d'opérations proche du potentiel en circuit ouvert. Le travail expérimental a aussi permis d'évaluer la performance de la pile à combustible par la mesure de courbes de polarisation.

Acknowledgements

This thesis is dedicated to my parents for their unconditional love and support rendered to me, and for being inspirational throughout this research project.

It is with immense gratitude that I acknowledge the guidance, expertise, support and help of my supervisor, Dr. Marten Ternan, all throughout the course of this research work. I am thankful to him for giving me the opportunity to improve my teamwork, presentation, and project management skills along with my research skills. I consider myself extremely fortunate for being associated with him.

I express my deepest sense of gratitude and acknowledge the gratefulness to my co-supervisor, Dr. Yves Bourgault, for his valuable guidance, constant encouragement, and keen interests in both the computational and experimental work of this research project. I am thankful to him for familiarizing me with the fundamentals of computational fluid dynamics, Linux Ubuntu terminal, and finite element numerical method.

I would like to sincerely acknowledge the contributions of my predecessors, Travis Robinson and Chidozie Isinguzo, in the domain of oscillations in a fuel cell.

I would like to acknowledge the support and prompt assistance received from the technical staff of Chemical and Biological Engineering Department, Louis Tremblay, Gérard Nina, and Franco Ziroldo, for helping me in building experimental set-ups and getting it functional.

Table of Contents

Abstract ii

Résumé iii

Acknowledgements iv

List of Figures vii

List of Tables xi

Nomenclature xii

Chapter 1: Introduction 1

- **1.1 The fuel cell and its technology** 1
- **1.2 Direct propane PEM fuel cell (DPFC)** 3
- **1.3 Research objectives** 4
- **1.4 Thesis structure** 4
- **1.5 References** 5

Chapter 2: Literature review 7

- **2.1 An overview of fuel cell technology** 7
- **2.2 Direct hydrocarbon fuel cells** 9
- **2.3 Direct hydrocarbon fuel cells with an aqueous electrolyte** 11
- **2.4 Direct hydrocarbon polymer electrolyte membrane fuel cell** 14
- **2.5 Direct hydrocarbon mixed oxide electrolyte fuel cell** 16
- **2.6 Direct hydrocarbon solid oxide fuel cell** 17
- **2.7 Oscillations in fuel cell** 19
- **2.8 Mathematical modeling in PEMFC** 26
- **2.9 References** 33

Chapter 3: A parametric study of a direct propane fuel cell (DPFC) using a computational fluid dynamics (CFD) model employing the finite element method 45

- **Abstract** 45
- **3.1 Introduction** 45
- **3.2 Model description** 49
- **3.3 Results and discussion** 54
- **3.4 Conclusions** 67

3.5 References 68

Chapter 4: Experimental work on low temperature direct propane fuel cell (DPFC) with a commercial Nafion membrane 72

Abstract 72

4.1 Introduction 73

4.2 Experimental 77

4.3 Results and discussion 84

4.4 Summary 104

4.5 Conclusions 107

4.6 References 108

Chapter 5: Linkages 113

5.1 Results and discussion 113

5.2 Recommendations 114

5.3 References 115

Chapter 6: Conclusions 116

6.1 Summary 116

6.2 Conclusions 116

6.3 Contribution to knowledge 117

6.4 References 117

Appendix A: Description of Equipment 118

Appendix B: Time-on-stream graphs of cell potential difference and current density 127

Appendix C: Thermodynamic calculations 136

List of Figures

Figure 1.1 Schematic diagram of a typical proton exchange membrane fuel cell (PEMFC) that uses hydrogen fuel. **2**

Figure 2.1 Schematic diagram of a typical proton exchange membrane fuel cell (PEMFC) that uses hydrogen fuel. **10**

Figure 3.1 The computational procedure with the time-stepping progressive iteration loop.. **51**

Figure 3.2 The effect of progressive and non-progressive time-stepping loop on the polarization curve for a direct propane fuel cell model (DPFC) at 150°C and 1 atm..... **52**

Figure 3.3 The effect of anodic exchange current density, $j_{0AN\text{-}ref}$ (A/m^2) on the polarization curve for a direct propane fuel cell model (DPFC) at 150°C and 1 atm. **55**

Figure 3.4 The effect of cathode exchange current density, $j_{0CA\text{-}ref}$ (A/m^2) on the polarization curve for a direct propane fuel cell (DPFC) model at 150°C and 1 atm. **56**

Figure 3.5 The effect of anode/ cathode catalyst layer thickness, Th_A/Th_C (μm) on the polarization curve for a direct propane fuel cell (DPFC) model at 150°C and 1 atm..... **57**

Figure 3.6 The effect of electrolyte (membrane) layer thickness, Th_M (μm) on the polarization curve for a direct propane fuel cell (DPFC) model at 150°C and 1 atm. **59**

Figure 3.7 The effect of membrane layer proton conductivity, σ_{ELY} (S/m) on the polarization curve for a direct propane fuel cell (DPFC) model at 150°C and 1 atm.. ..... **60**

Figure 3.8 The effect of proton diffusivity coefficient in electrolyte phase, $D_{H+\text{-}ZrP}$ (m^2/s) on the polarization curve for a direct propane fuel cell (DPFC) model at 150°C and 1 atm..... **61**

Figure 3.9 The effect of water diffusivity coefficient in electrolyte phase, $D_{H2O\text{-}ZrP}$ (m^2/s) on the polarization curve for a direct propane fuel cell (DPFC) model at 150°C and 1 atm. **62**

Figure 3.10 The effect of propane inlet mole fraction, y_{Pinput} on the polarization curve for a direct propane fuel cell (DPFC) model at 150°C and 1 atm. **63**

Figure 3.11 The effect of propane inlet molar flow rate, $\dot{m}_P$ (gmol/s) on the polarization curve for a direct propane fuel cell (DPFC) model at 150°C and 1 atm. **64**

Figure 3.12 The effect of fuel cell operating temperature, T (°C) on the polarization curve for a direct propane fuel cell (DPFC) model at 1 atm. **65**

Figure 3.13 The effect of fuel cell operating pressure, P (atm) on the polarization curve for a direct propane fuel cell (DPFC) model at 150°C. **67**

Figure 4.1A Experimental equipment used for a propane/nitrogen-air operation with an IDFF anode humidified with liquid water at 1 atm. **79**

Figure 4.1B Experimental equipment used for a hydrogen-air operation with an IDFF anode humidified with liquid water at 1 atm. **80**

Figure 4.1C Experimental equipment for a propane-air operation with an IDFF anode humidified with liquid water at 1 atm and no electrical connections to measure current. **81**

Figure 4.1D Experimental equipment used for a propane-air operation with a pin-type anode flow field and a bubble humidifier at 1 atm. **82**

Figure 4.1E Experimental equipment used for a hydrogen-air operation with a pin-type anode flow field and a bubble humidifier at 1 atm. **83**

Figure 4.1F Experimental equipment used for a propane-air operation with a pin-type anode flow field and a bubble humidifier at 1 atm. **84**

Figure 4.2 Cell potential difference, $\Delta\Phi_{cell}$ (V) versus time-on-stream, t (min) for a DPFC with 34% propane, IDFF anode humidified with liquid water, Pt anode catalyst, 65°C, 1 atm, and using fixed resistors of 1 MΩ, 10 kΩ, 980 Ω, 330 Ω, and 118 Ω..... **86**

Figure 4.3 Current density, j ($\mu A/cm^2$) versus time-on-stream, t (min) for a DPFC with 34% propane, IDFF anode humidified with liquid water, Pt anode catalyst, 65°C, 1 atm, and using fixed resistors of 1 MΩ, 10 kΩ, 980 Ω, 330 Ω, and 118 Ω..... **87**

Figure 4.4 Relationship between time-on-stream measurement of cell potential difference, $\Delta\Phi_{cell}$ (V) and current density, j ($\mu A/cm^2$) for a DPFC with 34% propane, IDFF anode humidified with liquid water, Pt anode catalyst, 65°C, 1 atm, and using a 1 MΩ fixed resistor..... **88**

Figure 4.5 Polarization curve of a DPFC with different propane inlet mole fractions at a time-on-stream of 14 minutes, IDFF anode humidified with liquid water, Pt anode catalyst, 65°C, 1 atm, and using different fixed resistors..... **89**

Figure 4.6 Polarization curve of a DPFC with 100% propane, IDFF anode humidified with liquid water, Pt anode catalyst, different fuel cell operating temperatures, 1 atm, and using different fixed resistors. **91**

Figure 4.7 Polarization curve of a DPFC with 100% propane, IDFF anode humidified with liquid water, different anode catalysts, 65°C, 1 atm, and using different fixed resistors. **92**

Figure 4.8 Polarization curve of a DPFC with 100% propane, different anode flow fields along with different humidification systems, Pt-Ru anode catalyst, 65°C, 1 atm, and using different fixed resistors. **94**

Figure 4.9 Polarization curve of a hydrogen fuel cell (after propane-air operation) with different anode flow fields along with different humidification systems, Pt-Ru anode catalyst, 65°C, 1 atm, and using the power-supply unit at a galvanostatic mode. **97**

Figure 4.10 Cell potential difference, $\Delta\Phi_{cell}$ (V) versus time-on-stream, t (min) for a DPFC with 100% propane, IDFF anode humidified with liquid water, Pt anode catalyst, 1 atm, a 118 Ω fixed resistor, and different fuel cell operating temperatures. **99**

Figure 4.11 Cell potential difference, $\Delta\Phi_{cell}$ (V) versus time-on-stream, t (min) for a DPFC with 100% propane, IDFF anode humidified with liquid water, different anode catalysts, 65°C, 1 atm, and using a 118 Ω fixed resistor. **100**

Figure 4.12 Cell potential difference, $\Delta\Phi_{cell}$ (V) versus time-on-stream, t (min) for a DPFC with 100% propane, different anode flow fields along with different humidification systems, Pt-Ru anode catalyst, 65°C, 1 atm, and using a 118 Ω fixed resistor. **101**

Figure 4.13 Cell potential difference, $\Delta\Phi_{cell}$ (V) versus time-on-stream, t (min) for a DPFC with 100% propane, different anode flow fields along with different humidification systems, Pt-Ru anode catalyst, 65°C, 1 atm, and no electrical connections to measure current (i.e. only thermo-chemical reaction possible). **102**

List of Tables

Table 2.1 The governing equations of the DPFC model. **32**

Table 3.1 Operational, electrochemical, and design parameters of the reference case of the DPFC model. **53**

Nomenclature

Abbreviations

Abbreviations	Definition
ACL	Anode catalyst layer
AFC	Alkaline fuel cell
CCL	Cathode catalyst layer
CFD	Computational fluid dynamics
CO	Carbon monoxide
DHFC	Direct hydrocarbon fuel cell
DMFC	Direct methane fuel cell
DMeFC	Direct methanol fuel cell
DME	Dimethyl ether
DPAFC	Direct phosphoric acid fuel cell
DPFC	Direct propane fuel cell
DPPAFC	Direct propane phosphoric acid fuel cell
EIS	Electrochemical impedance spectroscopy
FF	Flow field
GDL	Gas diffusion layer
GHG	Greenhouse gases
HFC	Hydrogen fuel cell
ICE	Internal combustion engine
IDFF	Interdigitated flow field
LPG	Liquefied petroleum gasoline
MCFC	Molten carbonate fuel cell

Abbreviations	Definition
MEA	Membrane electrode assembly
ML	Membrane or electrolyte layer
m-ZrP	Modified zirconium phosphate
OCP	Open-circuit potential
PAFC	Phosphoric acid fuel cell
Pd	Palladium
PEMFC	Proton exchange membrane fuel cell or polymer electrolyte membrane fuel cell
Pt	Platinum
PTFE	Polytetrafluoroethylene
Pt-Ru	Platinum-Ruthenium
RDE	Rotating disk electrode
Ru	Ruthenium
SCFC	Single chamber fuel cell
SEM	Scanning electron microscope
SOFC	Solid oxide fuel cell
TPO	Temperature programmed oxidation
ZrP	Zirconium phosphate

Symbols

Symbols	Definition
$\Delta\Phi_{cell}$	Cell potential difference
$\Delta\Phi_t$	Potential difference or instantaneous potential difference
$\Delta\Phi_{OCP}$	Open-circuit potential
$\Delta G°$	Standard Gibbs free energy change
$\Delta H°$	Standard enthalpy change
$\Delta S°$	Standard entropy change
D_{H+-ZrP}	Proton diffusivity coefficient in electrolyte phase
$D_{H2O-ZrP}$	Water diffusivity coefficient in electrolyte phase
$E°$	Standard electrochemical potential
F	Faraday constant
η	Overpotential
η_c	Conversion efficiency
η_{el}	Electrochemical efficiency
η_{th}	Thermodynamic efficiency
η_{FC}	Overall fuel cell efficiency
j	Current density
j_t	Current density or instantaneous current density
j_0	Electrode exchange current density
$j_{0AN-ref}$	Anodic exchange current density
$j_{0CA-ref}$	Cathode exchange current density
$\dot{m}_P$	Propane inlet molar flow rate
M	Molarity
n_E	Number of electrons transferred per molecule of hydrocarbon reacted

Symbols	Definition
N	Time-steps
P	Fuel cell operating pressure
P_{C3H8}	Partial pressure of propane
Φ_{Ag}	Potential difference at cathode
Φ_{Ni}	Potential difference at anode
R	Ideal gas constant
σ_{ELY}	Membrane layer proton conductivity
T	Fuel cell operating temperature
Th_A/Th_C	Anode/ cathode catalyst layer thickness
Th_M	Electrolyte (membrane) layer thickness
t	Time-on-stream or time
y_{Pinput} / $y_{propane}$ / y_{C3H8}	Propane inlet mole fraction
y_{water} / y_{H2O}	Water inlet mole fraction

Chapter 1: Introduction

1.1 The fuel cell and its technology

The history of fuel cells began in 1839. William Grove discovered the working principle of the fuel cell while reversing the water electrolysis process. He was successful in describing the fuel cell concept, and his description remains true today. Since then his concept has become a technology that is now used on a commercial scale [1,2]. A fuel cell is an electrochemical device that converts the chemical energy stored in fuels (e.g. hydrogen, H_2) directly into electrical energy along with some heat. If the fuel cell produces high temperature heat, the heat can be transformed into additional electrical energy. If the fuel cell produces low temperature heat, the heat is dissipated to the surroundings [3]. Fuel cell technology can be both clean and efficient [4,5]. The fuel cell power generation process is governed by an electrochemical reaction rather than a thermal one. Therefore, theoretically, its emission levels of global warming gases (or greenhouse gases, GHG), mainly carbon dioxide, could be decreased significantly (Section C.1, Appendix C). These attributes may make a fuel cell system a strong future competitor to the conventional internal combustion engine (ICE) system used in the transportation sector [6,7].

The fuel cell consists of three essential elements: the anode, the electrolyte, and the cathode. The type of electrolyte (membrane) is an important component often used to classify fuel cells. Based on the electrolyte type, most fuel cells can be categorized as one of the following: (a) alkaline fuel cell (AFC), (b) polymer electrolyte membrane fuel cell (PEMFC) or proton exchange membrane fuel cell (PEMFC), (c) phosphoric acid fuel cell (PAFC), (d) molten carbonate fuel cell (MCFC), and (e) solid oxide fuel cell (SOFC) [8]. The PEMFC is the one used most frequently in the transportation sector [5,9]. This is mainly due to the structure of the polymeric membrane [10], which eliminates the leakage issues of aqueous electrolytes.

The electrochemical reaction in a typical hydrogen proton exchange membrane fuel cell, H_2-PEMFC, containing a Nafion-Pt based membrane electrode assembly, MEA [11], is shown in Figure 1.1. The hydrogen gas, which is the fuel, is fed to the anode. It flows through the anode flow field, enters the gas diffusion layer, and then reaches the platinum (Pt) catalyst surface in

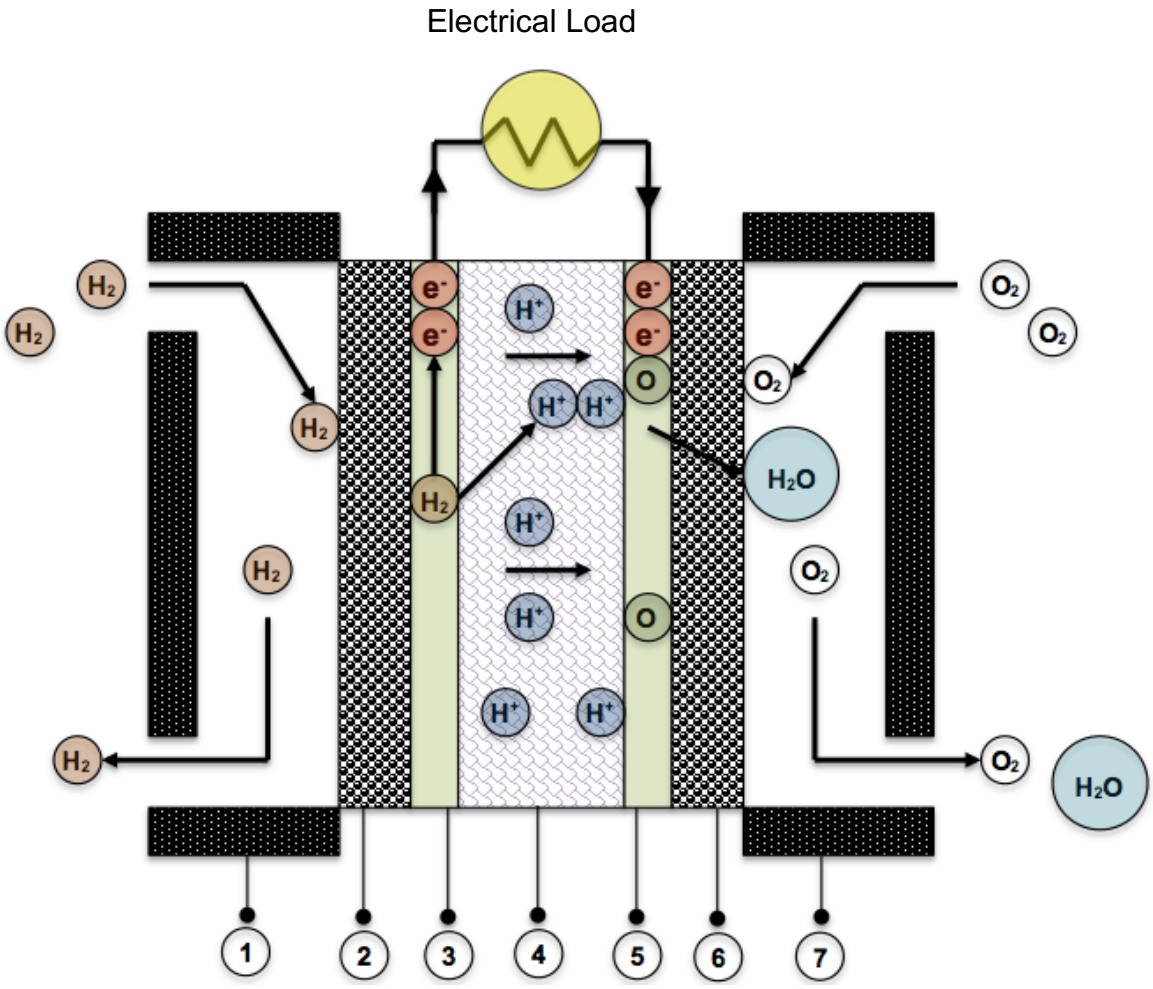


Figure 1.1 Schematic diagram of a typical proton exchange membrane fuel cell (PEMFC) that uses hydrogen fuel. Following are the parts: 1 - Anode flow field, 2 - Anode gas diffusion layer, 3 - Anode catalyst layer, 4 - Proton conducting electrolyte layer, 5 - Cathode catalyst layer, 6 - Cathode gas diffusion layer, and 7 - Cathode flow field.

the anode catalyst layer. At the cathode, the air, an oxidant, passes through the cathode flow field, the gas diffusion layer, and is adsorbed onto the Pt catalyst surface in the cathode catalyst layer.

The overall electrochemical reaction and the two half-cell reactions are [3,8]:

At anode: $H_2 \longrightarrow 2H^+ + 2e^-$ ---------- (1.1) Oxidation reaction

At cathode: $½O_2 + 2H^+ + 2e^- \longrightarrow H_2O$ ---------- (1.2) Reduction reaction

Overall: $H_2 + ½O_2 \longrightarrow H_2O$ ---------- (1.3) Overall reaction

Sufficient hydration of the MEA is necessary to provide protonic conductivity throughout the operation for the efficient performance of a PEMFC. Recent studies have shown that the protonic conductivity, as well as the hydration of the membrane, can be improved [10].

1.2 Direct propane PEM fuel cell (DPFC)

Extensive research on direct hydrocarbon fuel cells (DHFCs) was performed in the early 1960s [12] to utilize the abundance of fossil fuels. The working principle of a DHFC with a polymer electrolyte is the same as that of the hydrogen proton exchange membrane fuel cell (H_2-PEMFC) shown in Figure 1.1, except for the fuel fed to the anode. Hydrocarbons were considered as an alternative to hydrogen fuel for the following reasons: (i) storage as a liquid rather than gas, (ii) higher energy density, and (iii) the infrastructure that already exists [8,9]. Propane was chosen as the fuel for this DHFC project because it is available in rural areas. Since the delivery cost of electrical power in rural areas is greater than in urban areas, more expensive fuel cells might be justified in rural areas. Using hydrocarbon fuels for fuel cells eliminates the capital cost required for the processing plants that convert hydrocarbons to the hydrogen needed in a PEMFC. A direct propane fuel cell (DPFC) has a theoretical efficiency of 95% (Section C.1, Appendix C) in comparison to 65% for the Carnot cycle in thermal power plants [13].

The electrochemical reactions described below occur respectively on the catalyst surface of the following electrodes [14]:

The anode when humidified propane gas is fed:

$C_3H_8 + 6H_2O \longrightarrow 3CO_2 + 20H^+ + 20e^-$ ---------- (1.4) Oxidation reaction

The cathode when air is fed:

$5O_2 + 20H^+ + 20e^- \longrightarrow 10H_2O$ ---------- (1.5) Reduction reaction

The overall electrochemical reaction within a DPFC:

$C_3H_8 + 5O_2 \longrightarrow 3CO_2 + 4H_2O$ ---------- (1.6) Overall reaction

1.3 Research objectives

This research project is divided into following two parts:

Objective 1: Perform a parametric study using a mathematical model based on computational fluid dynamics (CFD) for a direct propane PEM fuel cell (DPFC) to identify significant experimental variables.

Objective 2: Perform laboratory experiments using a DPFC to investigate the trends predicted by the model.

1.4 Thesis structure

The thesis consists of six chapters. The first chapter presents an outline of the entire thesis. The second chapter is a survey of the scientific and technological literature that is related to the intended research work. The third and the fourth chapters are the two main chapters of the thesis covering objective 1 and objective 2 respectively. The third chapter describes the DPFC model. Different operational parameters were studied in detail. It also includes the predictions obtained from the parametric study. The fourth chapter describes the laboratory work conducted on a DPFC to investigate some of the significant parameters identified in the

modeling work. Critical observations are described, and are compared to the model results. The fifth chapter provides the linkages between the Chapters 3 and 4 and recommendations for the future work. The sixth chapter includes a summary, conclusions, and a list of contributions to knowledge.

1.5 References

[1] Johnson Matthey PLC 2016, "Fuel cell history," 2016. [Online]. Available: http://www.fuelcelltoday.com/history.

[2] H. A. Liebhafsky and L. W. Niedrach, "Fuel cells," *Journal of The Franklin Institute*, vol. 269, no. 4, pp. 257-267, 1960.

[3] G. Hoogers, “Introduction,” in *Fuel Cell Technology Handbook,* CRC Press, Boca Raton, 2003, pp. 2-37.

[4] T. Wilberforce, A. Alaswad, A. Palumbo, M. Dassisti, and A. G. Olabi, "Advances in stationary and portable fuel cell applications," *International Journal of Hydrogen Energy*, vol. 41, no. 37, pp. 16509-16522, 2016.

[5] Johnson Matthey PLC 2016, "Fuel cell introduction," 2016. [Online]. Available: http://www.fuelcelltoday.com/about-fuel-cells/introduction.

[6] A. D. S. Tantram, "Fuel cells: Past, present and future," *Energy Policy*, vol. 2, no. 1, pp. 55-66, 1974.

[7] M. L. Perry and T. F. Fuller, "A historical perspective of fuel cell technology in the 20th century," *Journal of The Electrochemical Society*, vol. 149, no. 7, pp. S59-S67, 2002.

[8] T. G. Services, *‘2004 fuel cell handbook: Advanced technology for generating electricity; series on renewable energy, Biofuels, Bioenergy, and Biobased products, 7th edition’*, 7th ed. Morgantown, WV: U.S. Department of Energy, Office of Fossil Energy, National Energy Technology Laboratory, 2004.

[9] J. O. Bockris and S. Srinivasan, “Fuel cells: Their electrochemistry,” in *Electrochemical Combustion of Organic Substances*, McGraw-Hill, New York, 1969, pp. 357-411.

[10] M. Liu, L. Chen, S. Lewis, S. Y. Chong, M. A. Little, T. Hasell, L. M. Aldous, C. M. Brown, M. W. Smith, C. A. Morrison, L. J. Hardwick, and A. I. Cooper, "Three-dimensional protonic conductivity in porous organic cage solids," *Nature Communications*, vol. 7, pp. 12750-12758, 2016.

[11] D. Stolten, R. C. Samsun, and N. Garland, “MEAs for PEM Fuel Cells,” in *Fuel Cells: Data, Facts, and Figures*, Wiley-VCH, Germany, 2016, pp. 110-118.

[12] H. G. Oswin, A. J. Hartner, and F. Malaspina, "A direct hydrocarbon/air fuel cell," *Nature*, vol. 200, no. 4903, pp. 256-257, 1963.

[13] M. Ternan, “The potential of direct hydrocarbon fuel cells for improving energy efficiency,” *2006 IEEE EIC Climate Change Conference*, vol. 1-2, pp. 504-507, 2006.

[14] W. T. Grubb and C. J. Michalske, "A high performance propane fuel cell operating in the temperature range of 150°C-200°C," *Journal of The Electrochemical Society*, vol. 111, no. 9, pp. 1015-1019, 1964.

Chapter 2: Literature review

2.1 An overview of fuel cell technology

A fuel cell is an energy-conversion device that electrochemically converts the chemical energy of a fuel directly into low-voltage electrical energy. It is driven by the electrochemical reaction occurring between a fuel (such as hydrogen, methanol) and an oxidant (such as oxygen or air) [1]. William Grove discovered the first fuel cell using hydrogen as the fuel in 1839, which was based on the concept explained by Humphry Davy in 1801 [2]. According to William Grove, his invention was about a gas battery that produced electrical power by reversal of the water electrolysis process. The gas battery was termed as a fuel cell in 1889 by Charles Langer and Ludwig Mond, who researched fuel cells that used coal gas fuel and less expensive nickel catalysts [3].

Fuel cells are classified by the type of electrolyte (membrane) used in the membrane electrode assembly (MEA). The desired operating temperature determines the choice of electrolyte. Based on the electrolyte type, there are the following different types of fuel cells: (a) alkaline fuel cell (AFC), (b) polymer electrolyte membrane fuel cell (PEMFC) or proton exchange membrane fuel cell (PEMFC), (c) phosphoric acid fuel cell (PAFC), (d) molten carbonate fuel cell (MCFC), and (e) solid oxide fuel cell (SOFC) [4]. Another criterion for the fuel cell classification is the fuel type. Hydrogen is the most common commercial fuel, followed by methanol. Other fuels that are not used commercially include ethanol, other oxygenated fuels (such as organic formates [5], organic hydrides [6]), and hydrocarbons (such as methane, propane, n-octane). They have been used in research studies [7].

Although the hydrogen fuel cell was discovered in the early 19th century, it took almost 160 years for hydrogen fuel cell technology to be established as an alternative energy generation system that can have minimal impact on the environment. The long waiting period

was caused by the performance of the Grove fuel cell being inferior to conventional energy conversion systems such as internal combustion engines (ICEs) and steam turbine systems. The major limitation of Grove's fuel cell was its very low power density i.e. 3.5 mA/cm^2 at 0.73 V. He noted that the reason for the low current density was the small effective area of the Pt electrodes. Langer and Mond developed the first practical fuel cell in 1889. It used a larger effective catalyst area for the hydrogen and air reactions and generated 50 times greater power density at the same voltage. However, among the existing fuel cell systems, it is the polymer electrolyte membrane fuel cell technology [8] and the solid oxide fuel cell technology that have advanced to become available on a commercial scale.

The application of hydrogen fuel cells can be divided into the following three important categories: (a) stationary, (b) portable, and (c) transport [11,12]. Since 1989 progress in the development of PEMFCs for the transportation sector has been significant and rapid. Past research studies have shown PEMFCs to be a viable and promising alternative to the conventional internal combustion engine (ICE). Due to the low operating temperature (less than 200°C) of the PEMFCs, it is possible to achieve quick start-up with low to zero emissions [8] using hydrogen fuel.

The 2016 Fuel Cell Annual Review [11], reported unexpected slow growth in the adoption of hydrogen fuel cell technology for the year 2015. As in previous years, the Asia Pacific market (primarily Japan and South Korea) dominated global fuel cell development. Nevertheless, the gap in fuel cell sales among the Asia Pacific, North American, and European markets has been diminishing. From 2013 to 2016, mostly stationary (SOFC) fuel cell systems were shipped. South Korea built and commissioned the world's largest fuel cell plant generating 58.8 MW (MCFC) and has announced plans for a 360 MW fuel cell power plant (PAFC) in Pyeongtaek City that was predicted to start full operation by 2018 [14].

In addition, the growth rate of hydrogen fuel cells for the transportation sector (PEMFC)

has been impressive. Hydrogen fuel cell systems can now be purchased on a commercial basis for the following transport applications: materials handling (fork-lifts), automotive vehicles, and buses. Other PEMFCs applications include: yachts, trains, and electric bicycles. PEMFCs are also being sold commercially for stand-by power / uninterrupted power applications. In 2009, PEMFCs used for transportation had typical lifetimes of 2500 h and costs of $61/kW [13]. Some of the major barriers that inhibit greater global commercialization of this technology are durability, cost, freeze-start (below 0°C) characteristics, and lifetime.

2.2 Direct hydrocarbon fuel cells

Theoretically, a direct hydrocarbon fuel cell can have an efficiency of 95% (Section C.1, Appendix C) [9], in comparison to 65% for the Carnot efficiency of an ICE. An important advantage of low temperature fuel cells is that their thermodynamic efficiency ($\Delta G/\Delta H$) does not have the material limitations of a high temperature Carnot cycle such as an ICE [10].

The working principle of a direct hydrocarbon fuel cell (DHFC) is the same as that of the hydrogen fuel cell (HFC) except for the fuel fed at the anode. A schematic diagram of a hydrogen fuel cell is shown in Figure 2.1. Within the fuel cell, a redox reaction, Eq. 2.1 to 2.3, takes place that generates electrical power. If the fuel cell is a PEMFC, the critical part is the membrane electrode assembly (MEA), which is located between the two flow fields i.e. Layers 2-6 of Figure 2.1. The MEA consists of the following five layers: the anode gas diffusion layer, the anode catalyst layer, the electrolyte (membrane) layer, the cathode catalyst layer, and the cathode gas diffusion layer [7].

In this process, the fuel is fed to the anode. There it flows sequentially through the anode flow fields, through the anode gas diffusion layer, and through the catalyst layer. The anode catalyst layer includes small Pt metal particles and electrolyte, where the reaction in Eq. 2.1 occurs. At the cathode, the air (oxygen), an oxidant, is fed through the cathode flow fields, through the gas diffusion layer, and through the catalyst layer. The cathode catalyst layer also

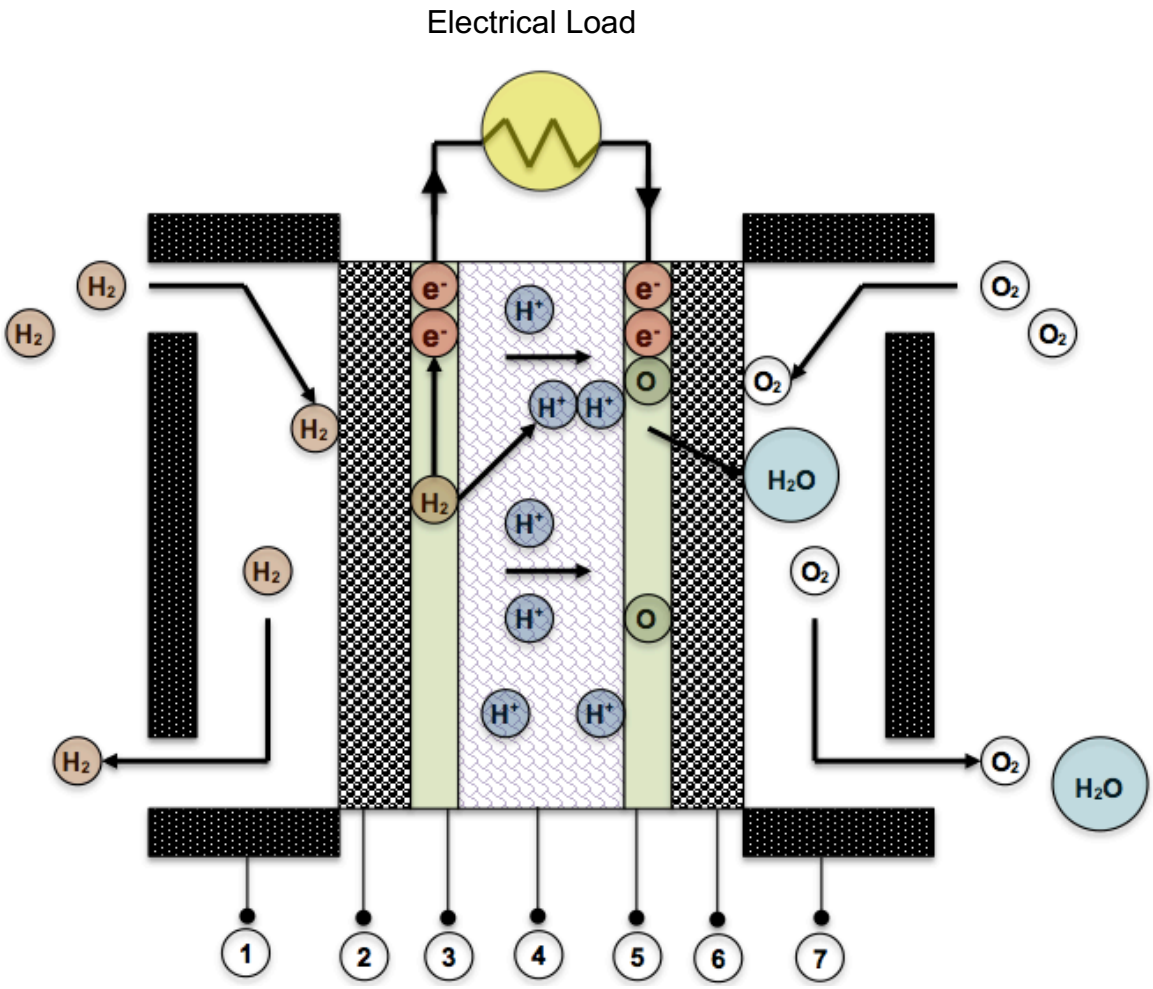


Figure 2.1 Schematic diagram of a typical proton exchange membrane fuel cell (PEMFC) that uses hydrogen fuel. Following are the parts: 1 - Anode flow field, 2 - Anode gas diffusion layer, 3 - Anode catalyst layer, 4 - Proton conducting electrolyte layer, 5 - Cathode catalyst layer, 6 - Cathode gas diffusion layer, and 7 - Cathode flow field.

includes small Pt metal particles and electrolyte, where the reaction in Eq. 2.2 occurs. The protons (H^+) generated at the anode migrate through the electrolyte layer to reach the cathode catalyst layer. The electrons (e^-) from the anode flow through the external circuit to reach the cathode catalyst layer, where they combine with protons from the electrolyte and the oxygen in air that entered the cathode, to form water.

The overall electrochemical reaction, Eq. 2.3 is divided into two half-cell reactions [7,10].

At anode: $H_2 \longrightarrow 2H^+ + 2e^-$ ---------- (2.1) Oxidation reaction

At cathode: $½O_2 + 2H^+ + 2e^- \longrightarrow H_2O$ ---------- (2.2) Reduction reaction

Overall: $H_2 + ½O_2 \longrightarrow H_2O$ ---------- (2.3) Overall reaction

The hydrocarbon fuels commonly used in research studies are mostly alkanes such as propane and methane. The reasons for choosing these fossil fuels included their availability through existing infrastructure, high storage density, and inexpensive production cost. These hydrocarbon fuels are fed directly to the anode without prior fuel processing. Therefore, the capital cost of a fuel processing system can be eliminated. The objective of the studies was to achieve complete conversion of the hydrocarbon fuels with substantially low GHG emissions [10].

2.3 Direct hydrocarbon fuel cells with an aqueous electrolyte

The application of hydrocarbon fuels in fuel cells was investigated extensively in the 1960s and early 1970s. Reviews of that work were prepared by Liebhafsky and Cairns [15], Bockris and Srinivasan [16], Bockris et al. [17], and Cairns [18]. That research focused on fuel cells with an aqueous electrolyte. Various hydrocarbon fuels (i.e. gasoline, diesel, methane, ethylene) were investigated at that time [10,15].

Many research studies have been performed in the past with hydrocarbons. In general, that research showed poor performance and usually generated current densities less than 20 mA/cm^2 at low cell potential values. In 1963, Oswin et al. [19] investigated a direct propane fuel cell (DPFC), which consisted of carbon-Pt electrodes and a phosphoric acid electrolyte. They reported the fuel cell performance at different electrolyte concentrations and at temperatures up to 220°C. Their investigation found reasonable performance of a DPFC at 160°C with an 85% wt. electrolyte concentration. They also observed that the DPFC generated current densities in the range of 100 to 200 mA/cm^2 at almost all cell potential values.

In 1964, Grubb and Michalske [20], reported a direct hydrocarbon fuel cell operating at 150°C using 85% wt. phosphoric acid electrolyte with porous Pt electrodes that delivered high performance. Various alkane hydrocarbon fuels such as methane, propane, n-octane, and n-hexadecane, were investigated in their research. Alkane hydrocarbons such as methane have low chemical reactivity. Their methane results showed chemical inertness at operating temperatures below 100°C. In general, the performance of their methane fuel cell was lower than that of a DPFC. However, when the fuel cell was operated at 150°C, the methane fuel cell performance exceeded that of a DPFC.

The electrochemical reactions given below occur within a direct methane fuel cell (DMFC) that operates with the following electrodes [20]:

The anode when humidified methane gas is fed:

$CH_4 + 2H_2O \longrightarrow CO_2 + 8H^+ + 8e^-$ ---------- (2.4) Oxidation reaction

The cathode when air is fed:

$2O_2 + 8H^+ + 8e^- \longrightarrow 4H_2O$ ---------- (2.5) Reduction reaction

The overall electrochemical reaction within a DMFC:

$CH_4 + 2O_2 \longrightarrow CO_2 + 2H_2O$ ---------- (2.6) Overall reaction

Grubb and Michalske [21], reported a high-performance DPFC that operated in the temperature range of 150 to 200°C. The DPFC consisted of porous Pt-electrodes and a phosphoric acid electrolyte. They observed complete electro-oxidation of propane fuel to carbon dioxide at 200°C. Their hypothesis was that the reaction intermediates had a tendency to adsorb more strongly on the anode catalyst surface compared to the propane molecules. This resulted in complete electrochemical oxidation of the propane molecules with approximately 99% yield of carbon dioxide. They suggested that some intermediate reactant species were strongly adsorbed on the catalyst surface and that others may have been inert to further anodic oxidation. They also obtained an increase in power density by increasing the DPFC operating

temperature from 25 to 200°C. At 200°C, a DPFC using a 95% wt. phosphoric acid electrolyte showed a high performance by producing a current density of 50 mA/cm^2 at 0.5 V cell potential (including the Ohmic losses). However, without including the Ohmic resistance losses, the fuel cell exhibited a higher performance by producing the same current density at 0.65 V cell potential. An interesting observation was the absence of a limiting current density up to a current density range of 200 mA/cm^2 in the measured polarization curves. Grubb [22] also reported complete electro-oxidation of propane using a DPFC that operated at 65°C. Grubb's work emphasized the role of electrocatalysts and fuel cell temperature in increasing the anodic oxidation using a direct hydrocarbon fuel cell.

The electrochemical reactions described below occur respectively on the catalyst surface of the following electrodes [21]:

The anode when humidified propane gas is fed:

$C_3H_8 + 6H_2O \longrightarrow 3CO_2 + 20H^+ + 20e^-$ ---------- (2.7) Oxidation reaction

The cathode when air is fed:

$5O_2 + 20H^+ + 20e^- \longrightarrow 10H_2O$ ---------- (2.8) Reduction reaction

The overall electrochemical reaction within a DPFC:

$C_3H_8 + 5O_2 \longrightarrow 3CO_2 + 4H_2O$ ---------- (2.9) Overall reaction

Cairns [23] performed studies on direct hydrocarbon fuel cells containing an aqueous electrolyte solution of cesium fluoride (CsF) and hydrogen fluoride (HF) salts at 150°C. He reported that an HF electrolyte generated high-performance in direct hydrocarbon fuel cells (DHFCs) using saturated hydrocarbons i.e. from ethane (C_2) to butane (C_4). He also observed that propane gets completely converted into carbon dioxide and water by using CsF-HF electrolytic solution within an operating temperature range of 105 to 166°C.

Natural gas is a rich and promising source of energy. It is easily produced, stored, and transported. Like propane, it is a hydrocarbon fuel that is inexpensive and readily available. The

following researchers had also performed direct hydrocarbon fuel cell studies using methane: (i) Cairns in 1971 [18], (ii) Hsieh and Chen in 1977 [25], (iii) Murray et al. in 1999 [26], (iv) Lee et al. in 2013 [27], (v) Baldinelli et al. in 2016 [28], and (vi) Choi et al. in 2016 [29].

2.4 Direct hydrocarbon polymer electrolyte membrane fuel cell

Cheng et al. [30] performed research on a DPFC with a phosphoric acid doped polybenzimidazole (PBI) electrolyte up to an operating temperature of 250°C. They observed blockage of some reaction sites on the noble metal catalyst by intermediate reactant species. As a result, the performance of the DPFC was poor at 200°C with current densities as low as 2 mA/cm^2 under anhydrous operating conditions. When the propane feed gas was humidified at 25°C, the performance of the fuel cell improved by producing current densities up to 15 mA/cm^2. However, in both the cases, the open-circuit potential (OCP) remained unchanged at 0.7 V.

In 1962, Niedrach [31] explored the possibility of using carbonaceous fuels using an ion exchange membrane, which was a sulfonated phenol-formaldehyde resin fuel cell with platinum (Pt) or palladium (Pd) based carbon electrodes. He investigated the following fuels, methane, ethylene, propane, propylene, and carbon monoxide (CO), with a Pt-based electrode. He observed that current densities were generally less than 5 mA/cm^2.

In 2001, Savadogo and Varela [32] compared low temperature direct propane PEMFC using different anode electrodes, Pt-CrO_3/C, Pt-Ru/C, and Pt/C with the same Pt/C cathode electrode. According to their study, both the anode electrodes Pt-CrO_3/C and Pt-Ru/C produced the highest power density i.e. 46 mW/cm^2 and 42 mW/cm^2 respectively at 95°C. The OCP of a direct propane fuel cell with a Pt-CrO_3/C anode electrode operating at 95°C was 0.98 V. The polarization curve showed a current density of 108 mA/cm^2 at 0.4 V.

In 2006, Varela and Savadogo [33] reported another study on low temperature direct propane fuel cells using a polymer electrolyte. In this study, they compared the performance of the DPFC with their lab prepared anode electrodes such as (PtO_x/C and Pt/C+CrO_3) and

commercial anode electrodes such as Pt-Ru/C and Pt/C. The DPFC was operated at 80°C and different pressure ratios of propane and oxygen. The DPFC consisted of a commercial non-modified MEA i.e. Nafion® 117. They found PtO_x/C anode electrode as the best option for efficient electro-oxidation of propane. For all the anode electrodes, they observed that a propane-oxygen pressure ratio of 2 gave the greatest power density. However, for hydrogen fuel, the fuel cell performance was superior using commercial anode electrodes than using their laboratory prepared ones.

In 2010, Al-Othman et al. [34] investigated a Nafion-free electrolyte that was designed to operate above 100°C. They found zirconium phosphate might be a potential alternative to the Nafion® electrolyte for the fuel cell operations above 100°C. They obtained a proton conductivity of 7.04×10^{-5} S/cm when the zirconium phosphate material was oven dried at a temperature of 70°C.

Various research studies in the past have shown the importance of feed gas humidification in elevating the performance of a PEMFC and increasing the fuel cell operation time. In 1997, Büchi and Srinivasan [35] investigated a PEMFC without external humidification of the feed gas. They observed that the performance of the fuel cell was lower by 20 to 40% when operated at a temperature of 60°C without an external humidification system. However, the fuel cell operated for about 1800 h without any trouble with the help of an internal humidification mechanism that provided water from the electrochemical reaction.

In 2011, Ramya et al. [36] investigated the performance of a PEMFC using an internal membrane humidifier and compared its performance to a conventional external humidification system. The performance of an H_2-PEMFC using an internal membrane humidifier that circulated water at 30°C, was evaluated at 68°C. Its performance was also compared to a conventional bubble humidifier. They observed the same performance for both humidification systems up to a current density of 175 mA/cm^2. At higher current densities, they reported some fluctuations in cell potential.

In 2016, Sanchez et al. [37] investigated the combined effect of relative humidity and operating temperature on the performance of a PEMFC. The effect of feed gas humidification on the fuel cell performance was studied by mapping the current density distribution along the MEA. The MEA was made of commercial Nafion XL membrane with a Pt catalyst loading of 0.3 mg/cm^2 on both the electrodes. Printed circuit board technology was employed to map the current density distribution along the MEA. A fuel cell with an electrode area of 142 cm^2 containing an MEA with a segmented area was placed between two current density measurement boards. The current flowing through each segment of the MEA was measured using the potential difference across the resistor and recorded by a data acquisition system. This configuration of the fuel cell was operated at both 60 and 80°C. They observed a decline in cell potential when operated at 80°C under low humidity conditions. Steady and stable fuel cell operations were observed at 60°C when the relative humidity of the cathode stream was in the range of 20 to 50%.

2.5 Direct hydrocarbon mixed oxide electrolyte fuel cell

In 2008, Heo et al. [38] carried out research on different hydrocarbon fuels using a fuel cell that operated within a temperature range of 100 to 300°C with an electrolyte formed from $Sn_{0.9}In_{0.1}P_2O_7$ powder that had been pressed into a pellet. Their catalysts were metal carbides on a carbon support. They reported current densities of 100 to 150 mA/cm^2 at 0.4 V cell potential. They investigated different hydrocarbon fuels such as methane, ethane, propane, and butane, with Pt-free anode electrodes. They observed a good fuel cell performance for butane and propane when operated at 300°C with Mo_2C-ZrO_2/C anode electrode. The open-circuit potential (OCP) for both butane and propane was 0.8 V and generated a current density of 100 mA/cm^2 at 0.5 V.

2.6 Direct hydrocarbon solid oxide fuel cell

In 2013, Lee et al. [27] investigated the performance of a SOFC fueled directly with methane using $La_2Sn_2O_7$–Ni–GDC (Oxide catalyst with Nickel and Gadolinia-doped ceria) anode at an operating temperature above 600°C. They observed that the $La_2Sn_2O_7$ nanopowder increased the coking tolerance as well as the chemical stability of the Ni-based ceria anode catalyst for dry methane gas at 650°C. They also observed that the direct methane fuel cell (DMFC) produced a peak power density of 0.94 W/cm^2 at 650°C.

In 2016, Ding et al. [43] reported a high-performance direct methane SOFC (DMFC) that consisted of ceramic oxide electrodes and operated within a temperature range of 550 to 700°C. The electrode material at the anode, $Sr_2FeNb_{0.2}Mo_{0.8}O_{6-\delta}$ (SFNM20) was synthesized by the reaction between strontium carbonate, $SrCO_3$, iron (III) oxide, Fe_2O_3, Niobium (V) oxide, Nb_2O_5, and Molybdenum (VI) oxide, MoO_3. This combination of solid compounds was later mixed with acetone and ball milled for 24 h followed by oven drying, grinding, and then calcination at 1200°C in air for 5 h. The DMFC that consisted of a highly conductive SFNM20 anode layer and a cathode layer of $PrBaCo_2O_{5+\delta}$ (PBCO) generated a peak power density of 0.38 W/cm^2 at 0.85 V and 800°C. An OCP of 0.81 V was observed at 800°C with a limiting current density of approximately 1.8 A/cm^2. They found that the SFNM20 had a high tolerance and chemical stability to the coking effect of methane fuel at different operating conditions. The nickel-free anode material exhibited a high catalytic reactivity during the electro-oxidation of the methane.

In 2016, Lee et al. [24] observed a high carbon monoxide (CO) tolerance of direct methane solid oxide fuel cell with ceria coated Ni catalyst at 610°C. Due to the reduced deposition of coke on the catalyst surface, the fuel cell operated continuously for more than 1000 h at a steady current density of 1.2 A/cm^2.

In addition to methane and propane hydrocarbon fuels, other saturated paraffin hydrocarbons such as butane, iso-octane, have also been investigated. The performance of

direct butane SOFC was investigated by Sumi et al. 2012 [39]. They compared the performance of a SOFC employing nickel with gadolinia doped ceria anode (Ni-GDC) with the conventional nickel-yttria stabilized zirconia anode (Ni-YSZ). They demonstrated a continuous production of power for 24 h by using a microtubular SOFC with a Ni-GDC anode that operated at 610°C. They observed slower deposition rate of carbon particles on the catalyst surface with the Ni-GDC anode than the Ni-YSZ anode. The coking effect of butane on the anode catalyst surface was suppressed due to the electrochemical reduction of ceria from Ce^{4+} to Ce^{3+}.

Liu et al. [40] investigated iso-octane as a fuel for a direct hydrocarbon fuel cell that was intended for the transportation sector. Their research described a direct solid oxide fuel cell (SOFC) operating at 750°C using a double-layered anode that was designed to eliminate extensive coke deposition that blocked the anode reaction sites. The double-layered anode that they synthesized consisted of an outermost catalyst layer and an inner electrochemical anode layer that was in contact with the electrolyte layer, YSZ. The catalyst layer was prepared by using a coating material $BaZr_{1-x}Y_xO_{3-\delta}$, BZY, on Ni-YSZ to form a layer of Ni-YSZ-BZY, that was used for catalytic reforming of iso-octane to form hydrogen in the absence of air or carbon dioxide. The hydrogen from reformed iso-octane was passed through the porous electrochemical anode, Ni-YSZ, where the fuel was electrochemically oxidized. This unique double-layered SOFC anode operated successfully with iso-octane fuel at 750°C and generated a peak power density of 0.6 W/cm^2.

Murray et al. 2006 [41] also investigated a direct iso-octane SOFC that operated at 750°C. Their study did not use any anode catalyst layer for internal reforming of the iso-octane fuel. Instead, they evaluated the anode performance of the SOFC by feeding the fuel directly to the anode, Ni-YSZ with a carrier gas, nitrogen. The composition of the iso-octane in the carrier gas was 5.3% by volume. They observed a peak power density of 0.34 W/cm^2 and an OCP of 1.078 V with a limiting current density of about 1 A/cm^2.

An investigation of a SOFC directly fueled with dimethyl ether (DME) hydrocarbon fuel at an operating temperature range of 550 to 650°C was performed by Murray et al. 2005 [42]. The SOFC consisted of yttria-stabilized zirconia electrolyte, YSZ, $La_{0.8}Sr_{0.2}MnO_3$-YSZ cathode, LSM-YSZ, and Ni-YSZ anode. They observed a maximum peak power density of 0.075 W/cm^2 at 650°C for both the anode fuels i.e. DME and DME (33%) + air mixture. Apparently, the performance curves of both the fuels were the same with an OCP of 1 V.

In addition to the hydrocarbon fuels described above, other fuels were also studied for use in directly fed fuel cell. They include: alcohols [44-45], formic acid [46], organic chemical hydrides [6], borohydride [47], and formate peroxide [5].

2.7 Oscillations in fuel cell

In 1967, Niedrach and Tochner [48] observed potential and current oscillations when using hydrocarbons from methane to butane. They investigated fuel cells with both perchloric acid and phosphoric acid electrolytes that operated over a temperature range of 60 to 120°C. They observed a connection between the accumulation of intermediate species and the fuel cell oscillations. They also found that the number of intermediate species produced increased from methane to butane.

In 1969, Deibert and William [49] reported natural oscillations of cell potential in a fuel cell system fed with H_2-CO at the anode at 95°C during galvanostatic mode of operation. The fuel cell consisted of Pt-based electrodes and a phosphoric acid electrolyte. They suggested that these oscillations may have been caused by continuous CO poisoning [50-51] combined with regeneration of the Pt-catalyst surface.

In 2000, Fukumoto et al. [52] observed oscillations in the potential produced by a PEMFC stack that had a Pt-Ru/C anode electrode and operated at a temperature below 60°C. The stack consisted of two single cells. Air was fed into the two cells in parallel. Fuel was fed into the two cells in series. The series arrangement of the fuel supply was such that the exhaust

anode gas of the first cell became the anode feed inlet gas of the second. With time they observed a greater decrease in the current density of the first cell than the second. They suggested that the reduced performance of the first cell indicated the occurrence of CO poisoning on the anode catalyst surface.

Lu et al. [53] demonstrated a similar concept in 2009 under the galvanostatic mode of operation. They observed spontaneous potential oscillations in the fuel cell performance when hydrogen contaminated by CO (at very low concentration in ppm) was the feed gas at the anode electrode (Pt-Ru/C). They observed oscillations at all current densities. They obtained steady potential oscillations at 0.6 V at a constant current density of 50 mA/cm^2 when the anode electrode was contaminated by 200 ppm CO concentration.

In 2011, Lu et al. [54] observed that the average output power density in the galvanostatic mode was higher than in the potentiostatic mode when operating a H_2-CO PEMFC system that had a Pt-Ru/C anode electrode. This was observed within the current density range of 25 to 200 mA/cm^2.

Lee et al. [55] reported electrochemical oscillations in a direct methanol fuel cell with Pt-based electrodes in 2002. In 2004, Zhang et al. [56] carried out a detailed mathematical analysis to understand the mechanism of potential oscillations at the anode fed with H_2-CO fuel in a Pt-based electrode PEMFC.

In 2008, Wang et al. [57] investigated a direct methane solid oxide fuel cell that consisted of $La_{0.75}Sr_{0.25}Cr_{0.5}Mn_{0.5}O_3$ (LSCM) based anode electrodes. They observed oscillations at open-circuit potential (OCP) with dry and wet methane. They reported significantly lower oscillations for dry methane. Their results indicated that the role of the fuel cell temperature and the presence of oxygen species on the catalyst surface were related to the occurrence of these potential oscillations.

In 2010, Hanke-Rauschenbach et al. [58] developed a one-dimensional isothermal

mathematical model to investigate the oscillatory behaviour of a PEMFC fed with H_2-CO fuel at a Pt-Ru/C anode electrode. The model used highly complex non-linear partial differential equations to describe the material and charge balances at the electrode channels and the electrolyte layer. The model predicted a pattern in the formation of intermediate species expected within a wide range of operating conditions, which was responsible for the electrical oscillations of the fuel cell.

In 2011, Lopes et al. [59] reported the occurrence of spontaneous potential oscillations over a wide range of parameters in a PEMFC with Pd-Pt/C anode electrode. They fed H_2 fuel that contained 100 ppm of CO to the anode and operated the PEMFC at 30°C under constant current. A steady oscillatory behaviour was demonstrated at a current density of 100 mA/cm^2. The results obtained were quite different from a PEMFC system with Pt-Ru/C anode electrode under similar operating conditions. They observed a very high amplitude of oscillations i.e. 0.8 V, which was nearly twice the amplitude of the oscillations for a similar operating system with Pd-Pt/C anode electrode. They also investigated the effect of the following two parameters on potential oscillations: (a) H_2-CO inlet flow rate and (b) the fuel cell current density. Their study showed that the oscillatory behaviour was mainly due to the presence of a CO adsorption and desorption mechanism that occurred at the PEMFC anode.

In 2011, Kadyk et al. [60] investigated the occurrence of autonomous potential oscillations in a PEMFC with both Pt/C and Pt-Ru/C anode electrodes at operating temperatures of 40, 60, and 80°C in a differential fuel cell. Their differential fuel cell was 1.6 mm wide and 63 mm long. It consisted of a commercial Nafion 1035 membrane with a Pt catalyst loading of 1 mg/cm^2 at both the electrodes. Graphite flow fields that consisted of 21 parallel flow channels were used for the distribution of gas at anode and cathode. The purpose of conducting experiments using a differential fuel cell was to eliminate the effect of gas starvation and the concentration gradient on the fuel cell performance. They used a differential H_2/H_2 PEMFC

system to eliminate the influence of oxygen at the cathode. They operated under the galvanostatic mode at 80°C with 0 to 200 ppm CO concentration. They also investigated an H_2/O_2 system at the same operating conditions. They observed the influence of the fuel cell temperature and the CO concentration on potential oscillations. They also found that these oscillations occurred at very high anode overpotentials. They used a model developed by Zhang et al. 2002 [61], which addressed CO poisoning in a PEMFC with Pt anode catalyst. They modified the model for Pt-Ru anode catalyst and fitted their experimental data to compare the two model results. They confirmed the influence of water dissociation on the cyclic behaviour of CO oxidation. Their model predicted higher kinetic rate constant values for water dissociation and CO oxidation in a Pt-Ru anode [62-63] catalyst than for a Pt-anode.

In 2012, Yoshizumi et al. [64] carried out an investigation on sulphur poisoning and reported potential oscillations in a SOFC that operated at 800°C. They used a Ni anode catalyst and a pre-reformed hydrocarbon fuel that mainly consisted of methane. They investigated different operational parameters in their study, which included fuel cell operating temperature, fuel inlet flow rate, fuel utilization, pre-reforming ratio, steam/carbon ratio, and current density. They observed degradation of the anode catalyst by hydrogen sulphide and sulphur dioxide, which was contained in the anode fuel. They also observed that the anode degradation was reversible when a sulphur adsorption/desorption process occurred before the fuel cell operation. Potential oscillations were observed when both sulphur and oxygen atoms were adsorbed on the Ni catalyst surface. The potential oscillations observed were reversible. They observed excess Ni oxidation when there were more oxygen atoms than sulphur atoms on the catalyst surface. However, they found that the Ni oxidation process was irreversible. After all the analysis, they concluded that the potential oscillations occurred at high fuel utilization and the Ni oxidation took place at high current densities.

In 2013, Gadacz et al. [65] observed oscillations of OCP and anodic conductivity when

operating a single-chamber fuel cell (SCFC) at an operating temperature range of 500 to 600°C. They defined SCFC as an alternative to SOFC without using two separate anode and cathode compartments. They fed a mixture of propane and oxygen into a single chamber of the SCFC. The SCFC was composed of an electrolyte, i.e. GDC ($Ce_{0.9}Gd_{0.1}O_{1.95}$), an anode i.e. Ni-GDC, and a cathode i.e. BSCF ($Ba_{0.5}Sr_{0.5}Co_{0.8}Fe_{0.2}O_{3-\delta}$). They varied the propane/oxygen mixture ratio from 0.2 to 0.66. They used scanning electron microscope (SEM) and temperature programmed oxidation (TPO) for their analysis. Using the SEM and TPO results, they concluded that the oscillations were caused by a deposition/oxidation cycle on carbon nanowires.

In 2013, Polverino et al. [66] investigated the relationship between water droplet interaction with gas flow and their effect on oscillations in a PEMFC by using a numerical model. They developed a single droplet lumped model that considered the drag force, surface tension force, and adhesive force on the single water droplet. They observed that the water entered through the gas diffusion layer (GDL) and formed a droplet that interacted with the gas flow channels. This interaction caused oscillations in the PEMFC. They also observed that the frequency of these oscillations during the growth and detachment from the GDL were a function of water droplet size.

In 2013, Zhai et al. [67] studied the effect of electrode contaminates such as propene, acetonitrile, and naphthalene on the performance of a PEMFC. They investigated different operating conditions: fuel cell temperature, current density, and contaminant concentration. They observed potential oscillations when the reaction sites of the PEMFC were exposed to naphthalene under an operating condition of higher contaminant concentration and lower temperature. They found that at higher contaminant concentrations, the PEMFC performance losses were higher, anode degradation was faster, and the performance recovery was faster. However, at lower fuel cell temperature, the performance recovery was slower. They also observed that at higher current densities, the PEMFC performance losses were higher, anode

degradation was faster, and the performance recovery was faster for all concentrations of the impurities. After an analysis of their electrochemical impedance spectroscopy (EIS) data, they concluded that the exposure to naphthalene and propene affected the overpotential and the mass transport regions of the fuel cell polarization curve. In contrast, the PEMFC exposure to acetonitrile affected the Ohmic resistance region.

In 2016, Nogueira et al. [68] investigated the kinetic instabilities in a direct methanol fuel cell (DMeFC) using a segmented anode flow field that consisted of 100 segments per channel. Each segment served as a current collection point. They used a patented printed circuit board technology for the current density measurement of the fuel cell. The current measurement board consisted of two gas flow channels, each 10 cm long and had 100 current collection points per channel. They operated a single cell with a face area of 10 cm^2 at an operating temperature of 25°C and under a galvanostatic mode of operation. They used a Nafion 111 MEA with Pt/C electrodes that had Pt catalyst loading of 0.3 mg/cm^2 at the anode and 0.55 mg/cm^2 at the cathode. The direct hydrocarbon PEMFC was fed with methanol fuel at the anode and pure oxygen at the cathode. Methanol fuel with concentrations of 0.5 and 1 M was supplied to the anode through a peristaltic pump. They used a half-cell set-up that consisted of a rotating disk electrode (RDE) and a stationary electrode, to study the electrochemical conditions of a DMeFC. They observed that the induction time after which the potential oscillations began was shorter for the stationary electrode than the rotating disk electrode, RDE. Through this observation, they confirmed that the emergence of potential oscillations in a DMeFC depended on the mass transport conditions in the anode diffusion layer. In general, they observed oscillations when the potential difference between the electrodes was less than 100 mV. They observed no particular waveform pattern for the potential oscillations. However, over a selected part of the series, the spontaneous oscillations had an amplitude of 0.08 to 0.15 V. Characterization of the fuel cell was done using EIS, which showed a negative differential

resistance for the DMeFC. They suggested that the presence of a negative resistance region within the DMeFC could be correlated with the occurrence of these potential oscillations under the constant current condition. The concept of a negative differential resistance (NDR) and its significance in a fuel cell operation was investigated by Hanke-Rauschenbach et al. 2011 [69]. They indicated that the common point in most of the non-linear cases reported in the literature was the observation of NDR. Autonomous oscillations in a fuel cell was a non-linear phenomenon that occurred due to the presence of a negative differential resistance in a part of the cell potential vs. current density curve of the fuel cell. In the Nyquist plots, the NDR is defined by a negative value of real impedance (Z_{Real}) in Ohms at zero frequency.

Oscillations in a direct methane SOFC at 800°C during a potentiostatic mode of operation were reported by Sands et al. 2016 [70]. They used three tubular SOFCs under a weakly humidified condition. The SOFC consisted of an electrolyte i.e. yttria-stabilized zirconia (YSZ), an anode i.e. nickel and yttria-stabilized zirconia (Ni/YSZ), and a cathode i.e. lanthanum strontium cobaltite ferrite (LSCF). A mixture of nitrogen and methane gas stream was passed through a humidifier before feeding the SOFC anode. They tested the fuel cells at constant applied potential of 0.8, 0.7, and 0.6 V. The fuel cells were operated continuously until a zero-current output state (i.e. the limiting current region) was reached. According to their prediction, the current oscillations in the fuel cell occurred just before approaching the zero-current output region due to the low methane concentration at the reaction sites. They observed current oscillations in all the three SOFCs, which began from a steady-state current region, then transited through a non-linear oscillatory phase, and finally reached a zero-current state. They also observed that the size of the oscillations grew with the decrease in the methane concentration. In general, they observed oscillations in the region of low methane concentration. The exact amplitude and period of the oscillations were not determined. However, the period of the oscillations was of the order of seconds. The experimental observations and results were

consistent with their model predictions as described in Sands et al. 2014 [71].

2.8 Mathematical modeling in PEMFC

Mathematical modeling is an important tool for understanding the overall performance of a fuel cell [72]. It is very helpful in predicting stable operating conditions for a fuel cell operating over a wide range of physical, electrochemical, and mass transfer parameters. In general, it plays a substantial role in the development of a fuel cell system. It provides a better understanding of the actual physical and chemical phenomena, occurring within the fuel cell. It also provides valuable information for the fuel cell design, optimization, and performance prediction at various operating conditions, thereby, saving time and money [73]. Several kinds of research in the past have described the advantages of using proton exchange membrane fuel cells (PEMFCs) for automotive applications. Application and development of transient energy models have been recommended for analysing the start-up running options in a fuel cell vehicle [74] with low carbon emissions [75].

A one-dimensional, steady-state, isothermal mathematical model for a hydrogen-oxygen PEMFC was developed by Springer et al. 1991 [76]. The model was designed for a Nafion 117 membrane electrode assembly (MEA) with an active area of 50 cm^2. The purpose of the model was to understand the water transport mechanism of the PEMFC and its effect on the fuel cell performance. In this model, an equilibrium condition was maintained between the liquid water-electrolyte phase and the water vapour-electrode phase at the electrolyte-electrode interface. The model described the phenomenon of electro-osmotic drag and diffusion driving forces for water in the electrolyte phase. A material balance was done for the reactant feed gases and the water vapour that included diffusion phenomenon at the electrodes. The model predicted a water to proton flux ratio of 0.2 at an operating temperature of 80°C, which was consistent with their experimental data.

In 1988, Verbrugge and Hill [77] developed a model using dilute solution theory to understand the transport mechanism in a fuel cell for perfluorosulfonate ionomers. Another model developed by Fales and Vandeborough, 1986 [78] provided insight into electrolyte humidification conditions based on the predicted water sorption isotherms. A different approach to model the transport mechanism occurring within a PEMFC was used by Bernardi and Verbrugge, 1992 [79]. According to their model, the transport mechanism was controlled by diffusion through the gas diffusion layers and hence, the electrolyte phase was completely hydrated.

In 1995, Amphlett et al. [80] developed an isothermal mathematical model for a PEMFC that predicted the fuel cell performance under different operating parameters. The model included both empirical and mechanistic techniques. The performance of the fuel cell was described by using the Stefan-Maxwell equation, the Tafel equation, the Nernst equation, the Nernst-Planck equation, and an Ohm's law equation. In general, the model used some assumptions and approximations to avoid modeling complexities. Nevertheless, the experimental data matched the model predictions quite well.

In 1995, Kim et al. [81] developed a simple mathematical model using an empirical equation for a PEMFC with air as the feed to the cathode. They used the following empirical equation to predict and analyze the performance of the PEMFC at different operating conditions such as fuel cell temperature, pressure, and feed concentration at the cathode.

$$E = E_0 - b \log i - Ri - m \exp (ni)$$

In the above empirical equation, the b log i term was used to define the overpotential loss region, Ri was used for the Ohmic loss region, and m exp (ni) term was used to represent the mass transport region of the polarization curve. They observed that the cell potential difference vs. the current density experimental data fitted the empirical model perfectly.

In 1995, Mosdale and Srinivasan [82] reviewed various mathematical models developed

by several research groups to understand the reason for the mass transport limitation that occurred within a PEMFC. They concluded that the performance of the fuel cell was enhanced when the electrode structure was modified to increase the diffusion of the oxygen at the cathode. They also observed that the thermal and water management issues within the PEMFC were resolved when adapted to the air-evaporative cooling mechanism. In this mechanism, the fuel cell stack placed within a chamber was supplied with water at the cathode such that the air was humidified and had a relative humidity of about 70%. The unreacted air was used to dissipate the heat generated during the fuel cell operation by evaporation of excess water at the cathode. Hence, in this way the dissipation of heat generated and drying out of the proton conducting membrane layer could be resolved. They also found some techniques to operate PEMFCs without reactant gas humidification. One of their methods was to use the product water to dissipate the heat generated within the fuel cell system. To accomplish this goal, they used a porous carbon flow field instead of a rib and channel structure to retain the water generated during the fuel cell operation.

In 1998, Wöhr et al. [83] developed a one-dimensional dynamic model for a hydrogen-air PEMFC to understand and resolve the water and thermal management issues of the fuel cell. The model considered the material and structural properties of the different fuel cell components, mainly the gas diffusion layer, the electrolyte layer, and the catalytic reaction layer. The individual cell components were defined through partial differential and algebraic equations and solved using a numerical method. The gas diffusion layer was described by a combination of the Stefan-Maxwell and the Knudsen diffusion equations. The catalytic reaction layer was defined by the Butler-Volmer equation. The water and proton transport through an electrolyte layer were described by the Stefan-Maxwell diffusion equation. The model results showed that at higher current densities, dehumidification occurred within the PEMFC. They also observed that water diffusion through the gas diffusion layer at the electrode-electrolyte interface was

increased by increased porosity, increased pore size and decreased gas diffusion layer thickness.

In 2000, Um et al. [84] developed a multi-dimensional isothermal model for hydrogen PEMFC using the finite-volume method in computational fluid dynamics (CFD). In their CFD model they considered, the electrochemical kinetics, the hydrodynamic properties, the current distribution phenomena, and the transport phenomena of the many species within the fuel cell. The conservation equations were developed for the flow channels, the diffusion layers, the catalytic reaction layers, and the electrolyte layer. These conservation equations were solved numerically using the finite-volume based method. The model reproduced the polarization curves of the experimental data obtained by Ticianelli et al. 1988 [85]. The model explored the hydrogen dilution phenomena in the anode fuel stream, which was limited by the mass transport phenomena at lower current densities. Similar research on the development of a three-dimensional CFD model for a PEMFC using conventional and interdigitated flow fields at the electrodes was carried out by Carcadea et al. 2005 [86].

The hydrogen dilution phenomena and its effect in a PEMFC were further investigated through a mathematical model by Springer et al. 2001 [87]. They have modeled the influence of hydrogen dilution on the anode performance with hydrogen mole fractions ranging from 0.40 to 0.74 using diluents such as nitrogen and carbon dioxide. They have also modeled the effect of CO surface poisoning on the anode performance under a high utilization rate of 90% with CO concentration of 10 to 100 ppm in 40% diluted hydrogen feed stream. In this model, the catalyst/ionomer interfacial kinetic equations were coupled with the Ohmic resistance and the reactant mass transfer limitations within the anode catalyst layer to determine the anode overpotentials.

In 2002, Berning et al. [88] reported a three-dimensional, non-isothermal CFD model for a PEMFC that considered phase change phenomenon within the fuel cell. The model provided

detailed information about the three-dimensional distribution of the fuel cell parameters such as current densities, mass transfer rates, flow velocities, species concentration, and the cell temperature. They predicted a temperature gradient within the fuel cell. The model included a mass transport mechanism and a limiting current condition. They also reported consistency of their model results with their experimental data. Furthermore, Weber and Newman in 2003 [89] and 2004 [90] investigated the mass transport mechanisms and water to proton flux ratio in a polymer electrolyte layer of the PEMFC using a simple two-dimensional pseudo-model.

In 2004, Um and Wang [91] developed a three-dimensional isothermal CFD model for a PEMFC using a parallel and an interdigitated flow field at the cathode. They observed a three-dimensional interaction of the electrochemical and mass transport kinetics for the species within the PEMFC. They also observed a higher mass transfer limiting current density when an interdigitated flow field (IDFF) was used for air at the cathode. Thus, the model showed that the forced draft convection induced by the IDFF had a positive impact on the mass transport limitations of the fuel cell. A parametric study for an intermediate temperature PEMFC, containing a polybenzimidazole (PBI) electrolyte, was conducted by Cheddie and Munroe, 2006 [92]. The model results showed that the mass transport limitations within the fuel cells occurred due to the lack of porosity in the electrode catalyst layers. The model predicted an increase in overall performance of the fuel cell by increasing the reaction rate of the cathode catalyst and by enhancing the polymer electrolyte proton conductivity.

In 2009, Baschuk and Li [93] developed an isothermal two-dimensional mathematical model for a PEMFC under steady-state operation. The model used non-equilibrium thermodynamics. Based on the model results, they concluded that the gas-flow channels with longer lengths gave rise to lower fuel cell performance. They reasoned that the lower performance was caused by an inefficient and non-uniform distribution of water. They also observed that sufficient humidification of the anode feed gas was necessary to enhance the

overall performance of the fuel cell. Later, Baschuk and Li, 2010 [94] presented an extensive mathematical model, which described the water and ion transport mechanism in an electrolyte layer of the PEMFC. They used the Stefan-Maxwell diffusion equation to model the transport phenomena. The equations in the model were solved using a finite-volume numerical method with the aid of simulation codes developed in-house. The model results showed that the majority of water at the anode was transported to the cathode. Hence, it was necessary to replenish the water consumed at the anode frequently.

An isothermal one-dimensional mathematical modeling for a direct propane fuel cell was developed by Psofogiannakis et al. 2006 [95] for an operating temperature less than 250°C. The model predicted the performance of a PAFC, fueled directly with propane at the anode, for both Pt anode catalyst supported on carbon and unsupported Pt black anode catalyst. The effect of the following parameters on the PAFC performance was investigated: fuel cell operating pressure, fuel cell operating temperature, concentration of the phosphoric acid electrolyte, Pt catalyst loading, and the percent conversion of reactant gases at the electrodes. In their work, the catalyst layer was modeled as a stack of spherical catalyst particles that were filled with the liquid electrolyte and externally surrounded by gas-filled porous structures. They observed that the largest resistance in the polarization curve for the direct propane PAFC (DPPAFC) anode was from the overpotential rather than the Ohmic and concentration resistances. They also observed that the performance of the DPPAFC was strongly affected by the electrolyte concentration. They found that, the performance of the DPPAFC was superior with a carbon supported Pt anode catalyst than with an unsupported Pt back anode catalyst.

In 2015, Khakdaman et al. [96] reported the first robust two-dimensional isothermal mathematical model for direct propane PEMFCs (DPFC) with interdigitated flow fields (IDFFs) at the electrodes. They developed a CFD model using FreeFem++ [97] open-source software. An investigation of the anode catalyst layer materials and the fuel cell operating conditions were

performed to improve the anode performance of the DPFC. The modeling domain consisted of the anode catalyst layer, the electrolyte layer, and the cathode catalyst layer. Each layer in the model was represented by partial different equations. The governing equations of the model are shown in Table 2.1.

Layer	Equations	Example
Anode and cathode catalyst layers	Reaction Mass transport PVT relation	Butler-Volmer equation or complex kinetics expressions Fick's law or Stefan-Maxwell equation Ideal gas law or equation of state
Electrolyte layer	Mass transport Membrane swelling PVT relation	Nernst-Planck or Stefan-Maxwell equation Empirical or thermodynamic models Ideal gas law or equation of state
Anode and cathode diffusion layers	Mass transport PVT relation	Fick's law or Stefan-Maxwell equation Ideal gas law or equation of state
Anode and cathode gas channels	Mass transport PVT relation	Fick's law or Stefan-Maxwell equation Ideal gas law or equation of state

Table 2.1 The governing equations of the DPFC model [96,98-99]

The partial differential equations were solved using a finite element numerical method. This was the first model that described the forces from the chemical potential and electrical potential

gradients being in opposite directions and thereby explained the proton transport phenomena accurately within the DPFC. In comparison to this model [96], their earlier models [98,99] had considered only the proton migration phenomena through the fuel cell electrolyte. The electrolyte material used in their DPFC models [96,98,99] was zirconium phosphate (ZrP), a Nafion-free proton conducting material. The models were developed for an operating temperature range of 150 to 200°C and a pressure of 1 atm. The maximum concentration of propane was maintained at the feed entrance by using IDFFs, which resulted in a relatively high anodic reaction rates. The DPFC model developed by Khakdaman et al. 2010 [98], operated at 150°C and used a ZrP and porous PTFE (polytetrafluoroethylene) electrolyte layer. The ZrP-PTFE electrolyte layer was chosen over the pure ZrP proton conducting material due to its better sustainability and ionic conductivity [100] at 150°C. They also observed that the performance of DPFC anode at 150°C improved when the anode catalyst layer thickness increased. Khakdaman et al. 2011 [99] investigated the performance a DPFC at 150°C using the ZrP-PTFE electrolyte layer. They compared its performance with the other proton conducting materials such as Nafion at 95°C, sulphuric acid doped polybenzimidazole (PBI) at 95°C, and phosphoric acid at 200°C. They observed that the performance of the DPFC model with ZrP-PTFE electrolyte layer at 150°C, was similar to others. However, by using ZrP-PTFE proton conducting material it was possible to operate a DPFC above 100°C and also, without the presence of a liquid phase electrolyte layer.

2.9 References

[1] H. A. Liebhafsky and L. W. Niedrach, "Fuel cells," *Journal of The Franklin Institute*, vol. 269, no. 4, pp. 257-267, 1960.

[2] Johnson Matthey PLC 2016, "Fuel cell history," 2016. [Online]. Available: http://www.fuelcelltoday.com/history.

[3] A. D. S. Tantram, "Fuel cells: Past, present and future," *Energy Policy*, vol. 2, no. 1, pp. 55-66, 1974.

[4] M. L. Perry and T. F. Fuller, "A historical perspective of fuel cell technology in the 20th century," *Journal of The Electrochemical Society*, vol. 149, no. 7, pp. S59-S67, 2002.

[5] Y. Li, "A liquid-electrolyte-free anion-exchange membrane direct formate-peroxide fuel cell," *International Journal of Hydrogen Energy*, vol. 41, no. 5, pp. 3600-3604, 2016.

[6] N. Kariya, A. Fukuoka, and M. Ichikawa, "Direct PEM fuel cell using 'organic chemical hydrides' with zero-CO_2 emission and low-crossover," *Physical Chemistry Chemical Physics*, vol. 8, no. 14, pp. 1724-1730, 2006.

[7] T. G. Services, *'2004 fuel cell handbook: Advanced technology for generating electricity; series on renewable energy, Biofuels, Bioenergy, and Biobased products, 7th edition'*, 7th ed. Morgantown, WV: U.S. Department of Energy, Office of Fossil Energy, National Energy Technology Laboratory, 2004.

[8] G. J. K. Acres, "Recent advances in fuel cell technology and its applications," *Journal of Power Sources*, vol. 100, no. 1-2, pp. 60-66, 2001.

[9] M. Ternan, "The potential of direct hydrocarbon fuel cells for improving energy efficiency," *2006 IEEE EIC Climate Change Conference*, vol. 1-2, pp. 504-507, 2006.

[10] G. Hoogers, "Introduction," in *Fuel Cell Technology Handbook,* CRC Press, Boca Raton, 2003, pp. 2-37.

[11] K. A. Adamson, "The fuel cell and hydrogen: Annual review, 2016," 4th Energy Wave, 2016.

[12] Johnson Matthey PLC 2016, "Fuel cell applications," 2016. [Online]. Available: http://www.fuelcelltoday.com/applications.

[13] Y. Wang, K. S. Chen, J. Mishler, S. C. Cho, and X. C. Adroher, "A review of polymer electrolyte membrane fuel cells: Technology, applications, and needs on fundamental research," *Applied Energy*, vol. 88, no. 4, pp. 981-1007, 2011.

[14] T. Wilberforce, A. Alaswad, A. Palumbo, M. Dassisti, and A. G. Olabi, "Advances in stationary and portable fuel cell applications," *International Journal of Hydrogen Energy*, vol. 41, no. 37, pp. 16509-16522, 2016.

[15] H. A. Liebhafsky and E. J. Cairns, “Direct hydrocarbon fuel cell with aqueous electrolytes,” in *Fuel Cells and Fuel Batteries*, Wiley, New York, 1968, pp. 458-523.

[16] J. O. Bockris and S. Srinivasan, “Fuel cells: Their electrochemistry,” in *Electrochemical Combustion of Organic Substances*, McGraw-Hill, New York, 1969, pp. 357-411.

[17] J. O. Bockris, E. Gileadi, and G. E. Stoner, "Anodic oxidation of saturated hydrocarbons. Mechanistic study," *The Journal of Physical Chemistry*, vol. 73, no. 2, pp. 427-434, 1969.

[18] E. J. Cairns, "The anodic oxidation of hydrocarbons and the hydrocarbon fuel cell," in *Advances in Electrochemistry and Electrochemical Engineering*, Wiley-Interscience, New York, 1971, vol. 8, pp. 337-392.

[19] H. G. Oswin, A. J. Hartner, and F. Malaspina, "A direct hydrocarbon/air fuel cell," *Nature*, vol. 200, no. 4903, pp. 256-257, 1963.

[20] W. T. Grubb and C. J. Michalske, "Electrochemical oxidation of methane in phosphoric acid fuel cells at 150°C," *Nature*, vol. 201, no. 4916, pp. 287-288, 1964.

[21] W. T. Grubb and C. J. Michalske, "A high performance propane fuel cell operating in the temperature range of 150°C-200°C," *Journal of The Electrochemical Society*, vol. 111, no. 9, pp. 1015-1019, 1964.

[22] W. T. Grubb, "Catalysis, electrocatalysis, and hydrocarbon fuel cells," *Nature*, vol. 198, no. 4883, pp. 883-884, 1963.

[23] E. J. Cairns, "Hydrocarbon fuel cells with fluoride electrolytes," *Journal of The Electrochemical Society*, vol. 113, no. 11, pp. 1200-1204, 1966.

[24] J. G. Lee, O. S. Jeon, H. J. Hwang, J. Jang, Y. Lee, S. H. Hyun, and Y. G. Shul, "Durable and high-performance direct-methane fuel cells with coke-tolerant ceria-coated Ni catalysts at reduced temperatures," *Electrochimica Acta*, vol. 191, pp. 677-686, 2016.

[25] S. Y. Hsieh and K. M. Chen, "Anodic oxidation of methane," *Journal of The Electrochemical Society*, vol. 124, no. 8, pp. 1171-1174, 1977.

[26] E. P. Murray, T. Tsai, and S. A. Barnett, "A direct-methane fuel cell with a ceria-based anode," *Nature*, vol. 400, no. 6745, pp. 649-651, 1999.

[27] J. G. Lee, C. M. Lee, M. Park, and Y. G. Shul, "Direct methane fuel cell with $La_2Sn_2O_7$–Ni–$Gd_{0.1}Ce_{0.9}O_{1.95}$ anode and electrospun $La_{0.6}Sr_{0.4}Co_{0.2}Fe_{0.8}O_{3-\delta}$–$Gd_{0.1}Ce_{0.9}O_{1.95}$ cathode," *RSC Advances*, vol. 3, no. 29, pp. 11816-11822, 2013.

[28] A. Baldinelli, L. Barelli, G. Bidini, A. Di Michele, and R. Vivani, "SOFC direct fuelling with high-methane gases: Optimal strategies for fuel dilution and upgrade to avoid quick degradation," *Energy Conversion and Management*, vol. 124, pp. 492-503, 2016.

[29] Y. Choi, E. C. Brown, S. M. Haile, and W. Jung, "Electrochemically modified, robust solid oxide fuel cell anode for direct-hydrocarbon utilization," *Nano Energy*, vol. 23, pp. 161-171, 2016.

[30] C. K. Cheng, J. L. Luo, K. T. Chuang, and A. R. Sanger, "Propane fuel cells using phosphoric-acid-doped polybenzimidazole membranes." *The Journal of Physical Chemistry B*, vol. 109, no. 26, pp. 13036-13042, 2005.

[31] L. W. Niedrach, "The performance of hydrocarbons in ion exchange membrane fuel cells," *Journal of The Electrochemical Society*, vol. 109, no. 11, pp. 1092-1096, 1962.

[32] O. Savadogo and F. J. Rodriguez Varela, "Low-temperature direct propane polymer electrolyte membranes fuel cell (DPFC)," *Journal of New Materials for Electrochemical Systems*, vol. 4, no. 2, pp. 93-97, 2001.

[33] F. J. Rodriguez Varela and O. Savadogo, "The effect of anode catalysts on the behavior of low temperature direct propane polymer electrolyte fuel cells (DPFC)," *Journal of New Materials for Electrochemical Systems,* vol. 9, no. 2, pp. 127-137, 2006.

[34] A. Al-Othman, A. Y. Tremblay, W. Pell, S. Letaief, T. J. Burchell, B. A. Peppley, and M. Ternan, "Zirconium phosphate as the proton conducting material in direct hydrocarbon polymer electrolyte membrane fuel cells operating above the boiling point of water," *Journal of Power Sources*, vol. 195, no. 9, pp. 2520-2525, 2010.

[35] F. N. Büchi and S. Srinivasan, "Operating proton exchange membrane fuel cells without external humidification of the reactant gases fundamental aspects," *Journal of the Electrochemical Society*, vol. 144, no. 8, pp. 2767-2772, 1997.

[36] K. Ramya, J. Sreenivas, and K. S. Dhathathreyan, "Study of a porous membrane humidification method in polymer electrolyte fuel cells," *International Journal of Hydrogen Energy*, vol. 36, no. 22, pp. 14866-14872, 2011.

[37] D. G. Sanchez, T. Ruiu, K. A. Friedrich, J. Sanchez-Monreal, and M. Vera, "Analysis of the influence of temperature and gas humidity on the performance stability of polymer electrolyte membrane fuel cells," *Journal of The Electrochemical Society*, vol. 163, no. 3, pp. F150-F159, 2016.

[38] P. Heo, K. Ito, A. Tomita, and T. Hibino, "A proton-conducting fuel cell operating with hydrocarbon fuels," *Angewandte Chemie International Edition*, vol. 47, no. 41, pp. 7841-7844, 2008.

[39] H. Sumi, T. Yamaguchi, K. Hamamoto, T. Suzuki, and Y. Fujishiro, "Impact of direct butane microtubular solid oxide fuel cells," *Journal of Power Sources*, vol. 220, pp. 74-78, 2012.

[40] M. Liu, Y. Choi, L. Yang, K. Blinn, W. Qin, and P. Liu, "Direct octane fuel cells: A promising power for transportation," *Nano Energy*, vol. 1, no. 3, pp. 448-455, 2012.

[41] E. P. Murray, S. J. Harris, J. Liu, and S. A. Barnett, "Direct solid oxide fuel cell operation using isooctane," *Electrochemical and Solid-State Letters*, vol. 9, no. 6, pp. A292–A294, 2006.

[42] E. P. Murray, S. J. Harris, J. Liu, and S. A. Barnett, "Direct solid oxide fuel cell operation using a dimethyl ether/air fuel mixture," *Electrochemical and Solid-State Letters*, vol. 8, no. 10, pp. A531-A533, 2005.

[43] H. Ding, Z. Tao, S. Liu, and Y. Yang, "A redox-stable direct-methane solid oxide fuel cell (SOFC) with $Sr_2FeNb_{0.2}Mo_{0.8}O_{6-\delta}$ double perovskite as anode material," *Journal of Power Sources*, vol. 327, pp. 573-579, 2016.

[44] J. Qi, N. Benipal, C. Liang, and W. Li, "PdAg/CNT catalyzed alcohol oxidation reaction for high-performance anion exchange membrane direct alcohol fuel cell (alcohol=methanol, ethanol, ethylene glycol and glycerol)," *Applied Catalysis B: Environmental*, vol. 199, pp. 494-503, 2016.

[45] S. Fan, D. P. Wilkinson, and H. Wang, "Performance of the vapor fed direct alcohol phosphoric acid fuel cell," *Journal of The Electrochemical* Society, vol. 159, no. 5, pp. B570-B577, 2012.

[46] A. Malolepszy, M. Mazurkiewicz, L. Stobinski, B. Lesiak, L. Kövér, J. Tóth, B. Mierzwa, A. Borodzinski, F. Nitze, and T. Wågberg, "Deactivation resistant Pd-ZrO_2 supported on multiwall carbon nanotubes catalyst for direct formic acid fuel cells," *International Journal of Hydrogen Energy*, vol. 40, no. 46, pp. 16724-16733, 2015.

[47] R. K. Raman, N. A. Choudhury, and A. K. Shukla, "A high output voltage direct borohydride fuel cell," *Electrochemical and Solid-State Letters*, vol. 7, no. 12, pp. A488-A491, 2004.

[48] L. W. Niedrach and M. Tochner, "Studies of hydrocarbon fuel cell anodes by the multipulse potentiodynamic method III. Behavior of saturated hydrocarbons on conducting porous teflon electrodes with a phosphoric acid electrolyte," *Journal of The Electrochemical Society*, vol. 114, no.1, pp. 17-22, 1967.

[49] M. C. Deibert and D. L. Williams, "Voltage oscillations of the H_2-CO system," *Journal of The Electrochemical Society*, vol. 116, no. 9, pp. 1290-1292, 1969.

[50] S. Balasubramanian and J. W. Weidner, "Analysis of an electrochemical filter for removing carbon monoxide from reformate hydrogen," *Journal of The Electrochemical Society*, vol. 162, no. 10, pp. E231-E236, 2015.

[51] Q. Li, R. He, J. Gao, J. O. Jensen, and N. J. Bjerrum, "The CO poisoning effect in PEMFCs operational at temperatures up to 200°C," *Journal of the Electrochemical Society*, vol. 150, no. 12, pp. A1599-A1605, 2003.

[52] H. Fukumoto, H. Maeda, and K. Mitsuda, "Oscillation phenomena on the cell voltage of PEFCs during CO poisoning," *Electrochemistry*, vol. 68, no. 10, pp. 794-800, 2000.

[53] H. Lu, L. Rihko-Struckmanna, R. Hanke-Rauschenbach, and K. Sundmacher, "Improved electrochemical CO removal via potential oscillations in serially connected PEM fuel cells with PtRu anodes," *Electrochimica Acta*, vol. 54, no. 4, pp. 1184-1191, 2009.

[54] H. Lu, L. Rihko-Struckmanna, and K. Sundmacher, "Spontaneous oscillations of cell voltage, power density, and anode exit CO concentration in a PEM fuel cell," *Physical Chemistry Chemical Physics*, vol. 13, no. 40, pp. 18179-18185, 2011.

[55] J. Lee, C. Eickes, M. Eiswirth, and G. Ertl, "Electrochemical oscillations in the methanol oxidation on Pt," *Electrochimica Acta*, vol. 47, no. 13, pp. 2297-2301, 2002.

[56] J. Zhang, J. D. Fehribach, and R. Datta, "Mechanistic and bifurcation analysis of anode potential oscillations in PEMFCs with CO in anode feed," *Journal of The Electrochemical Society*, vol. 151, no. 5, pp. A689-A697, 2004.

[57] W. Wang, L. Zhang, and S. P. Jiang, "Potential oscillation of methane oxidation reaction on $La_{0.75}Sr_{0.25}Cr_{0.5}Mn_{0.5}O_3$ electrodes of solid oxide fuel cells," *Journal of Power Sources*, vol. 178, no. 1, pp. 92-96, 2008.

[58] R. Hanke-Rauschenbach, S. Kirsch, R. Kelling, C. Weinzierl, and K. Sundmacher, "Oscillations and pattern formation in a PEM fuel cell with Pt/Ru anode exposed to H_2/CO mixtures," *Journal of the Electrochemical Society*, vol. 157, no. 11, pp. B1521-B1528, 2010.

[59] P. P. Lopes, E. A. Ticianelli, and H. Varela, "Potential oscillations in a proton exchange membrane fuel cell with a Pd-Pt/C anode," *Journal of Power Sources*, vol. 196, no. 1, pp. 84-89, 2011.

[60] T. Kadyk, S. Kirsch, R. Hanke-Rauschenbach, and K. Sundmacher, "Autonomous potential oscillations at the Pt anode of a polymer electrolyte membrane fuel cell under CO poisoning," *Electrochimica Acta*, vol. 56, no. 28, pp. 10593-10602, 2011.

[61] J. Zhang, T. Thampan, and R. Datta, "Influence of anode flow rate and cathode oxygen pressure on CO poisoning of proton exchange membrane fuel cells," *Journal of The Electrochemical Society*, vol. 149, no. 6, pp. A765-A772, 2002.

[62] H. A. Gasteiger, N. Marković, P. N. Ross, Jr., and E. J. Cairns, "Carbon monoxide electrooxidation on well-characterized platinum-ruthenium alloys," *The Journal of Physical Chemistry*, vol. 98, no. 2, pp. 617-625, 1994.

[63] Y. Si, R. Jiang, J. Lin, H. R. Kunz, and J. M. Fenton, "CO tolerance of carbon-supported platinum-ruthenium catalyst at elevated temperature and atmospheric pressure in a PEM fuel cell," *Journal of The Electrochemical Society*, vol. 151, no. 11, pp. A1820-A1824, 2004.

[64] T. Yoshizumi, S. Taniguchi, Y. Shiratori, and K. Sasaki, "Sulfur poisoning of SOFCs: Voltage oscillation and Ni oxidation," *Journal of The Electrochemical Society*, vol. 159, no. 11, pp. F693-F701, 2012.

[65] G. Gadacz, J. P. Viricelle, C. Pijolat, and M. Pijolat, "Voltage oscillations in single-chamber fuel cells operating under a C_3H_8/O_2 mixture," *Fuel Cells*, vol. 13, no. 6, pp. 1032-1039, 2013.

[66] P. Polverino, A. Esposito, and C. Pianese, "Experimental validation of a lumped model of single droplet deformation, oscillation and detachment on the GDL surface of a PEM fuel cell," *International Journal of Hydrogen Energy*, vol. 38, no. 21, pp. 8934-8953, 2013.

[67] Y. Zhai, J. St-Pierre, and M. S. Angelo, "The impact of operating conditions on the performance effect of selected airborne PEMFC contaminants," *ECS Transactions*, vol. 50, no. 2, pp. 635-647, 2013.

[68] J. A. Nogueira, I. K. Peña Arias, R. Hanke-Rauschenbach, T. Vidakovic-Koch, H. Varela, and K. Sundmacher, "Autonomous voltage oscillations in a direct methanol fuel cell," *Electrochimica Acta*, vol. 212, pp. 545-552, 2016.

[69] R. Hanke-Rauschenbach, M. Mangold, and K. Sundmacher, "Nonlinear dynamics of fuel cells: A review," *Reviews in Chemical Engineering*, vol. 27, no. 1-2, pp. 23-52, 2011.

[70] J. D. Sands, J. Uddin, and D. J. Needham, "Current Oscillations in solid oxide fuel cells under weakly humidified conditions," *Journal of The Electrochemical Society*, vol. 163, no. 8, pp. F856-F862, 2016.

[71] J. D. Sands, D. J. Needham, and J. Uddin, "A fundamental model exhibiting nonlinear oscillatory dynamics in solid oxide fuel cells," *Proceedings of The Royal Society A*, vol. 470, no. 2164, pp. 20130551-20130576, 2014.

[72] M. A. R. Sadiq Al-Baghdadi, "A simple mathematical model of performance for proton exchange membrane fuel cells," *International Journal of Sustainable Energy*, vol. 26, no. 2, pp. 79-90, 2007.

[73] H. Khakdaman, "A two dimensional model of a direct propane fuel cell with an interdigitated flow field", Ph.D., University of Ottawa, 2012.

[74] M. De Francesco and E. Arato, "Start-up analysis for automotive PEM fuel cell systems," *Journal of Power Sources*, vol. 108, no. 1, pp. 41-52, 2002.

[75] T. Nakata, D. Silva, and M. Rodionov, "Application of energy system models for designing a low-carbon society," *Progress in Energy and Combustion Science*, vol. 37, no. 4, pp. 462-502, 2011.

[76] T. E. Springer, T. A. Zawodzinski, and S. Gottesfeld, "Polymer electrolyte fuel cell model," *Journal of the Electrochemical Society*, vol. 138, no. 8, pp. 2334-2342, 1991.

[77] M. W. Verbrugge and R. F. Hill, "Experimental and theoretical investigation of perfluorosulfonic acid membranes equilibrated with aqueous sulfuric acid solutions," *The Journal of Physical Chemistry*, vol. 92, no. 23, pp. 6778-6783, 1988.

[78] L. J. Fales and N. E. Vandeborough, "The influence of ionomer channel geometry on ionomer transport", *Electrochemical Society Proceedings*, vol. 86, no. 13, pp. 179-191, 1986.

[79] D. M. Bernardi and M. W. Verbrugge, "A mathematical model of the solid-polymer-electrolyte fuel cell," *Journal of the Electrochemical Society*, vol. 139, no. 9, pp. 2477-2491, 1992.

[80] J. C. Amphlett, R. M. Baumert, R. F. Mann, B. A. Peppley, and P. R. Roberge, "Performance modeling of the Ballard Mark IV solid polymer electrolyte fuel cell I. Mechanistic model development," *Journal of the Electrochemical Society*, vol. 142, no. 1, pp. 1-8, 1995.

[81] J. Kim, S. Lee, and S. Srinivasan, "Modeling of proton exchange membrane fuel cell performance with an empirical equation," *Journal of the Electrochemical Society*, vol. 142, no. 8, pp. 2670-2674, 1995.

[82] R. Mosdale and S. Srinivasan, "Analysis of performance and of water and thermal management in proton exchange membrane fuel cells," *Electrochimica Acta*, vol. 40, no. 4, pp. 413-421, 1995.

[83] M. Wöhr, K. Bolwin, W. Schnurnberger, M. Fischer, W. Neubrand, and G. Eigenberger, "Dynamic modelling and simulation of a polymer membrane fuel cell including mass transport limitation," *International Journal of Hydrogen Energy*, vol. 23, no. 3, pp. 213-218, 1998.

[84] S. Um, C. Y. Wang, and K. S. Chen, "Computational fluid dynamics modeling of proton exchange membrane fuel cells," *Journal of The Electrochemical Society*, vol. 147, no. 12, pp. 4485-4493, 2000.

[85] E. A. Ticianelli, C. R. Derouin, and S. Srinivasan, "Localization of platinum in low catalyst loading electrodes to attain high power densities in SPE fuel cells," *Journal of Electroanalytical Chemistry and Interfacial Electrochemistry*, vol. 251, no. 2, pp. 275-295, 1988.

[86] E. Carcadea, H. Ene, D. B. Ingham, R. Lazar, L. Ma, M. Pourkashanian, and I. Stefanescu, "Numerical simulation of mass and charge transfer for a PEM fuel cell," *International Communications in Heat and Mass Transfer*, vol. 32, no. 10, pp. 1273-1280, 2005.

[87] T. E. Springer, T. Rockward, T. A. Zawodzinski, and S. Gottesfeld, "Model for polymer electrolyte fuel cell operation on reformate feed: Effects of CO, H_2 dilution, and high fuel utilization," *Journal of the Electrochemical Society*, vol. 148, no. 1, pp. A11-A23, 2001.

[88] T. Berning, D. M. Lu, and N. Djilali, "Three-dimensional computational analysis of transport phenomena in a PEM fuel cell," *Journal of Power Sources*, vol. 106, no. 1, pp. 284-294, 2002.

[89] A. Z. Weber and J. Newman, "Transport in polymer-electrolyte membranes I. Physical model," *Journal of the Electrochemical Society*, vol. 150, no. 7, pp. A1008-A1015, 2003.

[90] A. Z. Weber and J. Newman, "Modeling transport in polymer-electrolyte fuel cells," *Chemical Reviews*, vol. 104, no. 10, pp. 4679-4726, 2004.

[91] S. Um and C. Y. Wang, "Three-dimensional analysis of transport and electrochemical reactions in polymer electrolyte fuel cells," *Journal of Power Sources*, vol. 125, no. 1, pp. 40-51, 2004.

[92] D. Cheddie and N. Munroe, "Parametric model of an intermediate temperature PEMFC," *Journal of Power Sources*, vol. 156, no. 2, pp. 414-423, 2006.

[93] J. J. Baschuk and X. Li, "A comprehensive, consistent and systematic mathematical model of PEM fuel cells," *Applied Energy*, vol. 86, no. 2, pp. 181-193, 2009.

[94] J. J. Baschuk and X. Li, "Modeling of ion and water transport in the polymer electrolyte membrane of PEM fuel cells," *International Journal of Hydrogen Energy*, vol. 35, no. 10, pp. 5095-5103, 2010.

[95] G. Psofogiannakis, Y. Bourgault, B. E. Conway, and M. Ternan, "Mathematical model for a direct propane phosphoric acid fuel cell," *Journal of Applied Electrochemistry*, vol. 36, no. 1, pp. 115-130, 2006.

[96] H. Khakdaman, Y. Bourgault, and M. Ternan, "A Mathematical model of a direct propane fuel cell," *Journal of Chemistry*, vol. 2015, pp. 1-13, 2015.

[97] F. Hecht, O. Pironneau, A. LeHyaric, and K. Ohtsuka, "FreeFEM++ Version 3.32," 2014. [Online]. Available: http://www.freefem.org/ff++/index.htm.

[98] H. Khakdaman, Y. Bourgault, and M. Ternan, "Direct propane fuel cell anode with interdigitated flow fields: Two-dimensional model," *Industrial & Engineering Chemistry Research*, vol. 49, no. 3, pp. 1079-1085, 2010.

[99] H. Khakdaman, Y. Bourgault, and M. Ternan, "Computational modeling of a direct propane fuel cell," *Journal of Power Sources*, vol. 196, no. 6, pp. 3186-3194, 2011.

[100] M. Liu, L. Chen, S. Lewis, S. Y. Chong, M. A. Little, T. Hasell, L. M. Aldous, C. M. Brown, M. W. Smith, C. A. Morrison, L. J. Hardwick, and A. I. Cooper, "Three-dimensional protonic conductivity in porous organic cage solids," *Nature Communications*, vol. 7, pp. 12750-12758, 2016.

Chapter 3: A parametric study of a direct propane fuel cell (DPFC) using a computational fluid dynamics (CFD) model employing the finite element method

Abstract

A two-dimensional mathematical model based on computational fluid dynamics (CFD), specifically FreeFem++ software, was used to perform a parametric study of a direct propane fuel cell (DPFC). First, an existing mathematical model of a DPFC consisting of modified zirconium phosphate membrane electrode assembly (MEA) was improved. Then an isothermal parametric study was performed. Polarization curves predicted by the CFD model were used to indicate fuel cell performance. A total of eleven operational parameters were investigated to understand the overall performance of the fuel cell. The computational results showed that the parameters affecting the catalyst (the surface reaction rate) had the greatest effect on fuel cell performance.

3.1 Introduction

Although hydrogen is the most favored fuel for fuel cell performance, the technology for its storage and transportation cannot compete with that for hydrocarbon fuels such as gasoline [1] and propane (liquefied petroleum gasoline). This research is directed toward the development of a low temperature direct propane fuel cell (DPFC) operating above a temperature of 120°C [2]. From among the several types of fuel cells available [3,4], we have chosen a proton exchange membrane fuel cell (PEMFC). When fueled by hydrogen, it has become available commercially, and is now an alternative to the conventional internal combustion engine used in automobiles. Low temperature direct hydrocarbon fuel cells have many advantages. Hydrocarbons can be stored as liquids, rather than gas. They have greater energy densities than gases. Infrastructure for their production, transportation and storage already exists [5]. For example, propane (liquefied petroleum gasoline) is a hydrocarbon that is

widely available in rural areas. A fuel cell system has three components: (a) fuel processor, (b) fuel cell stack, and (c) power conditioner. Hydrocarbons can be fed directly to the anode of a fuel cell. They do not require any prior conversion, such as the fuel processing systems needed to make hydrogen for hydrogen fuel cells. Absence of a fuel processer unit decreases the capital cost of the fuel cell system by approximately one-third. A DPFC has a theoretical energy efficiency of 95% (Section C.1, Appendix C) in comparison to 65% for the Carnot cycle in thermal power plants [6]. However, direct hydrocarbon fuel cells have one major disadvantage. Their demonstrated energy efficiency is far less than those for fuels used in thermal power plants. The object of this research is to help to improve their energy efficiencies.

The use of hydrocarbon fuels in fuel cells was extensively investigated in the 1960s and early 1970s and has been reviewed by: Liebhafsky and Cairns [7], Bockris and Srinivasan [8], and Bockris et al. [9]. That research was focused on fuel cells with an aqueous electrolyte. Various hydrocarbon fuels (i.e. gasoline, diesel, methane, ethylene) were investigated. The results from previous research were poor. For example, the current densities at 0.5 V were often less than 100 mA/cm^2. Investigations specifically on DPFCs were performed by Oswin et al. 1963 [10], Grubb and Michalske 1964 [11], and Cheng et al. 2005 [12]. However, in recent years only a limited amount of work has been reported on DPFCs.

Mathematical models are useful for understanding the physical and chemical phenomena that occur in fuel cells. Specifically, fuel cell operating conditions can be predicted over a wide range of physical, electrochemical, and mass transfer parameters [13]. One of the first models for a hydrogen fuel cell was a one-dimensional, steady state, isothermal model that was developed by Springer et al. 1991 [14]. The model included a Nafion 117 membrane electrode assembly (MEA) with a face area of 50 cm^2. The purpose of the model was to understand the water transport mechanism within the PEMFC and its effect on the fuel cell performance. The model predicted the water flux to proton ratio of 0.2 at an operating

temperature of 80°C, which was consistent with an experimental value. Earlier, Verbrugge and Hill [15] developed a model using dilute solution theory to describe the migration of protons in a fuel cell having a perfluorosulfonate ionomer membrane. Another model, developed by Fales and Vandeborough in 1986 [16], used predicted water sorption isotherms to provide insight into electrolyte humidification. Bernardi and Verbrugge, 1992 [17] used a different approach to model the transport mechanism of several species within a PEMFC. According to their model, diffusion of dissolved gases to the catalyst limited catalyst utilization. In 1995, Amphlett et al. [18] developed an isothermal mathematical model for a PEMFC that predicted the fuel cell performance under different operating parameters. In 1995, Kim et al. [19] developed a simple empirical mathematical model using an analytical equation for a PEMFC with air as the feed to the cathode. In 1995, Mosdale and Srinivasan [20] reviewed various mathematical models developed by several research groups to understand the mass transport limitations that occur within a PEMFC. They concluded that the performance of the fuel cell could be enhanced if the electrode structure was modified to increase the diffusion of oxygen to the cathode. In 2000, Um et al. [21] developed a multidimensional isothermal model for hydrogen PEMFC using the finite-volume method commonly used in computational fluid dynamics (CFD). Their CFD model included electrochemical kinetics, hydrodynamic properties, current distribution phenomena, and transport phenomena of the various species within the fuel cell. Similar three-dimensional CFD models for a PEMFC have been developed. Carcadea et al. 2005 [22] developed models with both conventional and interdigitated flow fields. Um and Wang, 2004 [23] developed a three-dimensional isothermal CFD model for a PEMFC having both parallel and interdigitated cathode flow fields. In 2009, Baschuk and Li [24] developed an isothermal two-dimensional steady-state mathematical model for a PEMFC using non-equilibrium thermodynamics. Based on the model results, they concluded that the gas-flow channels with longer lengths gave rise to poorer fuel cell performance. Later, Baschuk and Li, 2010 [25] presented an extensive

mathematical model, which demonstrated the water and ion transport mechanism in an electrolyte layer of the PEMFC.

The work by our research group on computational modeling of a direct propane fuel cell (DPFC) began with a one-dimensional mathematical model developed by Psofogiannakis et al. 2006 [26] using phosphoric acid electrolyte and Pt anode catalyst. Their model showed that the performance of the fuel cell was controlled by the overpotential. Subsequently, Khakdaman et al. [2, 27-28] developed a two-dimensional mathematical model based on a proton exchange membrane and a Pt anode catalyst. In 2015, Khakdaman et al. [2] reported the first two-dimensional mathematical model of complete direct propane PEMFC. It was an isothermal model and it used interdigitated flow fields (IDFFs) at the electrodes. The model investigated the effects of anode catalyst layer materials and fuel cell operating conditions on the anode performance of the DPFC. The modeling domain consisted of the anode catalyst layer, the electrolyte layer and the cathode catalyst layer. Each layer in the model was represented by several partial different equations. The partial differential equations were solved by using the finite element numerical method and FreeFem++ software [29]. This model was more realistic than most DPFC models [27,28] because the migration proton flux caused by the electrical potential gradient was in the opposite direction to the diffusion proton flux, caused by the chemical potential. This model [2] considered both the migration and diffusion phenomena within the DPFC.

The two-dimensional mathematical model developed by Khakdaman et al. [2] was modified to conduct this parametric study. The purpose of the study was to identify parameter(s) that had a major effect on the overall performance of the DPFC. The intent was to use the performance predictions to guide the selection of experiments.

3.2 Model description

Khakdaman's CFD model on DPFC [2] was based on the migration and diffusion phenomena of the charged species (i.e. protons, H^+) through the membrane electrode assembly (MEA) of the fuel cell. The modeling domain of the DPFC consisted of an anode catalyst layer (ACL), an electrolyte (membrane) layer (ML), and a cathode catalyst layer (CCL). Zirconium phosphate ($Zr(HPO_4)_2 \cdot H_2O$ or ZrP) was the proton conducting material or the electrolyte used in the model. The membrane layer consisted of solid ZrP that filled the pores of porous polytetrafluoroethylene (PTFE). The catalyst layer was composed of carbon supported platinum (Pt) catalyst and ZrP electrolyte. Interdigitated flow fields (IDFF) were used both for the anode and cathode. One of the flow channels was used for the reactants and the other for the products. The catalyst layer was composed of three phases i.e. the gas phase, the solid electrolyte phase, and the solid catalyst phase. Four conservation equations were used in the model: the conservation of momentum, total mass, individual component species, and total charge. The governing equations of the model included (a) the conservation of mass in the gas phase, (b) the Ergun equation, (c) the Butler-Volmer equation was used to calculate the reaction rate at the anode and cathode, and (d) conservation equations for water and for protons in the electrolyte phase and in the two catalyst layers. Khakdaman et al. [2] have given a detailed description of the governing equations including their development.

Khakdaman's model [2] was modified to perform the parametric study being described here. The modification used a progressive time-stepping method in the iteration loop that included all the governing equations. The modified iteration loop is on the right-hand side of the modeling flow chart shown in Figure 3.1. This progressive time-stepping method speeds up the computation of the polarization curve by doing a fixed number (N=19 for $\Phi_{Ag} - \Phi_{Ni} \geq 0.793$ and N=39 for $\Phi_{Ag} - \Phi_{Ni} < 0.793$) of the time-steps. After the N time-steps, $\Phi_{Ag} - \Phi_{Ni}$ is decremented by a small value to proceed further down along the polarization curve instead of completing the

time loop before changing Φ_{Ag} - Φ_{Ni}. The progressive time-stepping method included a local overpotential cut-off value at the anode and cathode of 0.432 V. Any grid points where the overpotential was getting larger than 0.432 V was forced to take the value 0.432 V. This occurred at very few points in the anode and cathode. The value of 0.432 V was set by trial and error to limit the impact of this cut-off. Figure 3.2 shows performance prediction of the DPFC model [2] with and without the progressive time-stepping method in the iteration loop. The figure represents the polarization curve of the DPFC model at 150°C and 1 atm. It is a plot of cell potential difference, $\Delta\Phi_{cell}$ (V), versus current density, j (mA/cm^2). When using the progressive time-stepping method, the DPFC model converged up to a current density of 106 mA/cm^2 in comparison to 51 mA/cm^2 for the non-progressive model. The DPFC polarization curve shown in Figure 3.2 that resulted from the progressive time-stepping method was used as the reference case for the parametric study that is described here. The range of variables chosen for the investigation depended on the value of reaction rate (current density) obtained. This also affected the extent of the polarization curve achieved in each case. This difference in the extent of the polarization curve results from the DPFC numerical model [2] hardly converging to a steady-state past a threshold reaction rate, where the threshold is highly dependent on the value of the parameters. The input parameters for the DPFC model are shown in Table 3.1. The other design/ operational parameters remained the same as those reported by Khakdaman et al. [2].

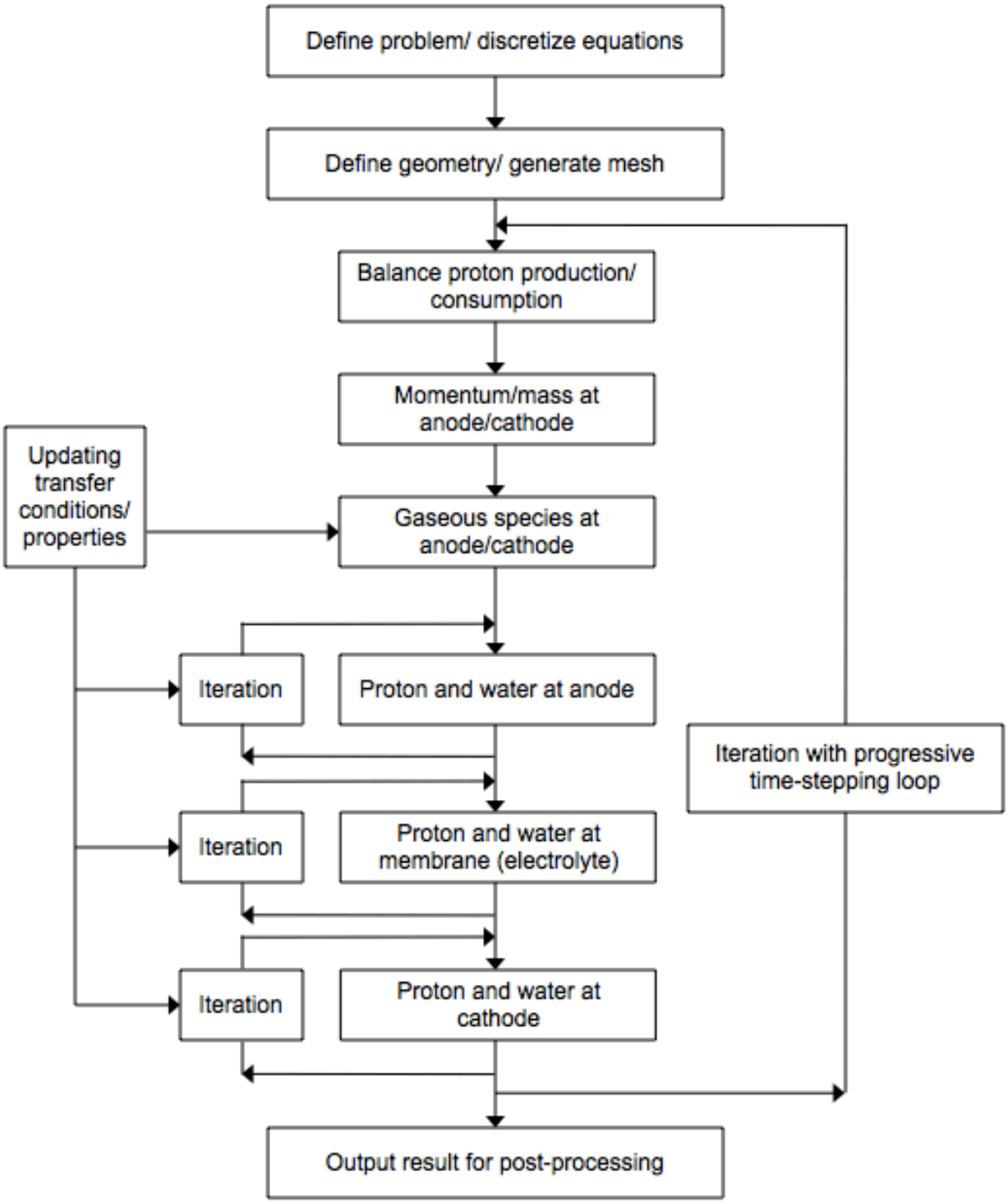


Figure 3.1 The computational procedure with the time-stepping progressive iteration loop [2].

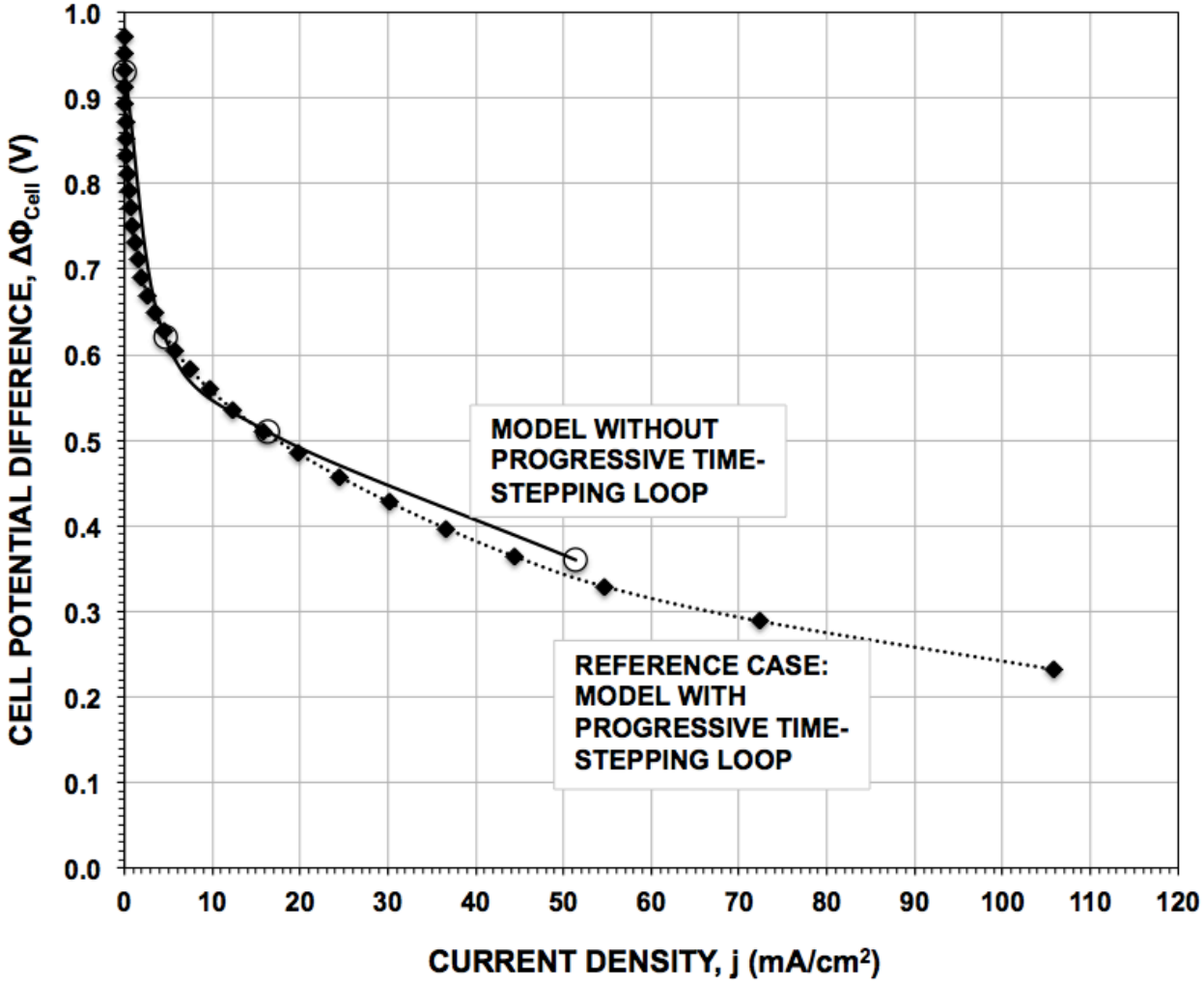


Figure 3.2 The effect of progressive and non-progressive time-stepping loop on the polarization curve for a direct propane fuel cell model (DPFC) at 150°C and 1 atm. The above two cases were represented by the following symbols: (i) open circle: model without progressive time-stepping loop, and (ii) solid diamond: model with progressive time-stepping loop with anode and cathode local overpotential cut-off value, 0.432 V (reference case).

Table 3.1 Operational, electrochemical, and design parameters of the reference case of the DPFC model (all taken from [2]).

Parameter	Value
Temperature, T	423 K
Pressure, P	1 atm
Propane inlet molar flow rate, $\dot{m}_P$	$8x10^{-6}$ gmol s^{-1}
Propane inlet mole fraction, y_{Pinput}	0.1
Reference exchange current density at the anode, $j_{0AN\text{-}ref}$	$7x10^{-5}$ A m^{-2} $_{Pt\text{-}catalyst}$
Reference exchange current density at the cathode, $j_{0CA\text{-}ref}$	$3x10^{-8}$ A m^{-2} $_{Pt\text{-}catalyst}$
Proton diffusivity coefficient in the electrolyte (ZrP) phase, $D_{H+\text{-}ZrP}$	$3x10^{-9}$ m^2 s^{-1}
Water diffusivity coefficient in the electrolyte (ZrP) phase, $D_{H2O\text{-}ZrP}$	$2x10^{-8}$ m^2 s^{-1}
Proton-water diffusivity coefficient, $D_{H2O\text{-}H+}$	$1.32x10^{-8}$ m^2 s^{-1}
Proton conductivity in the electrolyte (membrane) layer, σ_{ELY}	5 S m^{-1}
Specific surface area of carbon catalyst support in the anode and cathode, A_{CAT}	200 m^2 $_{catalyst}$ g^{-1} $_{catalyst}$
Land width, L_w	4.4 mm
Anode and cathode thickness, Th_A, Th_C	300 μm
Membrane thickness, Th_M	100 μm
Fluid channels width in bi-polar plates	0.2 mm
Electrical resistivity in membrane, R_{PTFE}	$1x10^{16}$ Ω m
Charge transfer coefficients, α_A and α_C	1

3.3 Results and discussion

Polarization curves are plots of potential difference between the anode and cathode, $\Delta\Phi_{cell}$, (V) versus current density, j, (mA/cm^2). Often they can be divided into different regions. In each region a different mechanism controls the performance of the fuel cell. At low current densities the reaction rate is controlled by the overpotential (the difference between the actual and the equilibrium potential difference at the electrode-electrolyte interface). At intermediate current densities Ohmic losses (across the electrolyte) control the reaction rate. Finally at high current densities, mass transfer limitations (e.g. oxygen diffusion through liquid water at the cathode) control the reaction rate. When a parameter was changed in this study, its effect on the polarization curve was used to determine its impact on the performance of the fuel cell.

The first parameter investigated was the electrode exchange current density (j_0). The operating conditions were 150°C and 1 atm. This parameter depends on the electrocatalytic properties of the catalyst used in the membrane electrode assembly (MEA) of the fuel cell. The Butler-Volmer equation for the anode can be written as: $j = j_0 * \{2 \sinh [(-½\ n_E F\ \eta)/RT]\}$, where j is the current density (mA/cm^2), j_0 is the exchange current density (mA/cm^2), n_E is the number of moles of electrons transferred per mole of hydrocarbon reacted, F is the Faraday constant (C/mol), η is the overpotential (V), R is the ideal gas constant (J/mol.K), and T is the fuel cell operating temperature (K). The exchange current density (j_0) is also directly proportional to the reaction rate constant (k). Therefore, changing the catalyst will change the rate constant and therefore, will change the exchange current density. The effect of the anodic exchange current density on the overall performance of a direct propane fuel cell (DPFC) is shown in Figure 3.3. A current density of 40 mA/cm^2 was chosen to compare the results obtained in Figure 3.3. As the anodic exchange current density ($j_{0AN\text{-}ref}$) increased by four orders of magnitude (i.e. from 0.07 to 7 to 700 mA/m^2) the potential difference between the fuel cell electrodes also increased (i.e. from 0.38 to 0.72 to 1.04 V respectively). These data indicate that the anodic exchange current

density has a large impact on fuel cell performance.

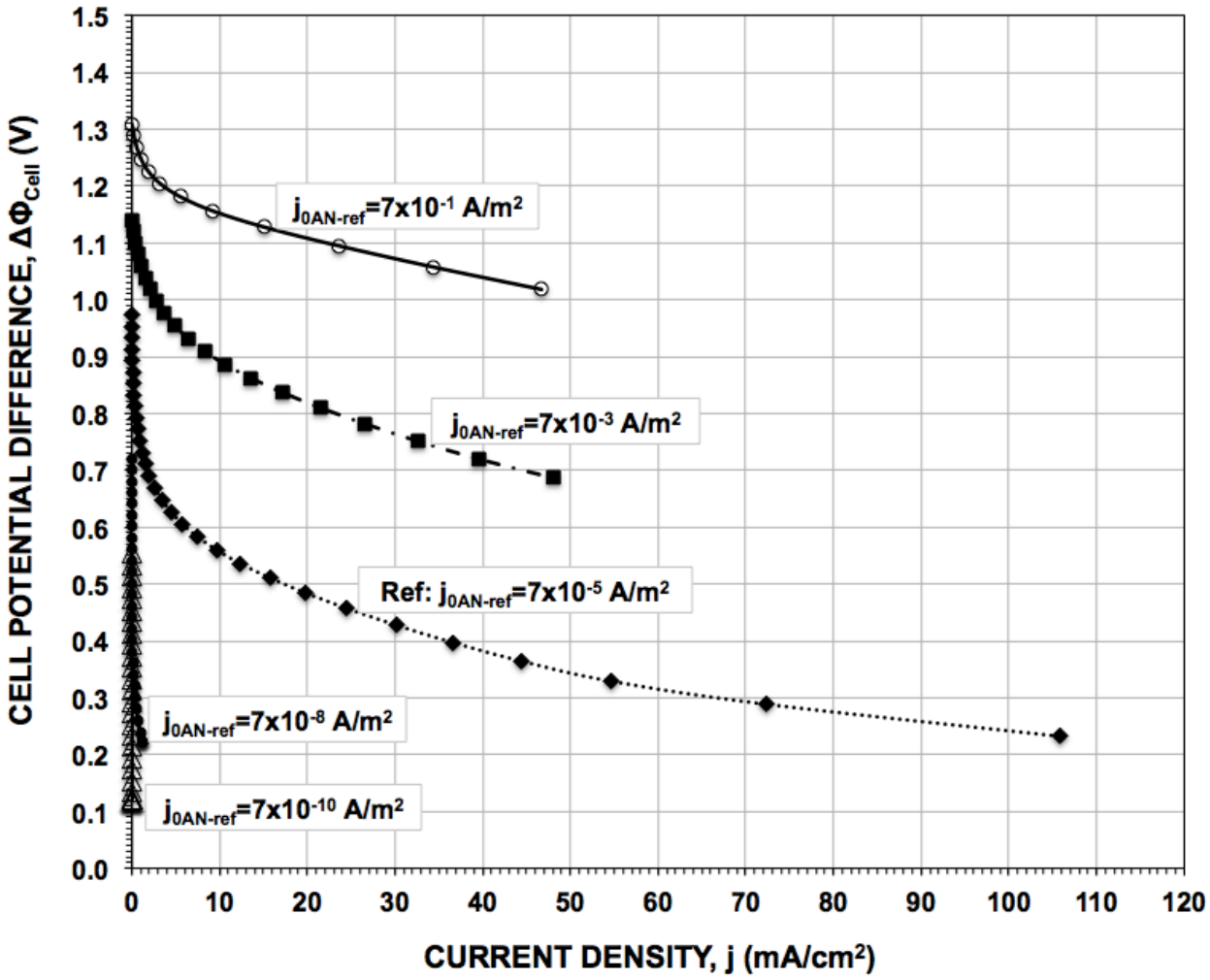


Figure 3.3 The effect of anodic exchange current density, $j_{0AN-ref}$ (A/m^2) on the polarization curve for a direct propane fuel cell model (DPFC) at 150°C and 1 atm. The value of $j_{0AN-ref}$ (A/m^2) for the above five cases were represented by the following symbols: (i) open circle: 7x10^{-1} A/m^2, (ii) solid square: 7x10^{-3} A/m^2, (iii) solid diamond: 7x10^{-5} A/m^2 (reference case), (iv) solid circle: 7x10^{-8} A/m^2, and (v) open triangle: 7x10^{-10} A/m^2. All other parameters were same as the reference case mentioned in Table 3.1.

The effect of the cathode exchange current density on the performance of the DPFC is shown in Figure 3.4. At a current density of 40 mA/cm^2, as the cathode exchange current density ($j_{0CA-ref}$) increased by two orders of magnitude (i.e. from 3 to 300 nA/m^2) the potential

difference between the fuel cell electrodes also increased (i.e. from 0.38 to 0.54 V respectively). From these observations, it was clear that the cathode exchange current density did not change the fuel cell performance as much as the anodic exchange current density. For instance, a

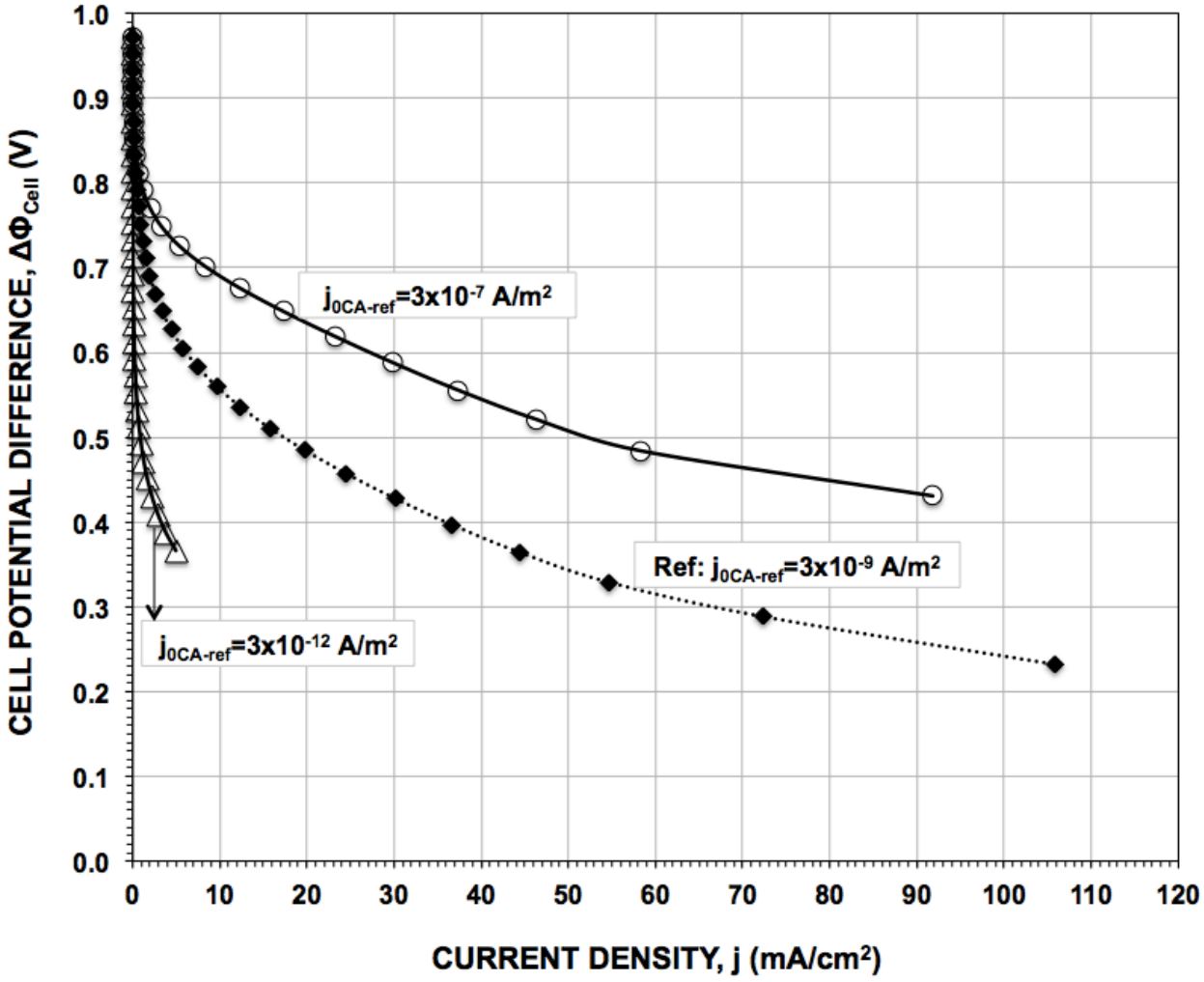


Figure 3.4 The effect of cathode exchange current density, $j_{0CA-ref}$ (A/m^2) on the polarization curve for a direct propane fuel cell (DPFC) model at 150°C and 1 atm. The value of $j_{0CA-ref}$ (A/m^2) for the above three cases were represented by the following symbols: (i) open circle: 3x10^{-7} A/m^2, (ii) solid diamond: 3x10^{-9} A/m^2 (reference case), and (iii) open triangle: 3x10^{-12} A/m^2. All other parameters were same as the reference case mentioned in Table 3.1.

change in the anodic exchange current density ($j_{0AN-ref}$) by two orders of magnitude (i.e. from 7x10^{-5} to 7x10^{-3} A/m^2) caused a cell potential difference change of 0.34 V at 40 mA/cm^2 (Figure

3.3). Whereas, in contrast, the same order of magnitude change in the cathode exchange current density ($j_{0CA\text{-}ref}$) (i.e. from $3x10^{-9}$ to $3x10^{-7}$ A/m^2) caused a cell potential difference change of 0.16 V at 40 mA/cm^2 (Figure 3.4). So, it shows that the change in the potential difference

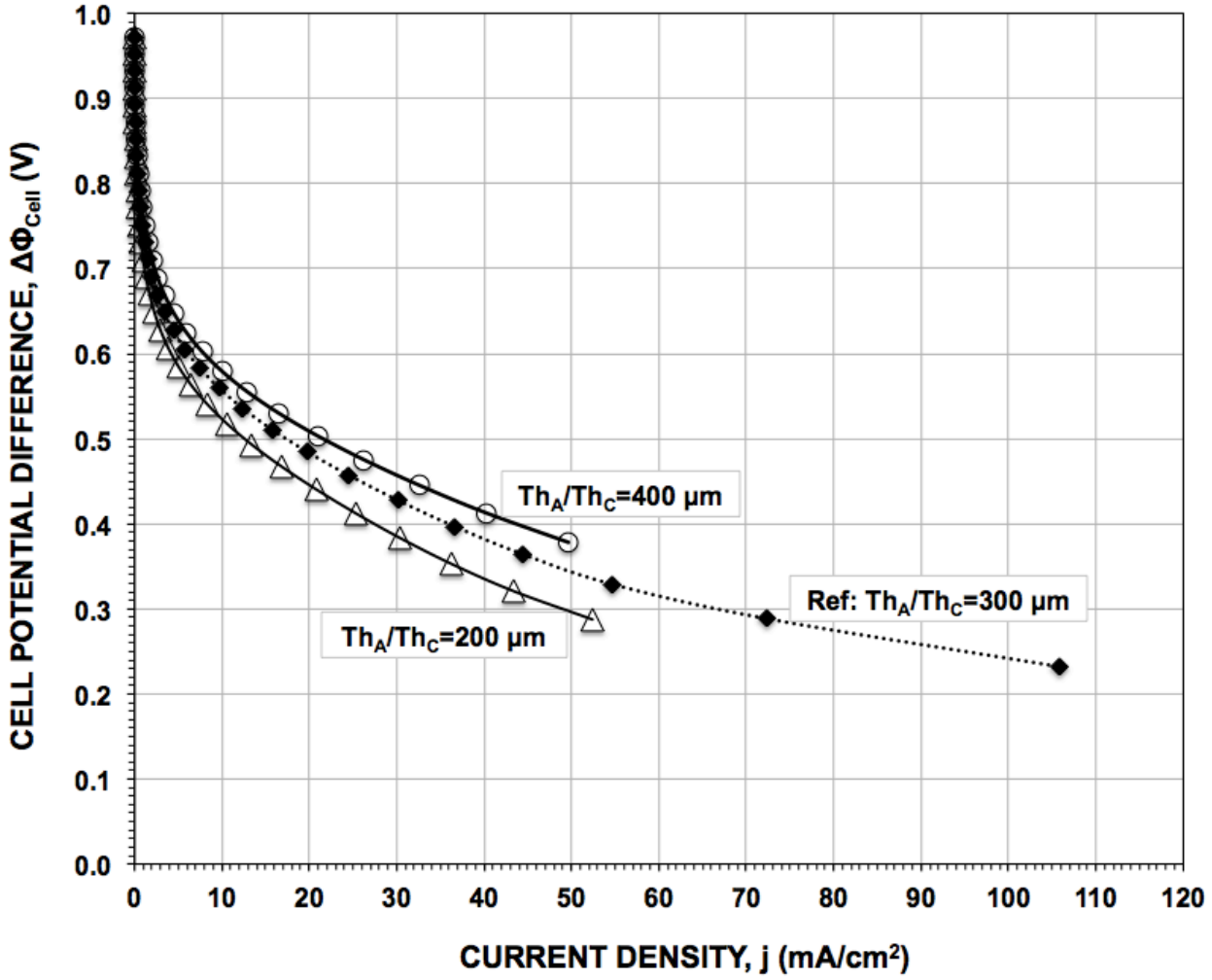


Figure 3.5 The effect of anode/ cathode catalyst layer thickness, Th_A/Th_C (μm) on the polarization curve for a direct propane fuel cell (DPFC) model at 150°C and 1 atm. The value of Th_A/Th_C (μm) for the above three cases were represented by the following symbols: (i) open circle: 400 μm, (ii) solid diamond: 300 μm (reference case), and (iii) open triangle: 200 μm. All other parameters were same as the reference case mentioned in Table 3.1.

across the fuel cell electrodes ($\Delta\Phi_{cell}$) is greater for the anode than the cathode. Hence, it can be concluded that the catalytic material on the anode-side has a greater impact on the overall

performance of the fuel cell than that on the cathode-side.

The catalyst layer thickness in both the anode (Th_A) and cathode (Th_C) are other parameters that could also affect the fuel cell performance, because they affect the volume of the catalyst available for the reaction. Both layers had the same thickness (Th_A/Th_C) in the polarization curves shown in Figure 3.5. At cell potential difference, $\Delta\Phi_{cell}$ of 0.4 V, the current density, j increased by 60% when the thickness of the catalyst layers increased from 200 to 400 μm. At a current density of 40 mA/cm^2, as the thickness of the catalyst layer (Th_A/Th_C) was increased (i.e. from 0.2 to 0.4 mm) the potential difference between the fuel cell electrodes also increased (i.e. from 0.335 to 0.41 V respectively). From these observations, it was evident that catalyst layer thickness did not have as large an impact on the overall performance of the DPFC when compared to the exchange current densities.

The parameter being investigated in Figure 3.6 was the membrane layer thickness (Th_M) of the fuel cell. Its effect can be seen where the Ohmic loss is rate controlling, often the middle part of a hydrogen polarization curve. At a current density of 40 mA/cm^2, as the thickness of the electrolyte (membrane) layer was decreased from 531 to 100 μm, the potential difference between the fuel cell electrodes increased from 0.35 to 0.38 V. Furthermore, when the membrane layer thickness (Th_M) was decreased from 100 to 25 μm, there were no significant changes in potential difference. From these observations, it was evident that the electrical resistance caused by the membrane layer thickness did not have a significant effect on the fuel cell performance in comparison to other parameters.

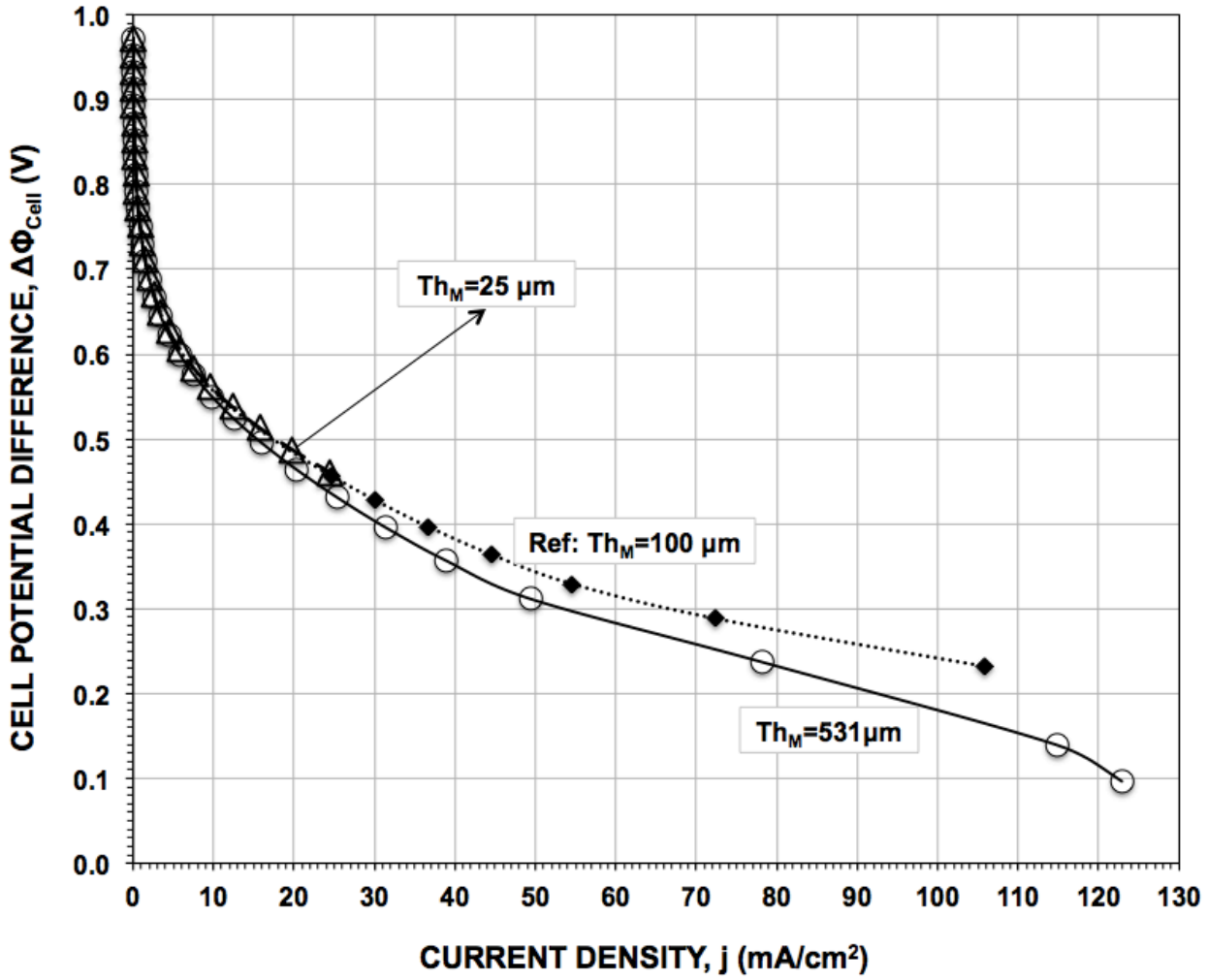


Figure 3.6 The effect of electrolyte (membrane) layer thickness, Th_M (μm) on the polarization curve for a direct propane fuel cell (DPFC) model at 150°C and 1 atm. The value of Th_M (μm) for the above three cases were represented by the following symbols: (i) open triangle: 25 μm, (ii) solid diamond: 100 μm (reference case), and (iii) open circle: 531 μm. All other parameters were same as the reference case mentioned in Table 3.1.

The proton conductivity (σ_{ELY}) of the membrane (electrolyte) layer was also investigated. The term proton conductivity refers to the migration of protons caused by an electrical potential gradient. It is different than proton diffusivity. The effect of the membrane layer proton conductivity (σ_{ELY}) on the fuel cell performance can be seen in Figure 3.7. At a current density of 40 mA/cm^2, when the proton conductivity of the electrolyte (membrane) layer (σ_{ELY}) was

increased from 5 S/m to $1x10^{20}$ S/m, there was no significant change in fuel cell performance. Therefore, the membrane layer proton conductivity was not rate limiting and had almost no effect on the performance of the DPFC.

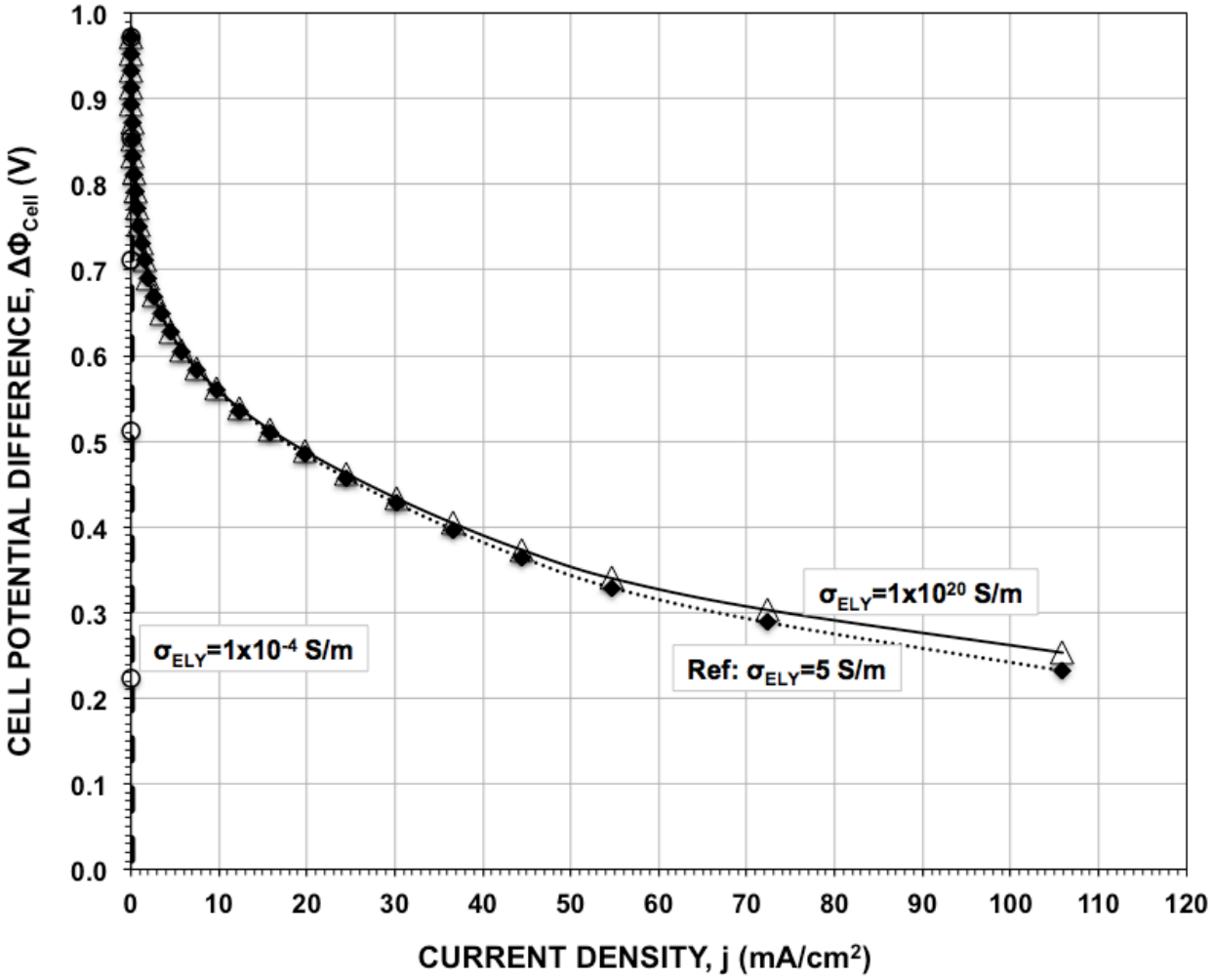


Figure 3.7 The effect of membrane layer proton conductivity, σ_{ELY} (S/m) on the polarization curve for a direct propane fuel cell (DPFC) model at 150°C and 1 atm. The value of σ_{ELY} (S/m) for the above three cases were represented by the following symbols: (i) open triangle: $1x10^{20}$ S/m, (ii) solid diamond: 5 S/m (reference case), and (iii) open circle: $1x10^{-4}$ S/m. All other parameters were same as the reference case mentioned in Table 3.1.

Proton diffusivity in the electrolyte phase was also investigated. The term proton diffusivity refers to the diffusion of protons caused by a concentration gradient. The effect of

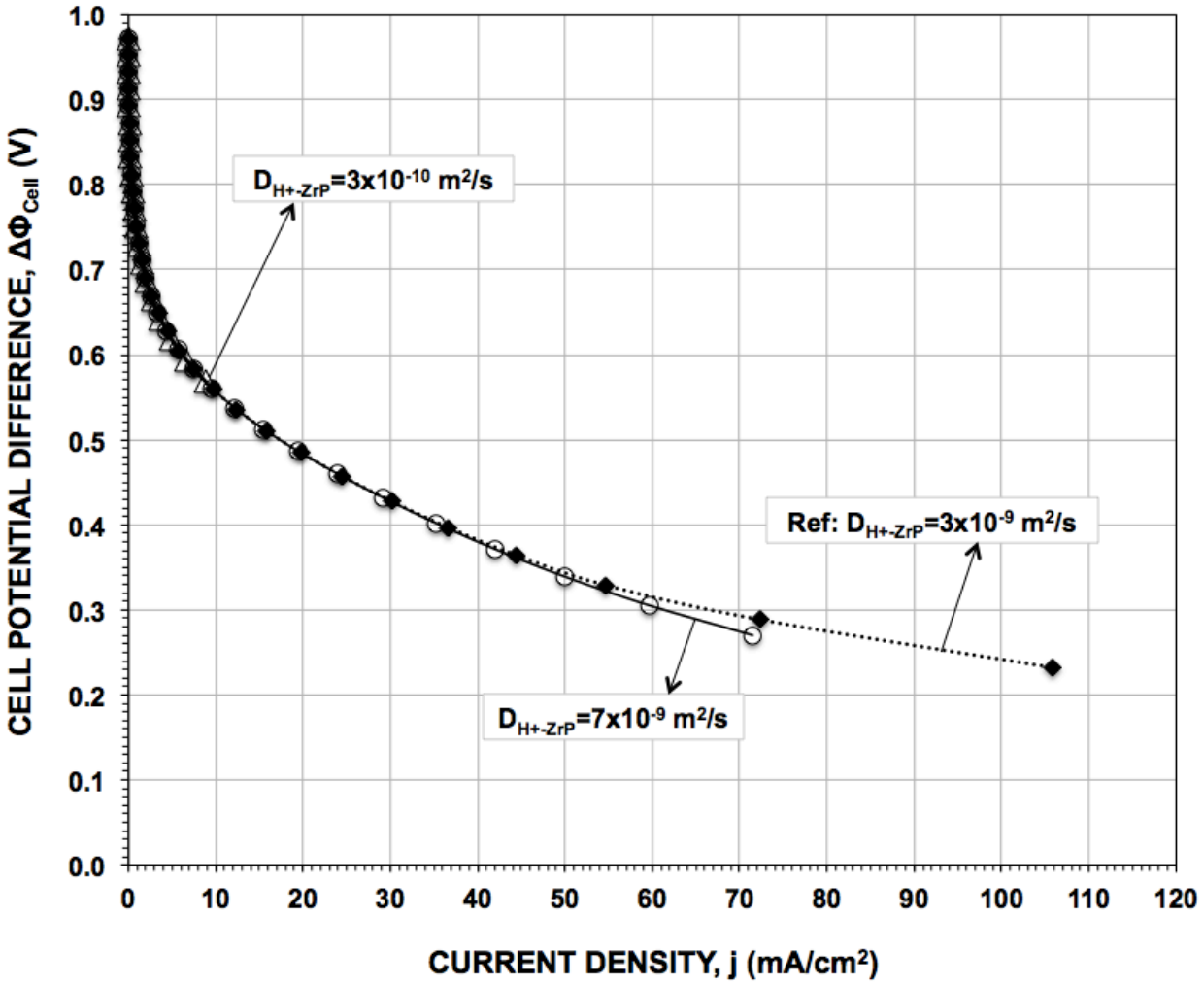


Figure 3.8 The effect of proton diffusivity coefficient in electrolyte phase, D_{H+-ZrP} (m^2/s) on the polarization curve for a direct propane fuel cell (DPFC) model at 150°C and 1 atm. The value of D_{H+-ZrP} (m^2/s) for the above three cases were represented by the following symbols: (i) open triangle: $3x10^{-10}$ m^2/s, (ii) solid diamond: $3x10^{-9}$ m^2/s (reference case), and (iii) open circle: $7x10^{-9}$ m^2/s. All other parameters were same as the reference case mentioned in Table 3.1.

proton diffusivity on the fuel cell performance is shown in Figure 3.8. When the proton diffusion coefficient (D_{H+-ZrP}) increased from $3x10^{-10}$ to $7x10^{-9}$ m^2/s, there was minimal change over the range of variables investigated. From these observations, it was concluded that the proton diffusion coefficient did not affect fuel cell performance when compared to the other parameters.

Water diffusivity in the electrolyte phase was also investigated. Its effect on the fuel cell performance is shown in Figure 3.9. When the water diffusion coefficient ($D_{H2O\text{-}ZrP}$) changed

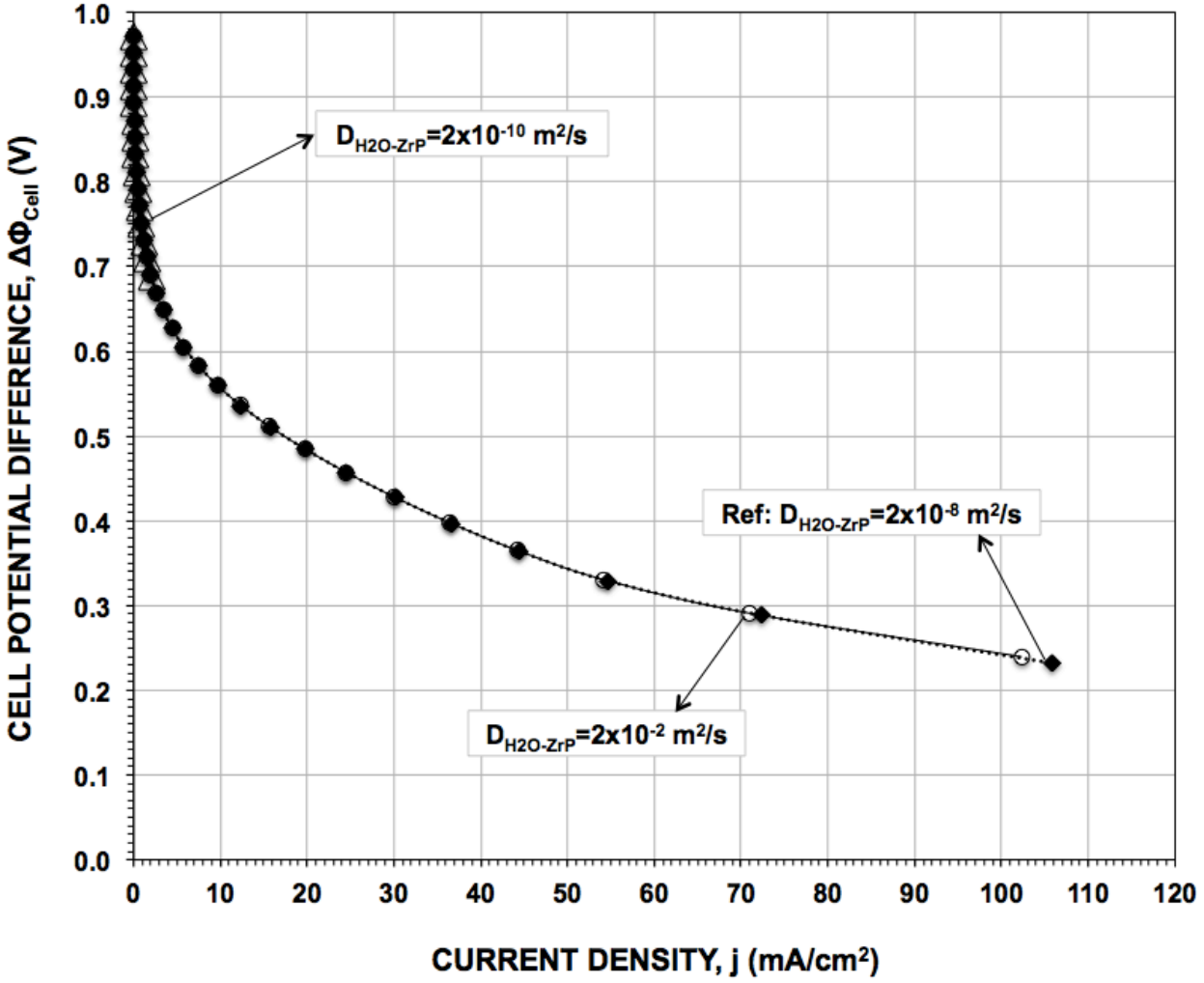


Figure 3.9 The effect of water diffusivity coefficient in electrolyte phase, $D_{H2O\text{-}ZrP}$ (m^2/s) on the polarization curve for a direct propane fuel cell (DPFC) model at 150°C and 1 atm. The value of $D_{H2O\text{-}ZrP}$ (m^2/s) for the above three cases were represented by the following symbols: (i) open triangle: $2x10^{-10}$ m^2/s, (ii) solid diamond: $2x10^{-8}$ m^2/s (reference case), and (iii) open circle: $2x10^{-2}$ m^2/s. All other parameters were same as the reference case mentioned in Table 3.1.

from $2x10^{-10}$ to $2x10^{-2}$ m^2/s, there was no noticeable change at any position in the polarization curve. Therefore, it was evident that changes to the water diffusion coefficient had virtually no effect on the overall performance of the DPFC.

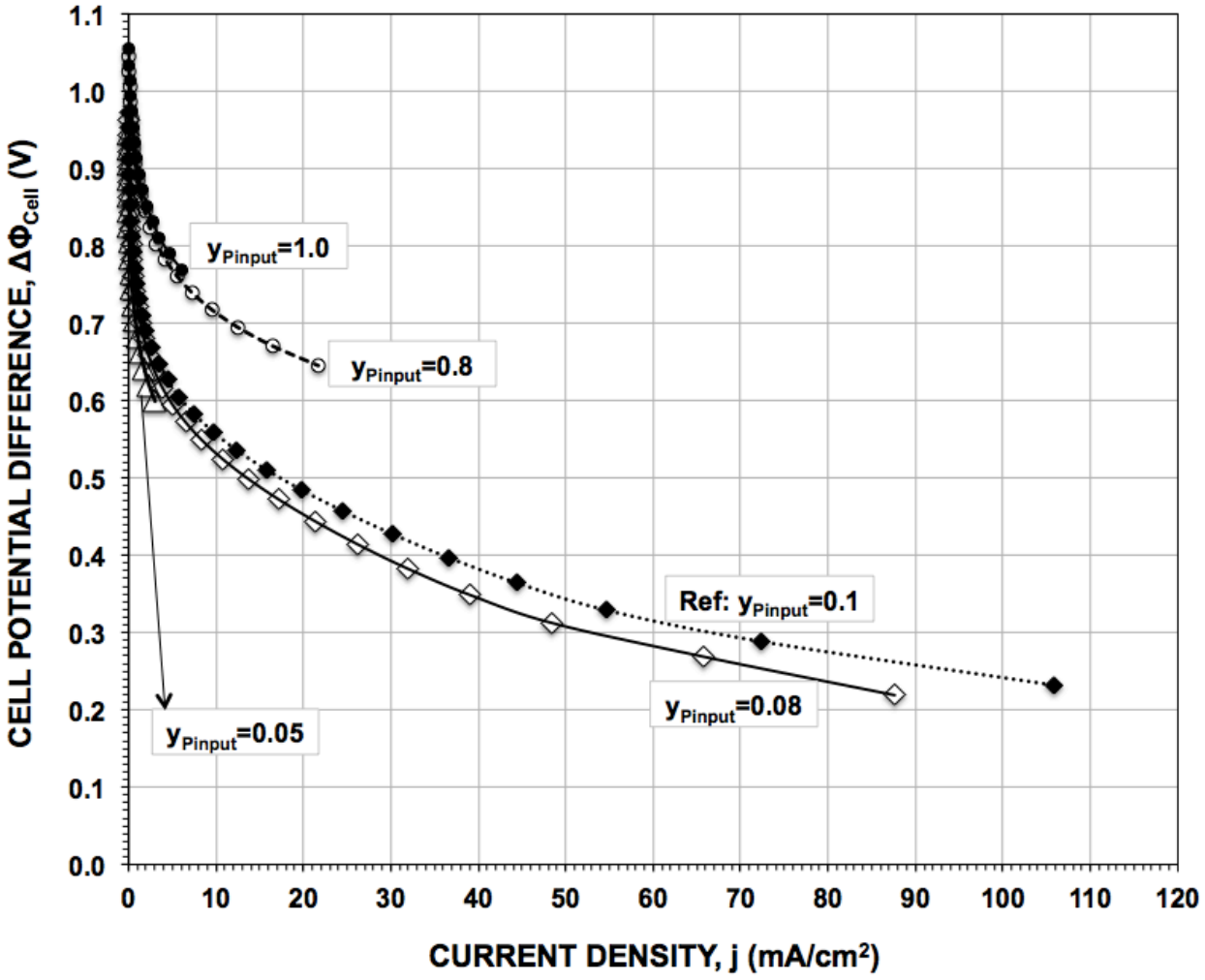


Figure 3.10 The effect of propane inlet mole fraction, y_{Pinput} on the polarization curve for a direct propane fuel cell (DPFC) model at 150°C and 1 atm. The value of y_{Pinput} for the above five cases were represented by the following symbols: (i) solid circle: 1, (ii) open circle: 0.8, (iii) solid diamond: 0.1 (reference case), (iv) open diamond: 0.08, and (v) open triangle: 0.05. All other parameters were same as the reference case mentioned in Table 3.1.

The propane inlet mole fraction in the feed to the fuel cell was also investigated, in order to vary the propane to water ratio. Its influence on the overall performance of the fuel cell is shown in Figure 3.10. At a current density of 20 mA/cm^2, as the propane inlet mole fraction (y_{Pinput}) increased (from 0.08 to 0.8) the potential difference between the fuel cell electrodes also increased (i.e. from 0.45 to 0.65 V).

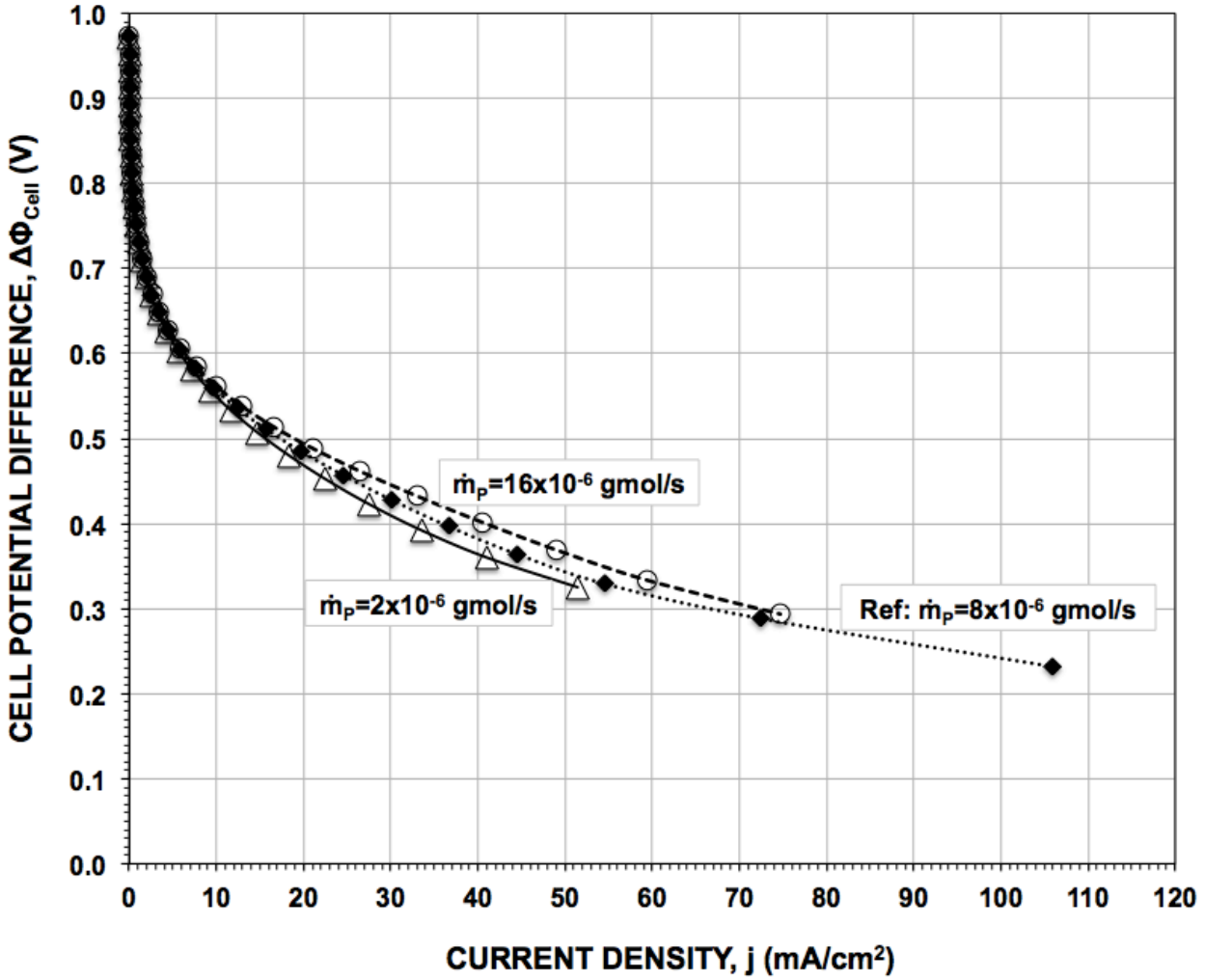


Figure 3.11 The effect of propane inlet molar flow rate, $\dot{m}_P$ (gmol/s) on the polarization curve for a direct propane fuel cell (DPFC) model at 150°C and 1 atm. The value of $\dot{m}_P$ (gmol/s) for the above three cases were represented by the following symbols: (i) open circle: 16×10^{-6} gmol/s, (ii) solid diamond: 8×10^{-6} gmol/s (reference case), and (iii) open triangle: 2×10^{-6} gmol/s. All other parameters were same as the reference case mentioned in Table 3.1.

Increasing the propane inlet mole fraction, y_{Pinput}, would increase the propane partial pressure and so, the propane adsorption rate. And, therefore, it had a large impact on the fuel cell performance.

The propane inlet molar flow rate was also investigated. Its effect on the overall performance of the fuel cell is shown in Figure 3.11. At a current density of 40 mA/cm^2, as the

propane inlet molar flow rate ($\dot{m}_P$) increased from $2x10^{-6}$ to $16x10^{-6}$ gmol/s the potential difference between the fuel cell electrodes also increased from 0.36 to 0.40 V. As discussed above, changing the propane inlet mole fractions has an impact on the propane partial pressure.

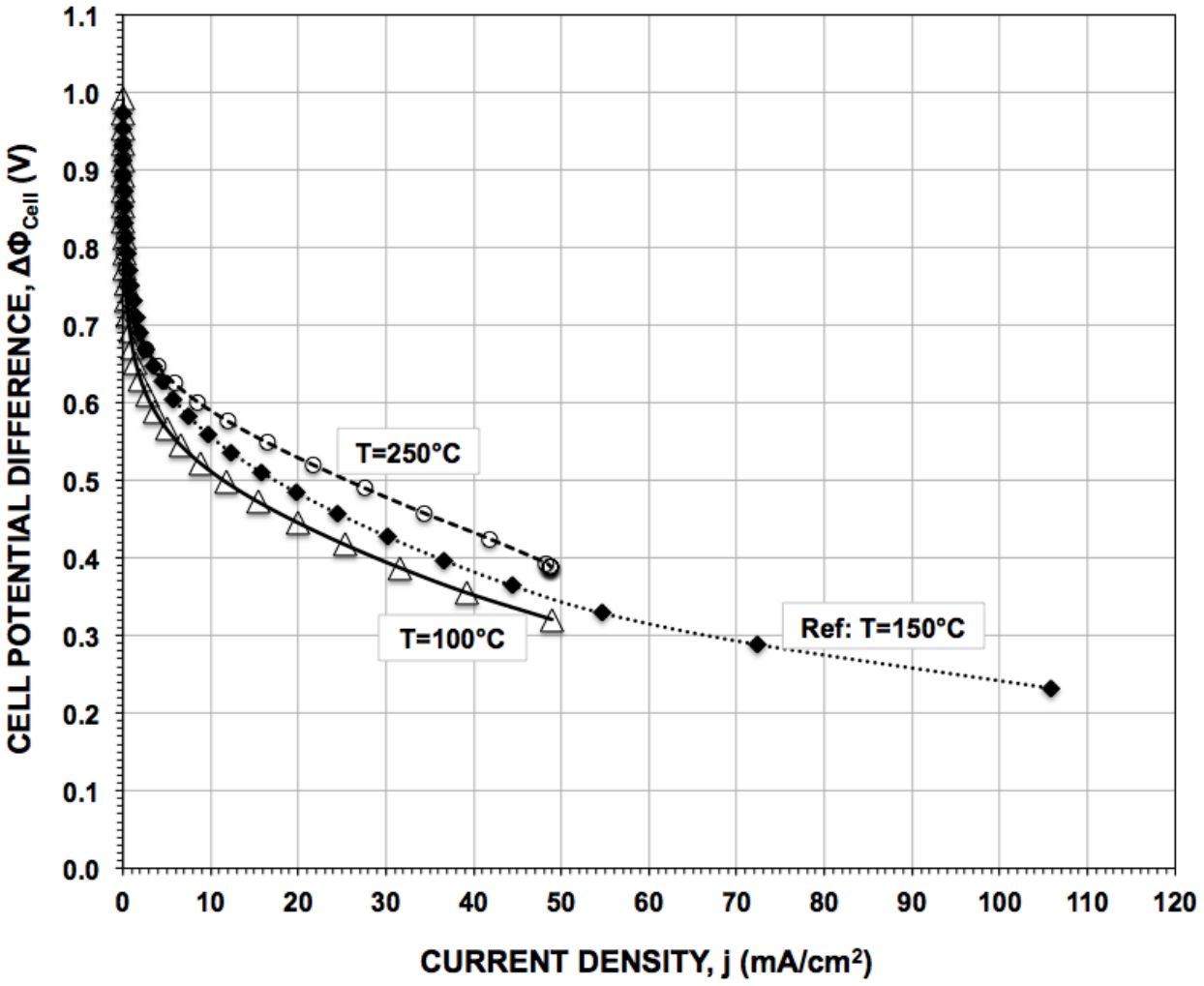


Figure 3.12 The effect of fuel cell operating temperature, T (°C) on the polarization curve for a direct propane fuel cell (DPFC) model at 1 atm. The value of T (°C) for the above three cases were represented by the following symbols: (i) open circle: 250°C, (ii) solid diamond: 150°C (reference case), and (iii) open triangle: 100°C. All other parameters were same as the reference case mentioned in Table 3.1.

However, the propane inlet molar flow rate will have little impact on the propane partial pressure. And so, at an inlet propane mole fraction of 0.1, the inlet propane flow rate only

caused a small change to the performance of the DPFC. Therefore, the utilization of propane feed gas at the anode was not affected since the propane partial pressure remained approximately constant.

The effect of the fuel cell operating temperature on its overall performance is shown in Figure 3.12. At a current density of 40 mA/cm^2, as the fuel cell operating temperature (T) increased from 100 to 250°C, the potential difference between the fuel cell electrodes increased, from 0.35 to 0.43 V. It was evident that temperature caused some improvement in the fuel cell performance.

The final parameter investigated was the anode and cathode operating pressures of the DPFC. Its effect on the overall performance of the fuel cell is shown in Figure 3.13. At a current density of 40 mA/cm^2, as the fuel cell operating pressure (P) increased from 1 to 11 atm the potential difference between the fuel cell electrodes increased from 0.38 to 0.71 V. From these observations, it was clear that the fuel cell operating pressure would increase the propane partial pressure and therefore, would play a major role in enhancing the overall performance of the DPFC.

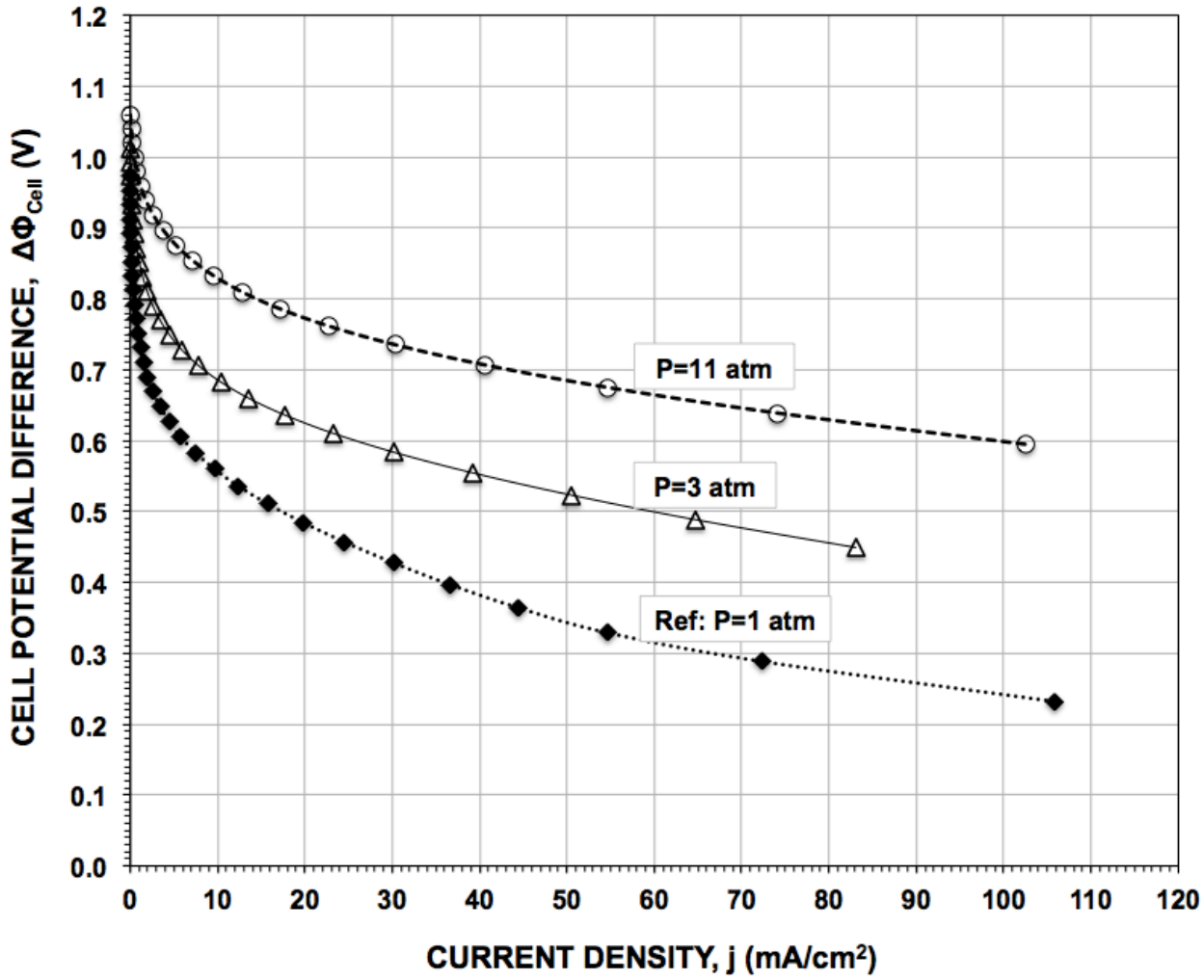


Figure 3.13 The effect of fuel cell operating pressure, P (atm) on the polarization curve for a direct propane fuel cell (DPFC) model at 150°C. The value of P (atm) for the above three cases ($y_{water}/y_{propane}$ = 9) were represented by the following symbols: (i) open circle: 11 atm, (ii) open triangle: 3 atm, and (iii) solid diamond: 1 atm (reference case). All other parameters were same as the reference case mentioned in Table 3.1.

3.4 Conclusions

A parametric study was successfully carried out with a two-dimensional mathematical model of a direct propane fuel cell (DPFC) using computational fluid dynamics (CFD) and FreeFem++ software. Almost every parameter investigated in the model had at least a minor

impact on the fuel cell polarization curve. Nevertheless, the computational results showed that the parameters having the largest effect were those that affected the fuel cell catalyst (the surface reaction rate). The parameters having the greatest effect on fuel cell performance were (i) Anodic exchange current density, (ii) Cathode exchange current density, (iii) Inlet propane mole fraction, (iv) Inlet propane molar flow rate, (v) Fuel cell operating pressure, and (vi) Fuel cell operating temperature. All of the above variables can have an influence on the catalyst performance. The catalyst layer thickness also had some effect on the overall performance of the fuel cell. Variables related to diffusion have little effect on the fuel cell performance. However, the effects of all other variables were minimal. In all of the figures reported in this work, the overall performance over the entirety of the computed polarization curve was influenced primarily by the electrochemical reaction rate (overpotential).

3.5 References

[1] M. L. Perry and T. F. Fuller, "A historical perspective of fuel cell technology in the 20th century," *Journal of The Electrochemical Society*, vol. 149, no. 7, pp. S59-S67, 2002.

[2] H. Khakdaman, Y. Bourgault, and M. Ternan, "A Mathematical model of a direct propane fuel cell," *Journal of Chemistry*, vol. 2015, pp. 1-13, 2015.

[3] G. Hoogers, “Introduction,” in *Fuel Cell Technology Handbook,* CRC Press, Boca Raton, 2003, pp. 2-37.

[4] Johnson Matthey PLC 2016, "Fuel cell technologies," 2016. [Online]. Available: http://www.fuelcelltoday.com/technologies.

[5] E. J. Cairns, "Anodic oxidation and molecular structure: Influence on performance of normal saturated hydrocarbons in fuel cells," *Science*, vol. 155, no. 3767, pp. 1245-1246, 1967.

[6] M. Ternan, “The potential of direct hydrocarbon fuel cells for improving energy efficiency,” *2006 IEEE EIC Climate Change Conference*, vol. 1-2, pp. 504-507, 2006.

[7] H. A. Liebhafsky and E. J. Cairns, “Direct hydrocarbon fuel cell with aqueous electrolytes,” in *Fuel Cells and Fuel Batteries*, Wiley, New York, 1968, pp. 458-523.

[8] J. O. Bockris and S. Srinivasan, “Fuel cells: Their electrochemistry,” in *Electrochemical Combustion of Organic Substances*, McGraw-Hill, New York, 1969, pp. 357-411.

[9] J. O. Bockris, E. Gileadi, and G. E. Stoner, "Anodic oxidation of saturated hydrocarbons. Mechanistic study," *The Journal of Physical Chemistry*, vol. 73, no. 2, pp. 427-434, 1969.

[10] H. G. Oswin, A. J. Hartner, and F. Malaspina, "A direct hydrocarbon/air fuel cell," *Nature*, vol. 200, no. 4903, pp. 256-257, 1963.

[11] W. T. Grubb and C. J. Michalske, "A high performance propane fuel cell operating in the temperature range of 150°C-200°C," *Journal of The Electrochemical Society*, vol. 111, no. 9, pp. 1015-1019, 1964.

[12] C. K. Cheng, J. L. Luo, K. T. Chuang, and A. R. Sanger, "Propane fuel cells using phosphoric-acid-doped polybenzimidazole membranes," *The Journal of Physical Chemistry B*, vol. 109, no. 26, pp. 13036-13042, 2005.

[13] H. Khakdaman, "A two dimensional model of a direct propane fuel cell with an interdigitated flow field", Ph.D., University of Ottawa, 2012.

[14] T. E. Springer, T. A. Zawodzinski, and S. Gottesfeld, "Polymer electrolyte fuel cell model," *Journal of the Electrochemical Society*, vol. 138, no. 8, pp. 2334-2342, 1991.

[15] M. W. Verbrugge and R. F. Hill, "Experimental and theoretical investigation of perfluorosulfonic acid membranes equilibrated with aqueous sulfuric acid solutions," *The Journal of Physical Chemistry*, vol. 92, no. 23, pp. 6778-6783, 1988.

[16] L. J. Fales and N. E. Vandeborough, "The influence of ionomer channel geometry on ionomer transport", *Electrochemical Society Proceedings*, vol. 86, no. 13, pp. 179-191, 1986.

[17] D. M. Bernardi and M. W. Verbrugge, "A mathematical model of the solid-polymer-electrolyte fuel cell," *Journal of the Electrochemical Society*, vol. 139, no. 9, pp. 2477-2491, 1992.

[18] J. C. Amphlett, R. M. Baumert, R. F. Mann, B. A. Peppley, and P. R. Roberge, "Performance modeling of the Ballard Mark IV solid polymer electrolyte fuel cell I. Mechanistic model development," *Journal of the Electrochemical Society*, vol. 142, no. 1, pp. 1-8, 1995.

[19] J. Kim, S. Lee, and S. Srinivasan, "Modeling of proton exchange membrane fuel cell performance with an empirical equation," *Journal of the Electrochemical Society*, vol. 142, no. 8, pp. 2670-2674, 1995.

[20] R. Mosdale and S. Srinivasan, "Analysis of performance and of water and thermal management in proton exchange membrane fuel cells," *Electrochimica Acta*, vol. 40, no. 4, pp. 413-421, 1995.

[21] S. Um, C. Y. Wang, and K. S. Chen, "Computational fluid dynamics modeling of proton exchange membrane fuel cells," *Journal of The Electrochemical Society*, vol. 147, no. 12, pp. 4485-4493, 2000.

[22] E. Carcadea, H. Ene, D. B. Ingham, R. Lazar, L. Ma, M. Pourkashanian, and I. Stefanescu, "Numerical simulation of mass and charge transfer for a PEM fuel cell," *International Communications in Heat and Mass Transfer*, vol. 32, no. 10, pp. 1273-1280, 2005.

[23] S. Um and C. Y. Wang, "Three-dimensional analysis of transport and electrochemical reactions in polymer electrolyte fuel cells," *Journal of Power Sources*, vol. 125, no. 1, pp. 40-51, 2004.

[24] J. J. Baschuk and X. Li, "A comprehensive, consistent and systematic mathematical model of PEM fuel cells," *Applied Energy*, vol. 86, no. 2, pp. 181-193, 2009.

[25] J. J. Baschuk and X. Li, "Modeling of ion and water transport in the polymer electrolyte membrane of PEM fuel cells," *International Journal of Hydrogen Energy*, vol. 35, no. 10, pp. 5095-5103, 2010.

[26] G. Psofogiannakis, Y. Bourgault, B. E. Conway, and M. Ternan, "Mathematical model for a direct propane phosphoric acid fuel cell," *Journal of Applied Electrochemistry*, vol. 36, no. 1, pp. 115-130, 2006.

[27] H. Khakdaman, Y. Bourgault, and M. Ternan, "Direct propane fuel cell anode with interdigitated flow fields: Two-dimensional model," *Industrial & Engineering Chemistry Research*, vol. 49, no. 3, pp. 1079-1085, 2010.

[28] H. Khakdaman, Y. Bourgault, and M. Ternan, "Computational modeling of a direct propane fuel cell," *Journal of Power Sources*, vol. 196, no. 6, pp. 3186-3194, 2011.

[29] F. Hecht, O. Pironneau, A. LeHyaric, and K. Ohtsuka, "FreeFEM++ Version 3.32," 2014. [Online]. Available: http://www.freefem.org/ff++/index.htm.

Chapter 4: Experimental work on low temperature direct propane fuel cell (DPFC) with a commercial Nafion membrane

Abstract

This chapter covers the experimental work performed using a low temperature direct propane fuel cell (DPFC) using commercial Nafion-Pt based membrane electrode assemblies (MEAs). The experiments were performed for two reasons: (i) to obtain a basis for comparison with the model predictions discussed in the previous chapter, and (b) to describe additional variables identified during the experimental work that were not included in the previous modeling (Chapter 3). The performance of the DPFC was analyzed at different operating conditions. It is the first report in the literature for a Pt-Ru (platinum-ruthenium) MEA being used in a DPFC. It was found that increasing the temperature, increased the desirable reaction rate but also the rate of deactivation. Unlike the modeling computation, the experimental work showed no change in the performance of the fuel cell when propane inlet mole fraction was changed from 0.34 to 1. This may have been caused by the experimental values of j (electrochemical reaction rate) being so much slower than the computational values of j, so that the experimental values of j were not influenced by the rate of propane adsorption. Also, it was the first study that fed liquid water continuously to a DPFC by using interdigitated flow field (IDFF) at the DPFC anode. The water reacted with propane feed gas and was used for electro-osmotic drag through the electrolyte. During the experiments oscillations were observed at very low current densities i.e. in nA/cm^2. Such low current densities have not been reported in the literature to date. This observation has raised serious concerns about the existence of absolute open-circuit cell potential difference for a DPFC. The cycling behaviour observed with DPFC indicated the presence of a continuous degradation-regeneration process on the catalyst surface near open-circuit potential. The experimental work evaluated the fuel cell performance

by measuring polarization curves. The phenomenon of potential oscillations at minuscule current density range was investigated. The role of liquid water was identified, specifically its presence in the anode gas diffusion layer, and how that may have affected the oscillating nature of the DPFC performance. Finally, the performance of the DPFC was analyzed by using two different anode humidification methods i.e. liquid water and a bubble humidifier.

4.1 Introduction

In the previous computational work (Chapter 3), a parametric study was conducted that identified some key parameters that had an impact on the overall performance of the DPFC such as fuel cell operating pressure and temperature, and electrode exchange current density. However, a few other parameters were identified that had little impact on the fuel cell performance such as membrane and catalyst layer thickness, and electrolyte proton conductivity. The objective of the experimental work was to investigate some of the significant parameters that were identified in the modeling study. The parameters investigated were anodic exchange current density, fuel cell operating temperature, and propane inlet mole fraction. During the course of the work, some additional important parameters were identified that were not included in the model and those were: (a) deactivation, (b) humidification, and (c) oscillation.

A fuel cell is an energy-conversion device that electrochemically converts the chemical energy of a fuel directly into electrical energy. It is driven by the electrochemical reaction occurring between a fuel (such as hydrogen or methanol) and an oxidant (such as oxygen or air) [1]. The application of fuel cells is broadly divided into the following three important categories: (a) stationary, (b) portable, and (c) transportation [2,3]. Within a fuel cell, a redox reaction takes place that generates electrical power. The polymer electrolyte membrane fuel cell used in these studies consisted of two flow fields and a membrane electrode assembly (MEA). The MEA is divided into the following five layers: the anode gas diffusion layer, the anode

catalyst layer, the electrolyte (membrane) layer, the cathode catalyst layer, and the cathode gas diffusion layer [4].

Polymer electrolyte membrane fuel cell (PEMFC) technology has advanced enormously over the past three decades. It is capable of generating about 1000 mA/cm^2 at 0.7 V [5]. The working principle of a direct hydrocarbon fuel cell (DHFC) having a polymer electrolyte is the same as that of hydrogen proton exchange membrane fuel cells (PEMFCs) except for the fuel being fed at the anode. The motivation for these studies was the complete conversion of the hydrocarbon fuels to carbon dioxide and water accompanied by no other emissions. The advantages of feeding a hydrocarbon fuel such as propane directly to the fuel cell were the elimination of the fuel processing cost to convert propane to hydrogen, the existing infrastructure for propane in the form of liquefied petroleum gasoline (LPG), the ease of delivering propane especially in the rural areas, its high storage density in the liquid phase, and its comparative inexpensive cost [6]. Research on direct propane fuel cells (DPFC) has been published by: Oswin et al. 1963 [7], Grubb, 1963 [8], Grubb and Michalske, 1964 [9], Savadogo and Varela, 2001 [10], Cheng et al. 2005 [11], and Varela and Savadogo, 2006 [12].

The importance of feed gas humidification in increasing the performance and operation time of a PEMFC has been demonstrated. In 1997, Büchi and Srinivasan [13] investigated a PEMFC without external humidification of the feed gases. At a temperature of 60°C without an external humidification system the performance of the fuel cell decreased by 20 to 40%. However, the fuel cell operated for 1800 h with an internal humidification mechanism that involved the electrochemical reaction. The performance of a PEMFC using an internal membrane humidifier was compared with a conventional external humidification system by Ramya et al. 2011 [14]. Sanchez et al. 2016 [15] investigated the effect of feed gas relative humidity and fuel cell operating temperature on the performance of a PEMFC. Wood et al. 1998 [16] observed improved fuel cell performance when liquid water was fed through an inter-

digitated flow field (IDFF) at the anode rather than at cathode. They also observed that water management and mass transport phenomena were superior with an IDFF compared to a conventional parallel serpentine flow field.

Many researchers reported potential oscillations in hydrogen fuel cells. Niedrach and Tochner, 1967 [17] observed a connection between the accumulation of intermediate species and fuel cell oscillations. In 1969, Deibert and Williams [18] reported natural oscillations in cell potential when H_2-CO mixtures were fed to the anode at 95°C, under a galvanostatic mode of operation. These oscillations were attributed to continuous CO poisoning [19,20] and regeneration of the Pt-catalyst surface [21]. In 2000, Fukumoto et al. [22] observed potential oscillations in a PEMFC stack with a Pt-Ru/C anode electrode at a temperature below 60°C. They suggested that CO poisoning of the catalyst surface was the cause. In 2009, Lu et al. [23] observed spontaneous potential oscillations under a galvanostatic mode of fuel cell operation when CO (at very low concentration in ppm) contaminated the anode (Pt-Ru). Furthermore, they observed oscillations at all current densities. For example, they obtained steady potential oscillations at 0.6 V at a constant current density of 50 mA/cm^2 when the anode electrode was contaminated by a 200 ppm CO concentration. In 2011, Lu et al. [24] observed a higher average output power density for a Pt-Ru anode electrode H_2-CO PEMFC system that operated in the galvanostatic mode rather than the potentiostatic mode. This was observed within a current density range of 25 to 200 mA/cm^2. Lee et al. reported electrochemical oscillations in a direct methanol fuel cell with Pt-based electrodes in 2002 [25]. In 2004, Zhang et al. [26] performed a detailed mathematical analysis to understand the mechanism of potential oscillations at the anode fed with H_2-CO fuel in a Pt-based electrode PEMFC. In 2011, Lopes et al. [27] reported the occurrence of spontaneous potential oscillations over a wide range of parameters in a PEMFC having a Pd-Pt/C anode electrode. They fed H_2 fuel containing 100 ppm of CO to the anode and operated the PEMFC at 30°C under constant current. Steady oscillatory behavior

was demonstrated at a current density of 100 mA/cm^2. The results obtained were quite different from a PEMFC system with Pt-Ru/C anode electrode under similar operating conditions. They observed a very high amplitude of oscillations i.e. 0.8 V, which was nearly twice the amplitude of oscillations reported previously for similar operating systems. Their study showed that the oscillatory behavior was mainly due to the presence of CO adsorption and desorption mechanism that occurred at the PEMFC anode. In 2011, Kadyk et al. [28] investigated the occurrence of autonomous potential oscillations in a PEMFC with both Pt/C and Pt-Ru/C anode electrodes at fuel cell operating temperatures of 40, 60, and 80°C. They observed the influence of the fuel cell temperature and CO concentration on the existence of potential oscillations. They also found that oscillations occurred at very high anode overpotentials. They confirmed the influence of water dissociation on the cyclic behavior of CO oxidation. They observed higher values of the kinetic rate constants for water dissociation and CO oxidation with a Pt-Ru anode [29,30] catalyst model than with a Pt anode catalyst model. Performance degradation of a direct hydrocarbon fuel cell due to poisoning of the catalyst surface was also observed by Zhu et al. 2015 [31]. They investigated the performance of a direct phosphoric acid fuel cell (DPAFC) having Pt electrode catalysts at 190°C using petroleum diesel. They observed initial performance degradation followed by a steady state operation of the DPAFC for 15 h at a cell potential difference of 0.38 V. In their work, extensive coking was reported, which made a major contribution to the poor performance of the DPAFC.

In 2013, Polverino et al. [32] investigated the relationship between water droplet interaction with gas flow and the oscillations in a PEMFC by using a numerical model. They developed a single droplet lumped model that considered the drag force, surface tension force and adhesive force on the single water droplet. They observed that the water entered through the gas diffusion layer (GDL) and formed a droplet that interacted with the gas flow channels. The gas/air-water interaction led to oscillation phenomenon within the PEMFC. They also

observed that the frequency of these oscillations during the growth and detachment from the GDL were a function of water droplet size. Zhai et al. 2013 [33] observed potential oscillations when the reaction sites of the PEMFC were exposed to naphthalene under an operating condition of higher contaminant concentration and lower temperature. At higher current densities, the PEMFC performance losses were higher, the anode degradation was faster and the performance recovery was faster for the impurities (i.e. naphthalene and propene). Nogueira et al. 2016 [34] confirmed that the existence of potential oscillations in a direct methanol fuel cell depended on the mass transport conditions. In general, they observed oscillations when the potential difference between the electrodes was less than 100 mV. They observed no particular waveform pattern for the potential oscillations. However, over a selected region of the series, the spontaneous oscillations had amplitude of 0.08 to 0.15 V.

4.2 Experimental

The experimental work discussed here, of a single direct propane fuel cell (DPFC), was broadly divided into two cases (i.e. case i and ii). In both cases a pin-type flow field was used at the cathode without humidification. The humidification method employed at the anode was the basis for the classification of case i or case ii. Case i was a DPFC with an interdigitated serpentine-type flow field (IDFF) with one of the anode channels filled with liquid water and the other anode channel filled with dry propane gas. Case ii was a DPFC with a pin-type anode flow field and a bubble humidifier before the anode. In each case, the anode of the DPFC was fed continuously with either propane gas or hydrogen gas at the anode and compressed air (medical grade) at the cathode. Nitrogen gas was mixed with propane gas when the propane mole fraction in the anode feed gas was varied (Figure 4.1 A). Rotameters measured the flow rates of gases used for the DPFC. They were calibrated with a bubble flow meter. The exit lines from the fuel cell anode, and the cathode were bubbled through their respective water-filled open jars, placed inside the fume hood. In general, every propane-air operation was followed by

hydrogen-air operation to regenerate the catalyst reaction sites. In this work, the criterion for catalyst regeneration was the reproduction of the hydrogen open-circuit potential. The experimental equipment used for the hydrogen-air operation for both case i, and case ii is shown in Figures 4.1B and 4.1E respectively. In Figures 4.1B and 4.1E, the hydrogen-air operation used a power-supply unit (Kikusui PBX 20-10 Bipolar Power Supply) in the galvanostatic mode.

Figure 4.1A is the experimental equipment of a DPFC at 1 atm with IDFF anode and liquid water for anode humidification. Liquid water was fed to the anode through a 15-inch tubing Masterflex peristaltic pump that consisted of a 75 ml vessel for feeding and recirculating water. Two different Nafion Pt-based MEAs were used with an effective area of 25 cm^2. Experiments were conducted using a Nafion 212 MEA, which had a Pt (platinum) catalyst loading of 1 mg/cm^2 at both the electrodes. While the other set of experiments were performed using a Nafion 117 MEA that had a catalyst loading of 4 mg/cm^2 for both Pt-Ru (platinum-ruthenium) catalyst at the anode and Pt catalyst at the cathode. The experimental equipment shown in Figure 4.1A was used to perform experiments with different anode propane inlet mole fractions (i.e. 0.34 to 1), different fuel cell operating temperatures (i.e. 23 and 65°C), and different anode catalysts (i.e. Pt and Pt-Ru).

The deactivation process of the DPFC was sufficiently fast that a polarization curve could not be generated at currents greater than 10^4 μA. The power-supply unit could not provide sufficiently small currents. Therefore, in order to obtain an appropriate μA current range the propane-air operation was conducted by putting a fixed resistor and an ammeter in the fuel cell circuit instead of a power-supply unit. The electrical circuit of the DPFC with a fixed resistor is shown in Figures 4.1A and 4.1D.

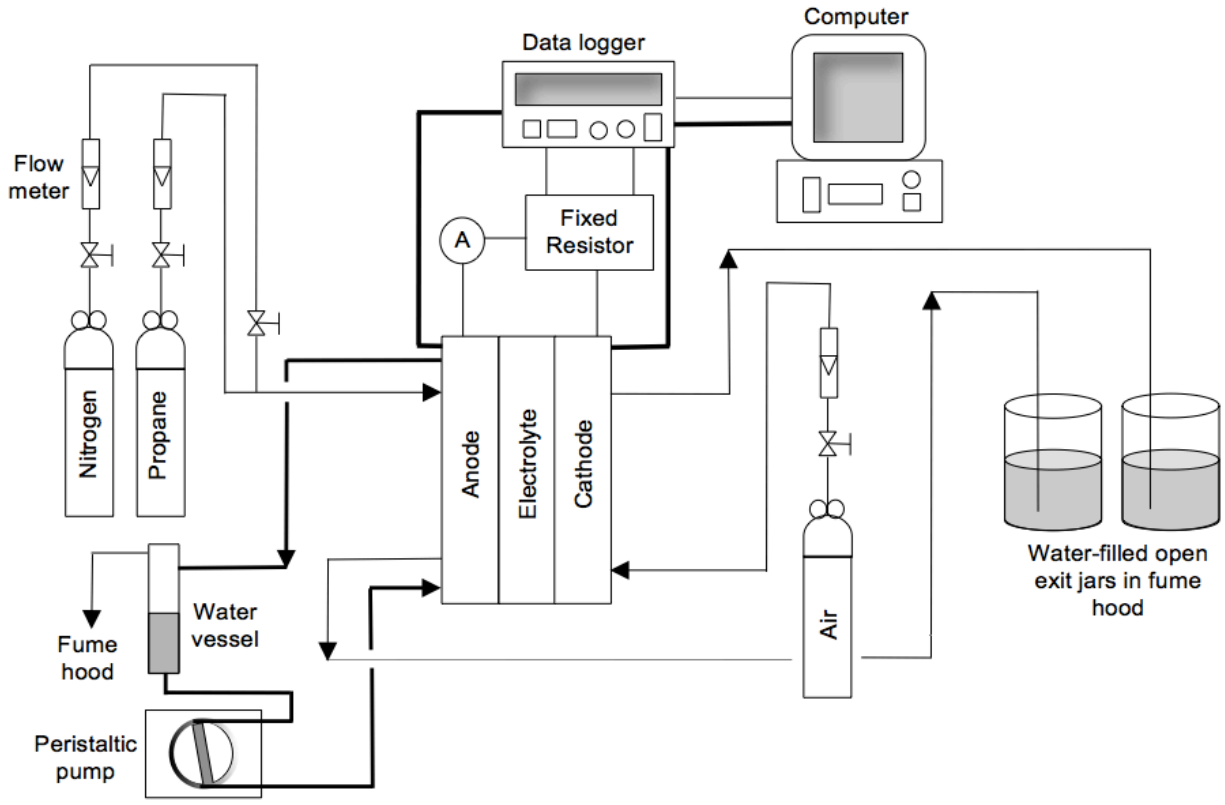


Figure 4.1A Experimental equipment used for a propane/nitrogen-air operation with an IDFF anode humidified with liquid water at 1 atm. Fixed resistors of 1 MΩ, 10 kΩ, 980 Ω, 330 Ω, and 118 Ω were used.

The time-on-stream measurement of cell potential was obtained by measuring the potential difference between the DPFC electrodes. The time-on-stream measurement of current density was achieved by measuring the potential difference across the fixed resistor. In Figures 4.1A and 4.1D, the time-on-stream measurements of potential difference and current were recorded using a Fluke hydra data logger.

The performance of the DPFC was analyzed by measuring the cell potential difference and the current density as a function of time-on-stream. The following five resistors were used: 1 MΩ, 10 kΩ, 980 Ω, 330 Ω, and 118 Ω. The current ranges provided by the resistors were as follows: (a) 1 MΩ: 0 to 1 μA, (b) 10 kΩ: 1 to 100 μA, (c) 980 Ω: 100 to 1000 μA, (d) 330 Ω: 1000

to 2000 μA, and (e) 118 Ω: 2000 to 4000 μA. In each case the current varied with the extent of deactivation.

The experimental equipment used for propane-air operations at near open-circuit potential (OCP) in case i, and case ii is shown in Figures 4.1C and 4.1F respectively. In Figures 4.1C and 4.1F, the fuel cell circuit was maintained at open-circuit potential (OCP) by disconnecting the electrical connections that had been used to measure current. The electrical connections used to measure potential difference across the fuel cell remained in place. In some cases, this measured value of OCP varied with the extent of deactivation caused by the propane-air thermo-chemical reaction.

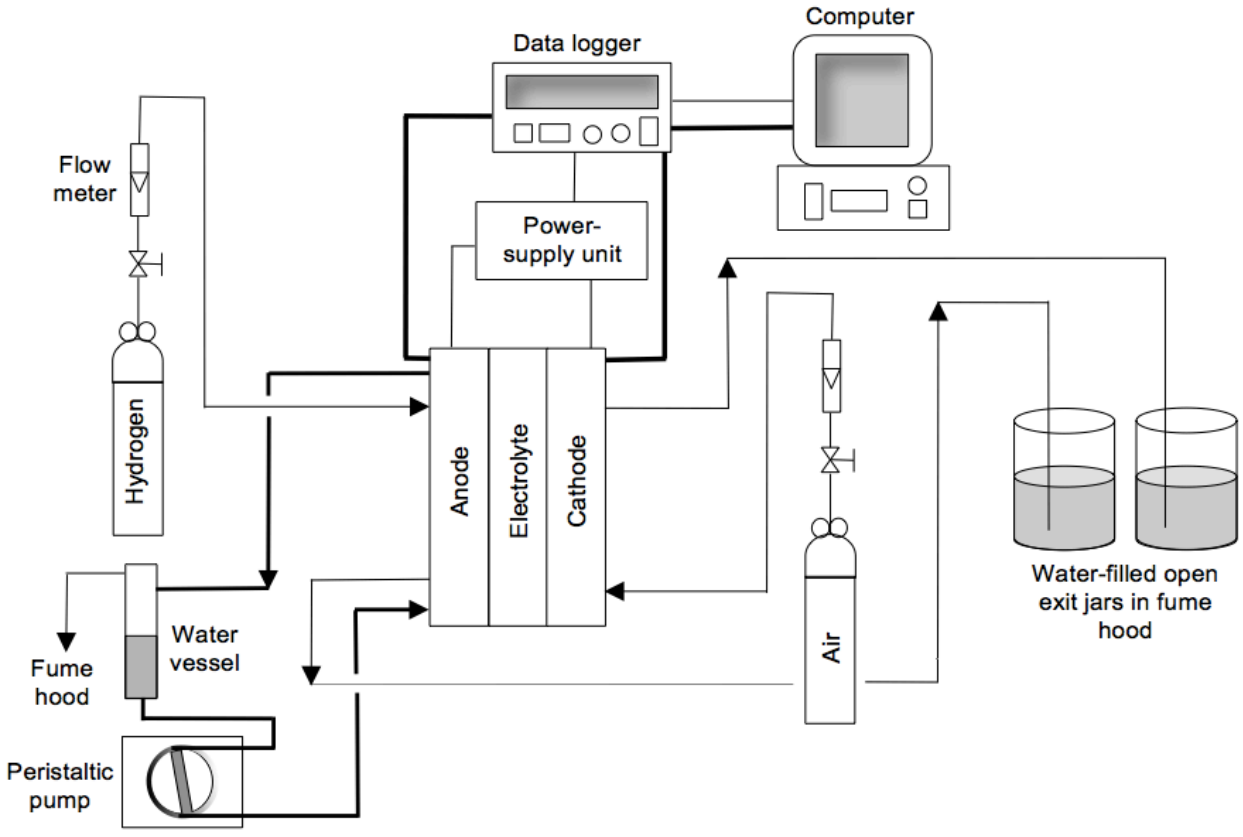


Figure 4.1B Experimental equipment used for a hydrogen-air operation with an IDFF anode humidified with liquid water at 1 atm, using a power-supply unit (galvanostatic mode).

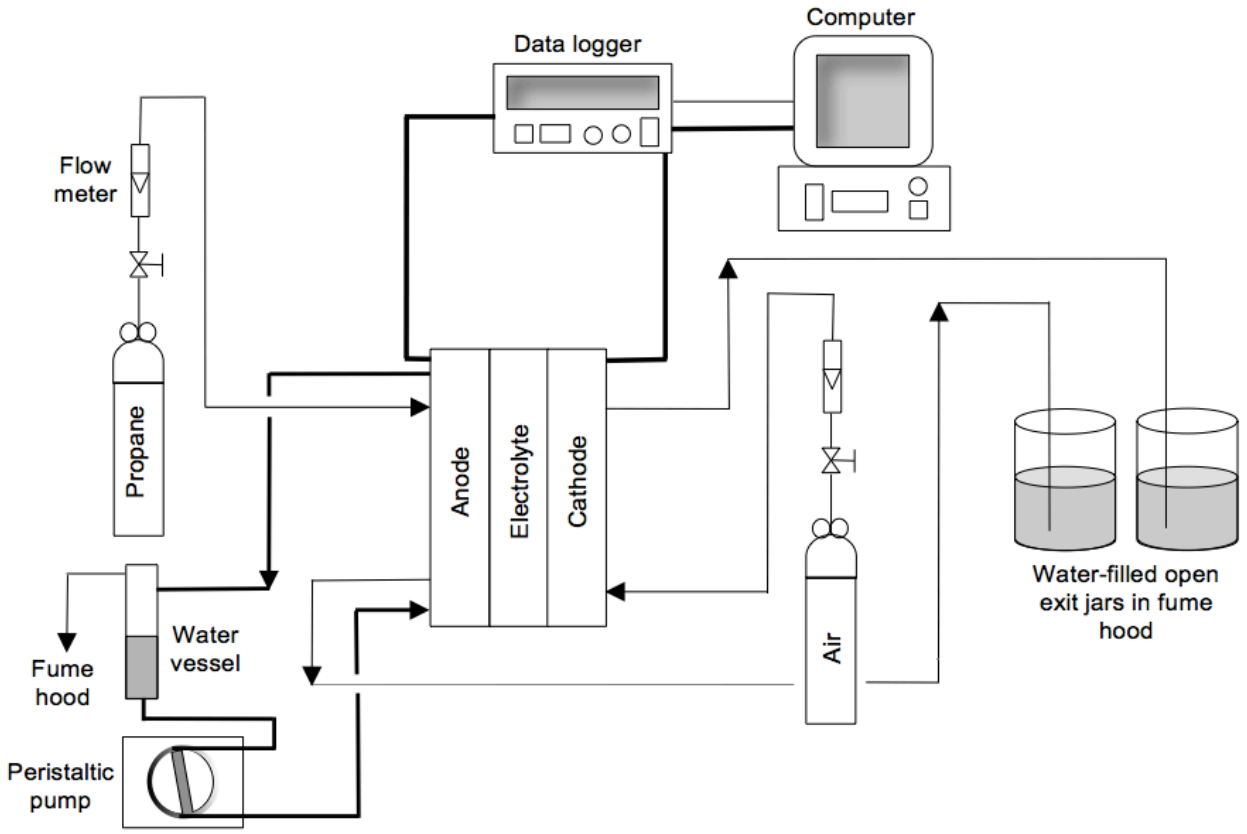


Figure 4.1C Experimental equipment for a propane-air operation with an IDFF anode humidified with liquid water at 1 atm and no electrical connections to measure current (i.e. no power-supply unit in galvanostatic mode).

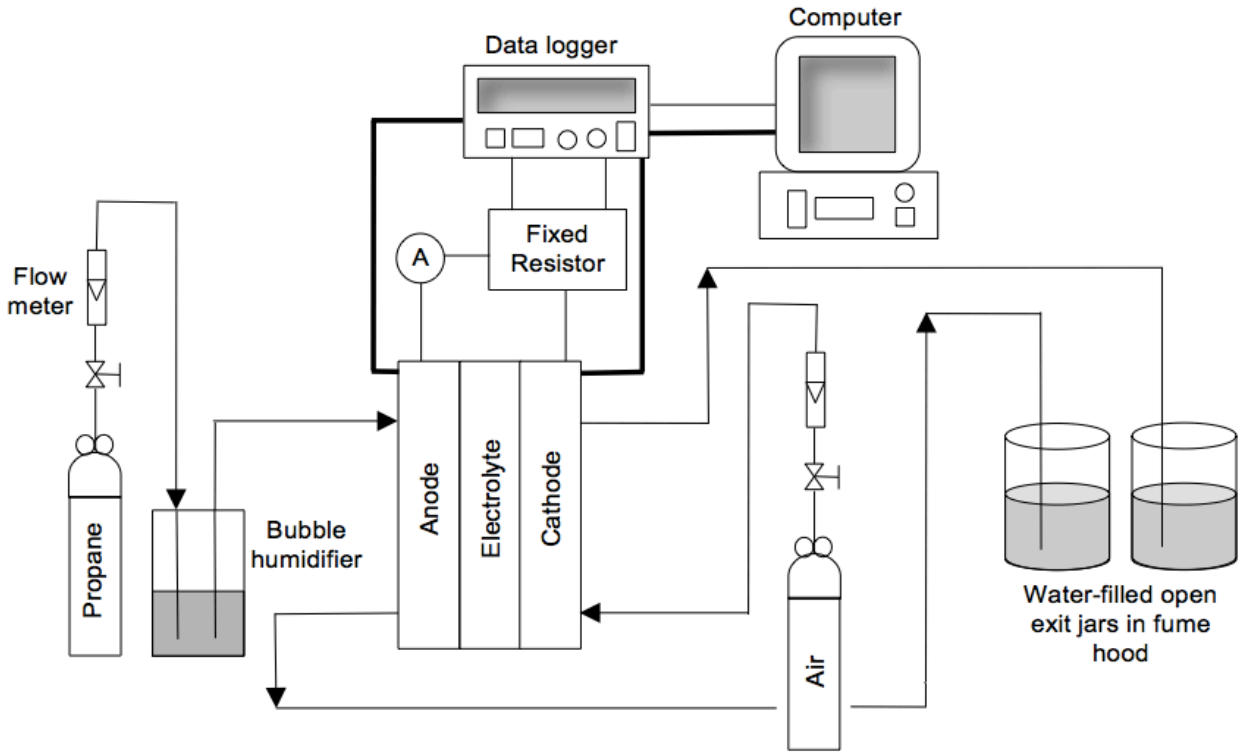


Figure 4.1D Experimental equipment used for a propane-air operation with a pin-type anode flow field and a bubble humidifier at 1 atm. The following fixed resistors were used: 1 MΩ, 10 kΩ, 980 Ω, 330 Ω, and 118 Ω.

Figure 4.1D shows the DPFC experimental equipment used at 65°C and 1 atm, with 100% propane at the anode inlet, a Pt-Ru anode catalyst, and a pin-type anode with a bubble humidifier for anode humidification. A steady and continuous operation of the fuel cell at 65°C was achieved by maintaining the bubble humidifier (capacity, 1100 ml) at 85°C and the fuel cell inlet line from the humidifier to the fuel cell at 115°C.

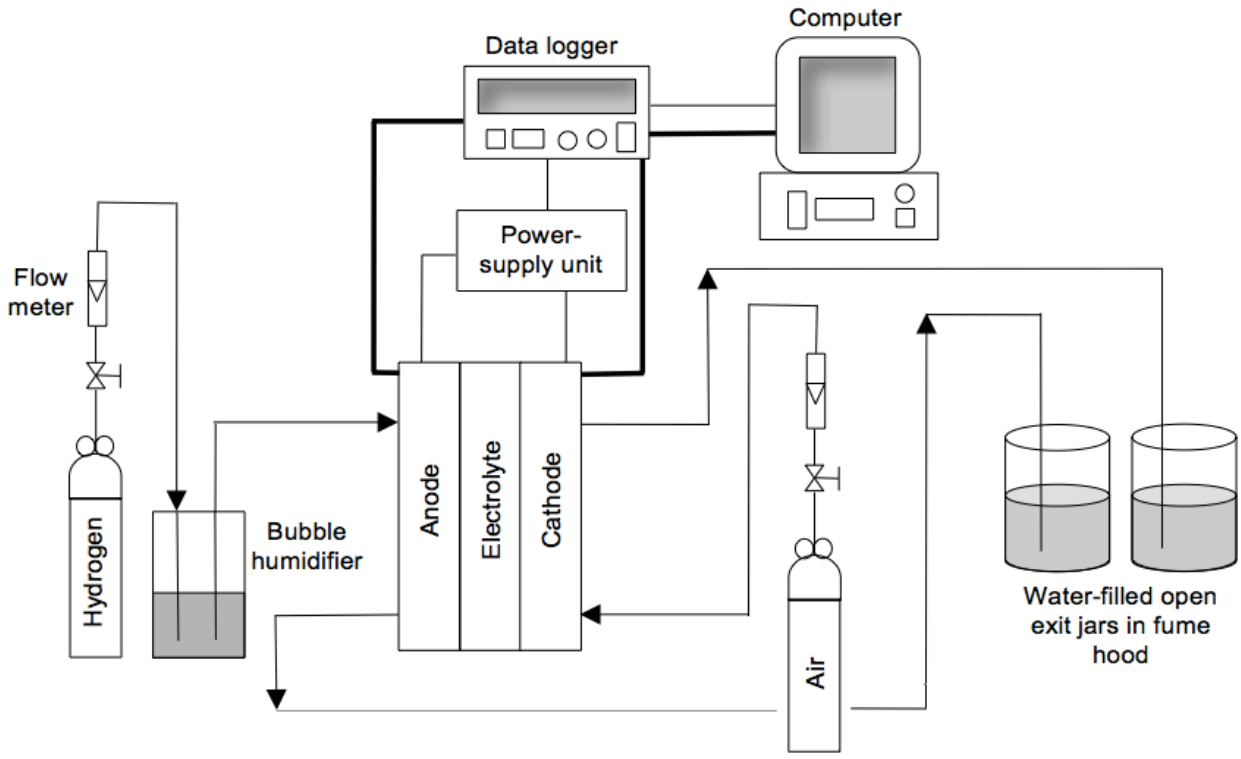


Figure 4.1E Experimental equipment used for a hydrogen-air operation with a pin-type anode flow field and a bubble humidifier at 1 atm. A power-supply unit (in galvanostatic mode) was used.

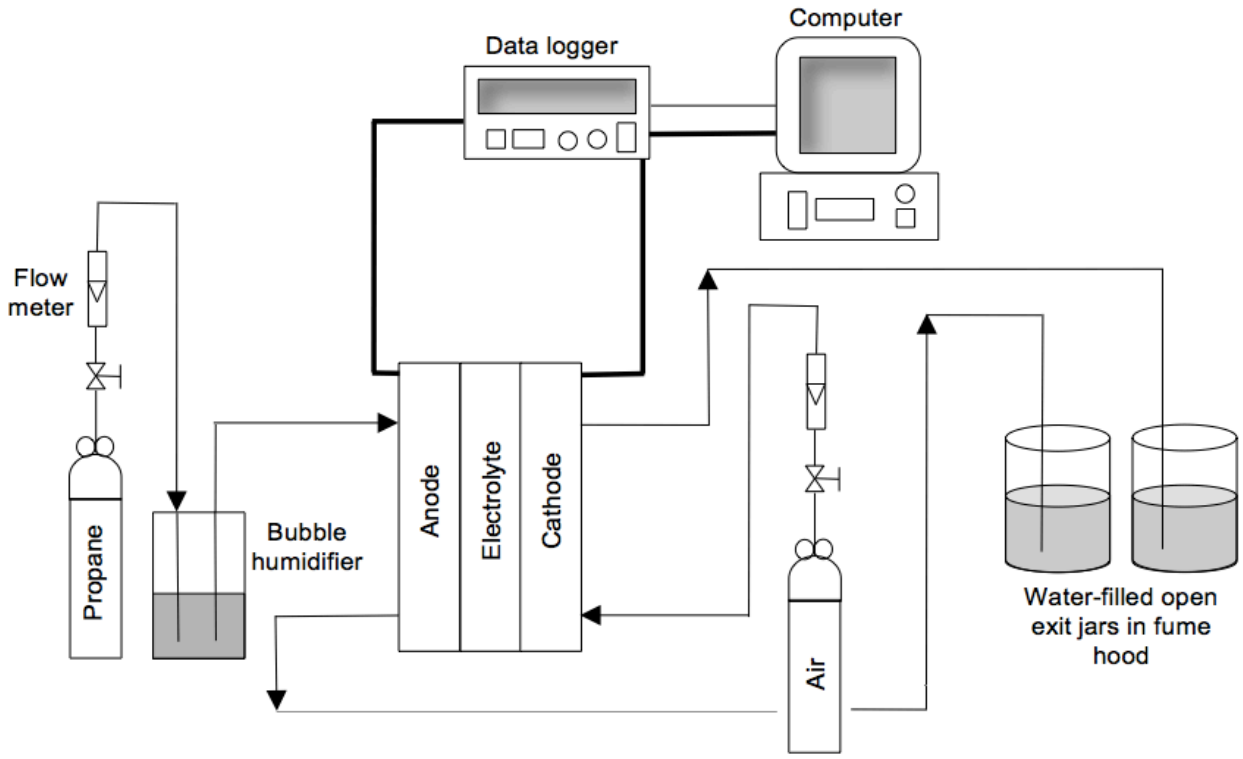


Figure 4.1F Experimental equipment used for a propane-air operation with a pin-type anode flow field and a bubble humidifier at 1 atm. No electrical connections were used to measure current (i.e. no power-supply unit in galvanostatic mode).

4.3 Results and discussion

In this work, the potential difference between the fuel cell anode and cathode, $\Delta\Phi_{cell}$ (V) and the current, (that was reported as current density, j, $\mu A/cm^2$) were measured as a function of the fuel cell operating time, t (min) or time-on-stream. The DPFC was regenerated with hydrogen at the anode and air at the cathode before each experiment was performed with propane at the anode. In all experiments the cathode had a pin-type flow field and was not humidified. The effects obtained by varying fuel cell operating conditions are described in the following material.

4.3.1 Platinum anode catalyst at 65°C

Several experiments were performed with a platinum anode catalyst at 65°C. Pure propane and two different mixtures of nitrogen and propane were used to vary the inlet propane mole fraction. The results from the 65°C experiment with pure propane were compared with results of experiments performed at a variety of other operating conditions.

The data shown in Figure 4.2 were obtained using an anode feed gas, a propane-nitrogen mixture having a propane mole fraction of 0.34. For this experiment, (case i described in section 4.2), the DPFC had a Nafion 212 MEA, a Pt anode catalyst, and an IDFF anode that was humidified by water in the liquid phase. The experimental equipment is shown in Figure 4.1A. The following fixed resistors were used: 1 MΩ, 10 kΩ, 980 Ω, 330 Ω, and 118 Ω in separate experiments. The results from each of those experiments are shown as a separate line in Figure 4.2.

All the curved lines on the graph in Figure 4.2 indicate that deactivation (decrease in $\Delta\Phi_{cell}$ with time-on-stream) was occurring. They all consist of a series of five features that appear consecutively as a function of time-on-stream. The first feature at the shortest time-on-stream is the small peaks in $\Delta\Phi_{cell}$ that occurred in most experiments during the first 5 minutes. The causes of those peaks are unknown. Nevertheless, some possibilities can be suggested. For example, after the regeneration experiment air would have been introduced into the gas feed lines when the anode feed gas was changed from hydrogen to propane. That air may have reacted with hydrocarbon intermediates remaining on the anode catalyst surface after regeneration to form hydrogen that became protons. At longer time-on-stream there is an almost linear deactivation, the second feature. Next, the shape of the deactivation curve becomes concave downward, the third feature. Then, the fourth feature is a concave upward portion of the deactivation curve. Finally, there is another almost uni-directional part of the

deactivation curve that consists of a series of small oscillations. They had peak-to-peak frequencies of about 2 minutes and their peak-to-valley heights were about 0.02 V.

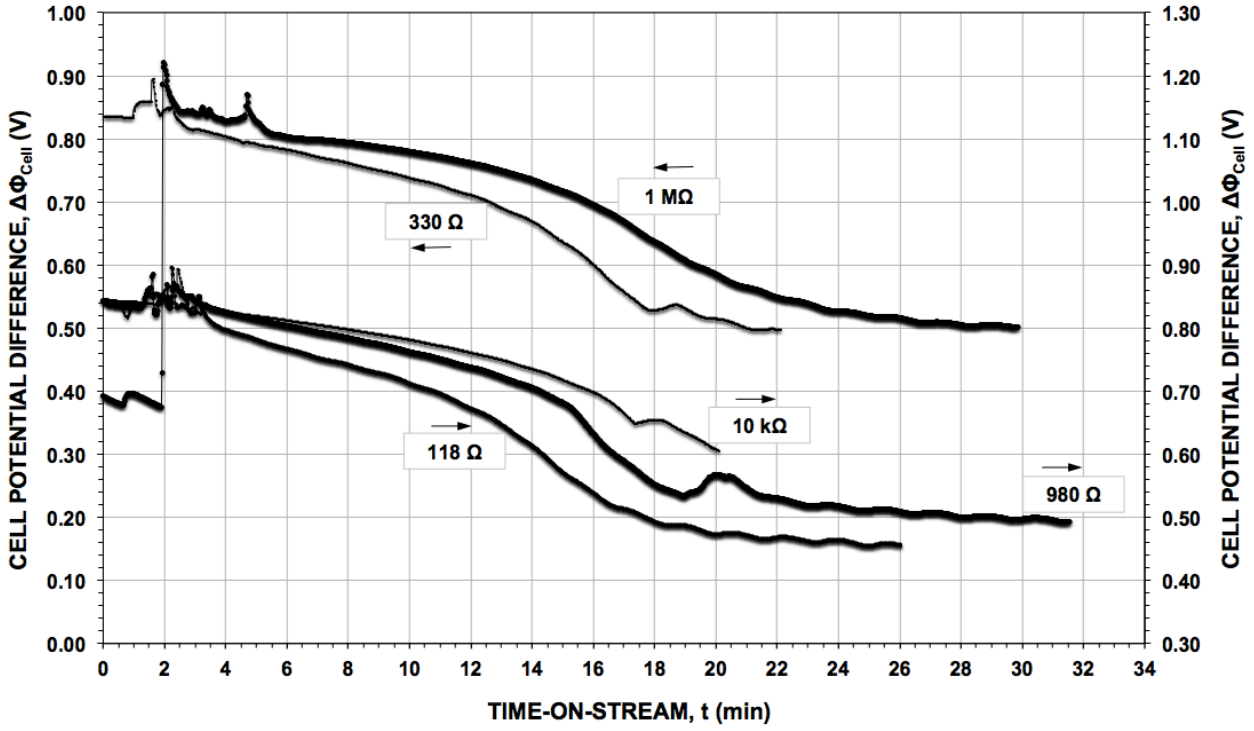


Figure 4.2 Cell potential difference, $\Delta\Phi_{cell}$ (V) versus time-on-stream, t (min) for a DPFC with 34% propane, IDFF anode humidified with liquid water, Pt anode catalyst, 65°C, 1 atm, and using fixed resistors of 1 MΩ, 10 kΩ, 980 Ω, 330 Ω, and 118 Ω.

The current densities, j, in Figure 4.3 are those corresponding to the potential differences across the fuel cell shown in Figure 4.2. For the same potential difference across a fuel cell significantly more current (i.e. four orders of magnitude more, in μA) passes through a 118 Ω resistor than through a 1 MΩ resistor. In spite of that difference in current all of the potential difference curves and all of the current density curves appear to be more or less similar as a function of time-on-stream. That suggests that at least part of deactivation is independent of the amount of current flowing through the fuel cell circuit, or in other words not caused by the electrochemical reaction.

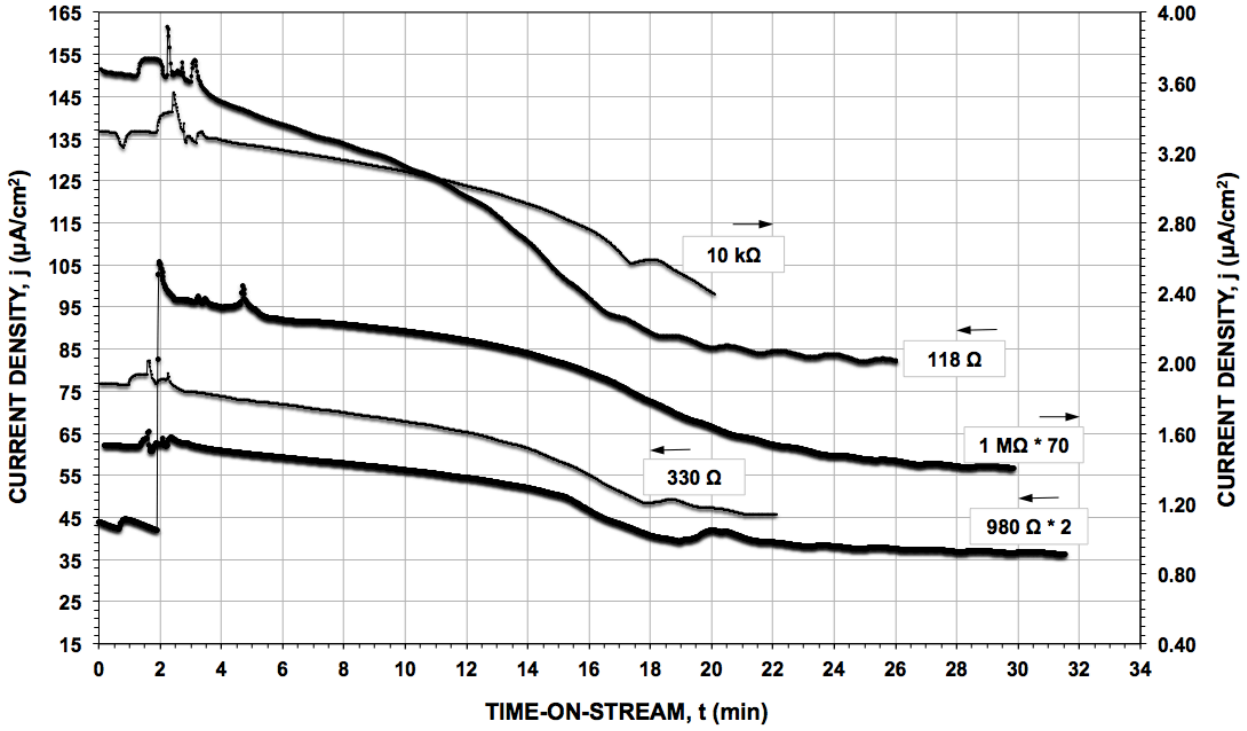


Figure 4.3 Current density, j ($\mu A/cm^2$) versus time-on-stream, t (min) for a DPFC with 34% propane, IDFF anode humidified with liquid water, Pt anode catalyst, 65°C, 1 atm, and using fixed resistors of 1 MΩ, 10 kΩ, 980 Ω, 330 Ω, and 118 Ω. A factor of 2 and 70 has been multiplied to the curve data of 980 Ω and 1 MΩ respectively.

The data in Figures 4.2 and 4.3 were used to plot a polarization curve at a time-on-stream of 14 minutes. The potential difference at 14 minutes for each curve in Figure 4.2 was matched with the current density for each curve in Figure 4.3. Thereby different data points were obtained. Those data points are shown as open circles in Figure 4.5. Together they make a polarization curve that corresponds to 14 minutes time-on-stream. Although the 14 minute time was an arbitrary choice, it generally represents a time towards the end of the first linear portion of the deactivation curve.

A linear relationship between the cell potential difference, $\Delta\Phi_{cell}$ and the current density, j, both measured at the same time-on-stream is shown in Figure 4.4. The data in this figure are for the propane-air operation of the fuel cell using a 1 MΩ fixed resistor. Similar linear

relationships were observed for all five resistors and in all experiments with a fixed resistor. Relationships between the fuel cell potential difference and current density are Ohm's law relationships and are therefore, not surprising. However, it is important to note that the Ohm's law relationships were observed even when oscillations occurred.

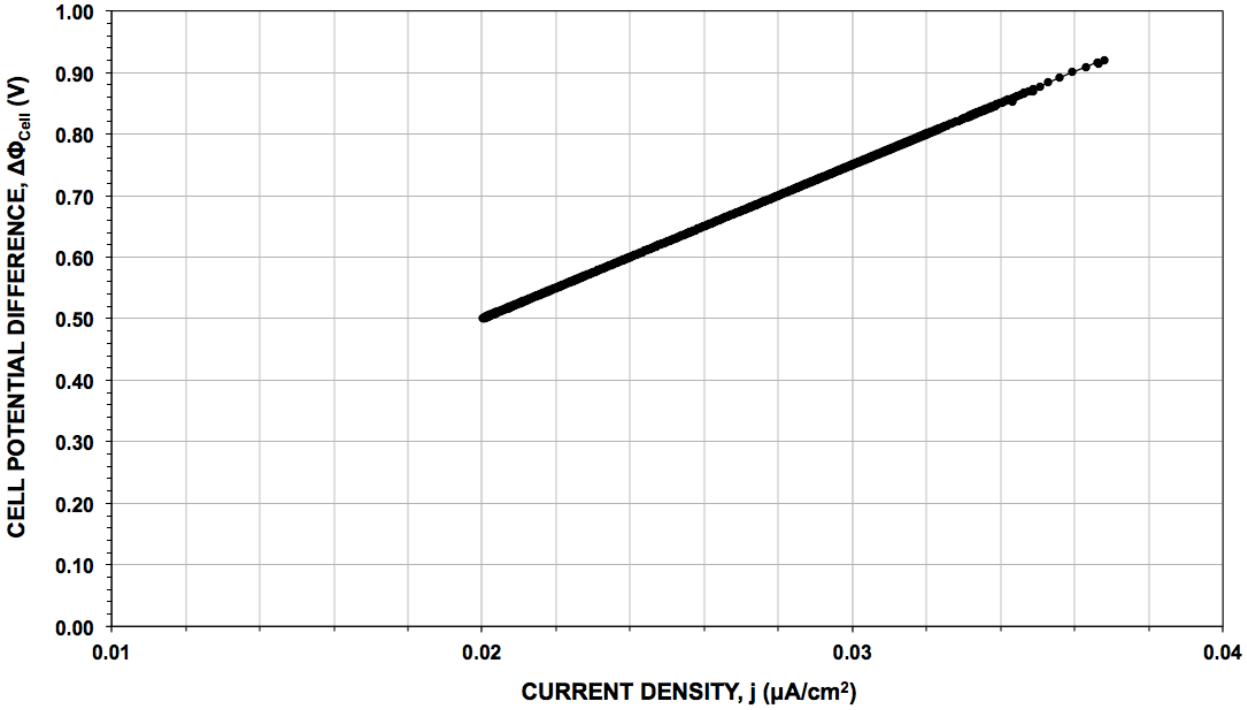


Figure 4.4 Relationship between time-on-stream measurement of cell potential difference, $\Delta\Phi_{cell}$ (V) and current density, j ($\mu A/cm^2$) for a DPFC with 34% propane, IDFF anode humidified with liquid water, Pt anode catalyst, 65°C, 1 atm, and using a 1 MΩ fixed resistor.

Liquid water was observed flowing from the interdigitated channels at the anode and exited through both the anode and cathode gas exit lines. However, most of the liquid water fed at the anode-water inlet exited through the anode-water exit line and recirculated back into the water feed vessel of the peristaltic pump shown in Figure 4.1A. The flow rate of liquid water was comparatively higher for the anode exit gas stream than the cathode. This observation was based on the greater water level observed in the anode exit jar compared to the cathode exit jar.

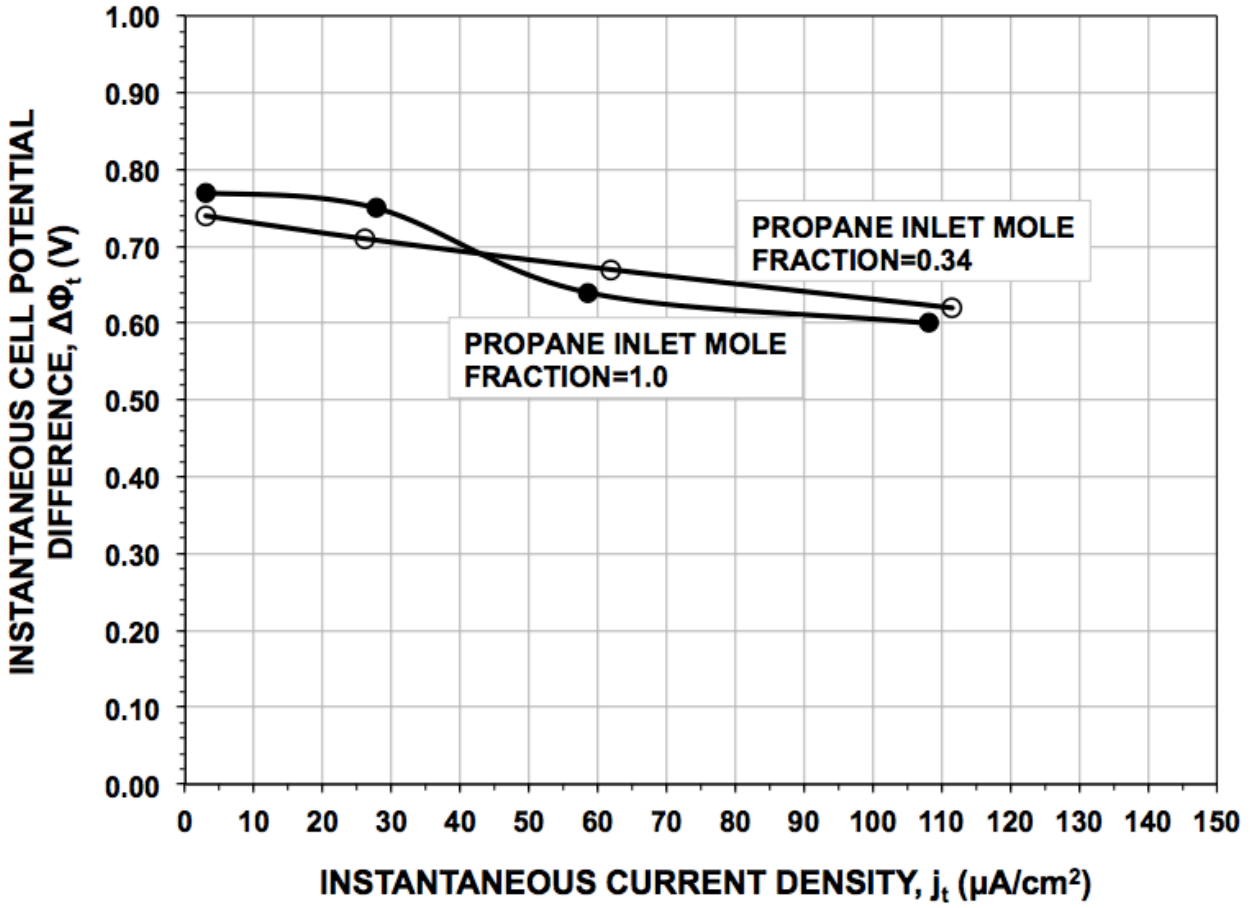


Figure 4.5 Polarization curve of a DPFC with different propane inlet mole fractions at a time-on-stream of 14 minutes, IDFF anode humidified with liquid water, Pt anode catalyst, 65°C, 1 atm, and using different fixed resistors. The value of propane inlet mole fraction for the above two cases were represented by the following symbols: (i) solid circles: 1.0 mole fraction, and (ii) open circles: 0.34 mole fraction.

The points seen in Figure 4.5 indicate that when the rate of the electrochemical reaction was held constant the performance of the DPFC, as indicated by the potential difference across the fuel cell, was almost the same with 1.0 and 0.34 propane mole fractions at the anode inlet. That indicates the performance of the DPFC was not affected by anode inlet propane mole fractions ranging from 0.34 to 1.0. This observation is consistent with the fact that the propane flow rate in the anode feed gas was much greater than the rate of propane used by the fuel cell

at all propane mole fractions. Furthermore, the partial pressure of propane in the gas phase in contact with the anode catalyst provided propane to the catalyst as fast as the electrochemical reaction was using it. This indicates that the rate of propane adsorption is not rate limiting.

4.3.2 Platinum anode catalyst at 23°C

The polarization curve data for a propane mole fraction of 1.0, in Figure 4.5, were used as the base case for several comparisons. Temperature was the variable changed for the comparison shown in the polarization curve data of Figure 4.6. All the conditions used to obtain the 23°C data in Figure 4.6 were the same as the base case except that the base case temperature was 65°C. The 23°C data in Figure 4.6 were obtained using exactly the same method that was used to obtain the data in Figure 4.5. The values of $\Delta\Phi_t$ and j_t at 14 minutes time-on-stream were obtained from their respective plots of cell potential difference, $\Delta\Phi_{cell}$ and current density, j, versus time-on-stream (Figures B.5 and B.6, Appendix B).

Temperature makes a difference. The OCP of 0.78 V at 23°C is slightly greater than the OCP of 0.77 V at 65°C. The potential difference ($\Delta\Phi_t$) across the fuel cell (driving force), in Figure 4.6, is consistently greater at 23°C than at 65°C. At constant current density, the value of ($E° - \Delta\Phi_t$), where $E°$ is the standard electrochemical potential (V), represents the energy needed for operating the fuel cell. At constant current density, $\Delta\Phi_t$ represents the energy produced by the fuel cell. The reason the fuel cell performance, as measured by the potential difference ($\Delta\Phi_t$) across the fuel cell, is consistently greater at 23°C than at 65°C might be that the deactivation rate is slower at 23°C than at 65°C. This comparison in Figure 4.6, at constant current density, suggests that at least one of the reactions that cause deactivation is not directly related to the electrochemical reaction. When the electrochemical reaction is constant, the current density is constant. Therefore, if different temperatures produce different results at the same current density (the same electrochemical reaction rate), then some variable other than the electrochemical reaction must be responsible for the difference in results.

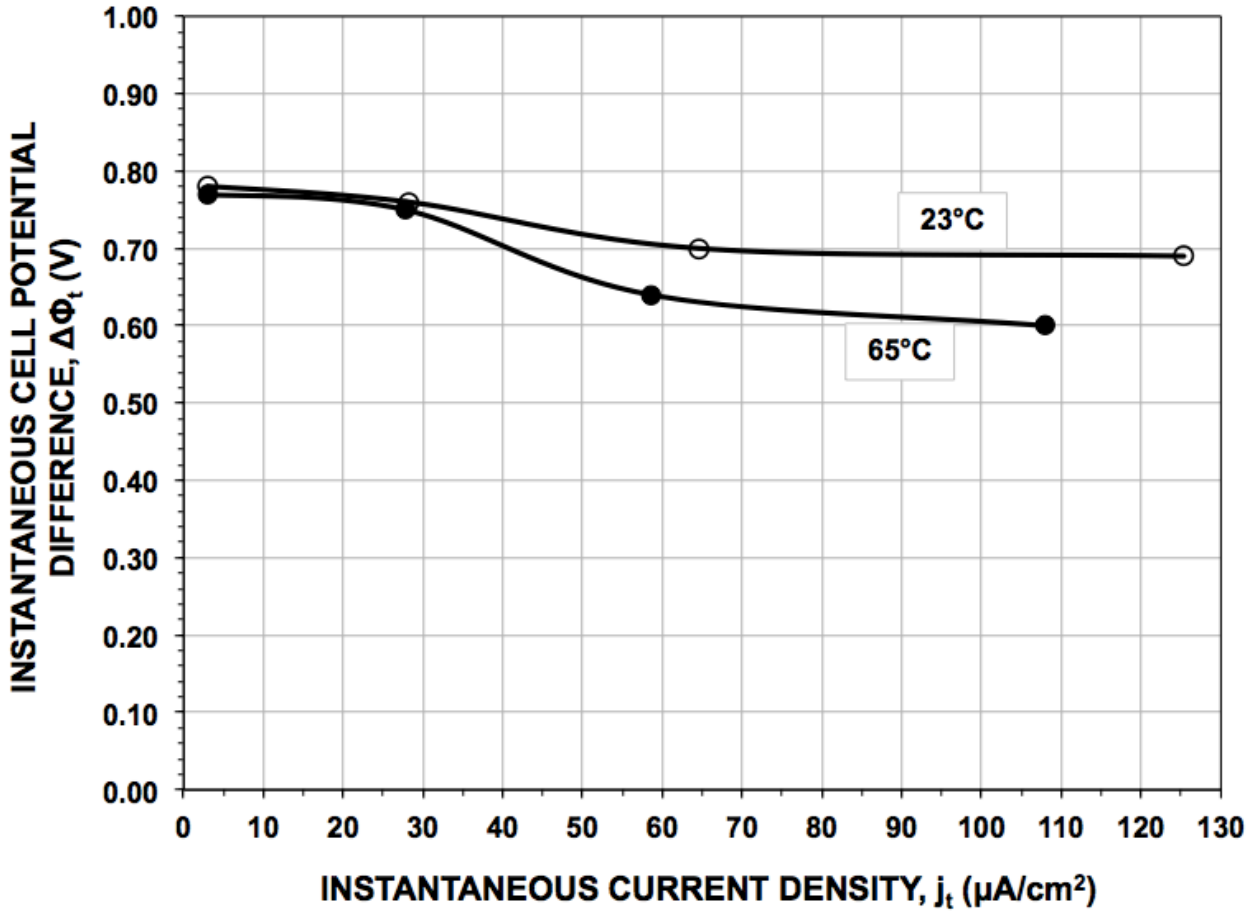


Figure 4.6 Polarization curve of a DPFC with 100% propane, IDFF anode humidified with liquid water, Pt anode catalyst, different fuel cell operating temperatures, 1 atm, and using different fixed resistors. The value of fuel cell operating temperature for the above two cases were represented by the following symbols: (i) solid circles: 65°C, and (ii) open circles: 23°C.

4.3.3 Platinum-Ruthenium anode catalyst at 65°C

The 65°C data in Figure 4.7 were obtained at almost the same conditions as the propane mole fraction of 1.0 data in Figures 4.5 and 4.6. There were two differences. First, a platinum-ruthenium (Pt-Ru) catalyst replaced the platinum catalyst at the anode. Second, the Nafion 117 MEA (1100 equivalent weight and 7/1000 inch = 128 μm thickness) that was used with Pt-Ru anode catalyst replaced the Nafion 212 MEA (2100 equivalent weight and 2/1000 inch = 51 μm thickness) that was used with the Pt anode catalyst. The modeling result

demonstrated that membrane thickness and other variables related to the membrane had essentially no effect on the overall performance of the fuel cell. The equivalent weight is the

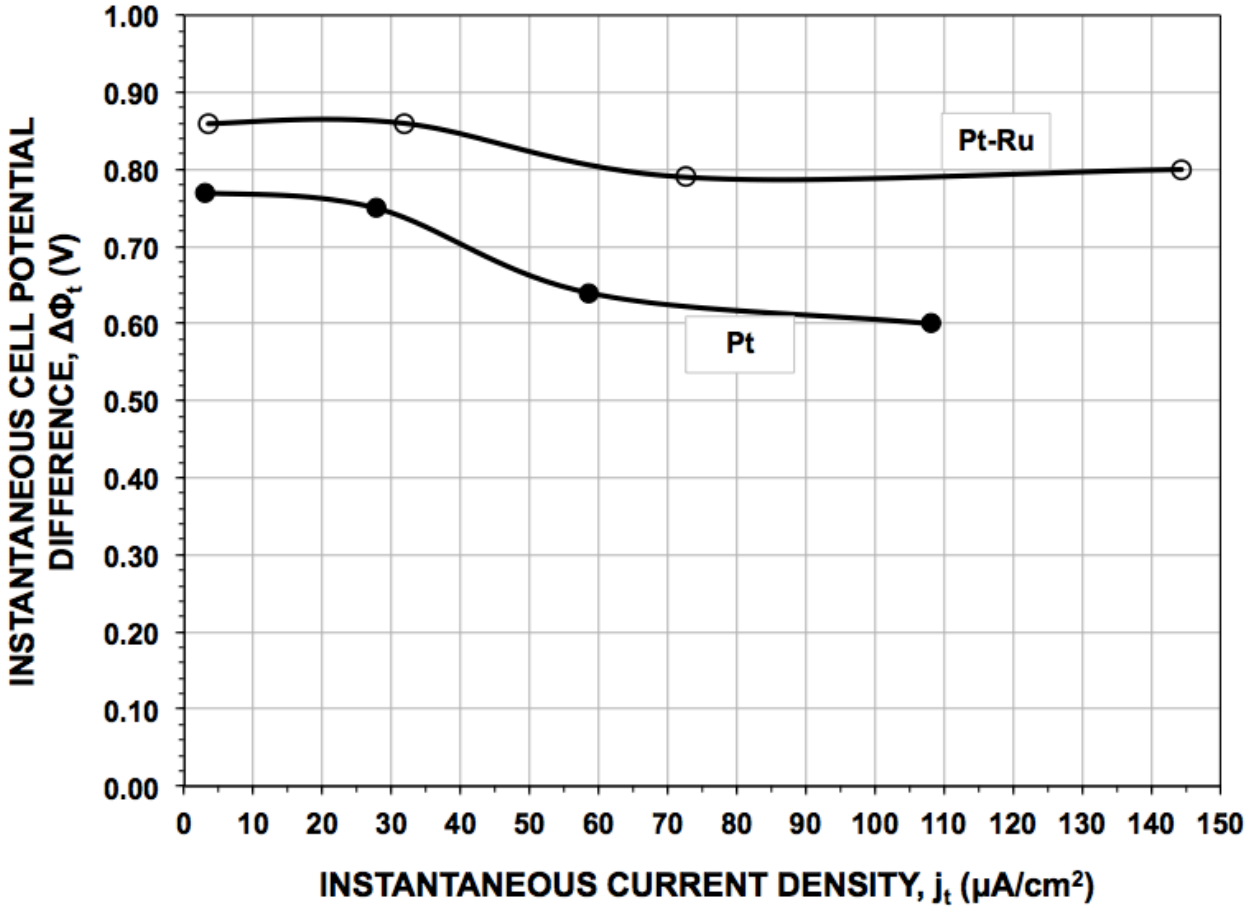


Figure 4.7 Polarization curve of a DPFC with 100% propane, IDFF anode humidified with liquid water, different anode catalysts, 65°C, 1 atm, and using different fixed resistors. The anode catalyst for the above two cases were represented by the following symbols: (i) solid circle: Pt (platinum), and (ii) open circle: Pt-Ru (platinum-ruthenium).

weight of Nafion polymer per sulphonic acid group in the polymer. The values of $\Delta\Phi_t$ and j_t at 14 minutes time-on-stream in Figure 4.7 were obtained from their respective plots of cell potential difference, $\Delta\Phi_{cell}$ and current density, j, versus time-on-stream (Figures B.7 and B.8, Appendix B).

Catalyst composition also makes a difference. The OCP of 0.86 V for the Pt-Ru anode catalyst was greater than the value of 0.77 V for the Pt anode catalyst. The fuel cell performance, as measured by the potential difference ($\Delta\Phi_t$) across the fuel cell, was better with Pt-Ru anode catalyst than with the Pt anode catalyst.

The improved fuel cell performance with Pt-Ru anode catalyst may be related to CO being one of the deactivating species. Ideally direct propane fuel cells will convert all the carbon atoms in propane to carbon atoms in CO_2 molecules. CO is one of the reaction intermediates that are formed as a precursor to obtaining CO_2. Many studies on hydrogen fuel cells have been performed with CO as an impurity in the hydrogen. CO is known to poison Pt catalysts. Water is known to dissociate into H and OH species more readily (at a lower overpotential) on the Ru component of Pt-Ru catalysts than on Pt catalysts without Ru. The hydrogen fuel cell studies with CO as an impurity in the hydrogen have consistently shown that better fuel cell performance is obtained with Pt-Ru anode catalysts than with Pt anode catalysts. The fact that the comparison in Figure 4.7 showed that the Pt-Ru catalyst was superior to the Pt catalyst raises the possibility that CO may be one of the deactivating species in this work.

4.3.4 Platinum-Ruthenium anode catalyst with a pin-type anode flow field at 65°C

The data in Figure 4.7, for a Pt-Ru catalyst, obtained using an interdigitated flow field, were compared in Figure 4.8 with data obtained at exactly the same conditions except that a pin-type flow field (fed by propane humidified by a bubble humidifier) replaced the interdigitated flow field (in which one of the channels had been filled with water in the liquid phase). Values of $\Delta\Phi_t$ and j_t at 25 minutes time-on-stream were obtained from their respective plots of cell potential difference, $\Delta\Phi_{cell}$ and current density, j, versus time-on-stream (Figures B.9 and B.10, Appendix B). A 25 minute time-on-stream comparison was chosen because short-term fluctuations, in some of the curves of $\Delta\Phi_{cell}$ versus time-on-stream, had prevented representative deactivation from occurring before the 14 minutes time-on-stream.

As seen in Figure 4.8, the fuel cell performance with an interdigitated flow field, having excess water and approximately 80% less reaction volume than the pin-type, at the anode was better than with a pin-type flow field at the anode. One of the differences between the two was

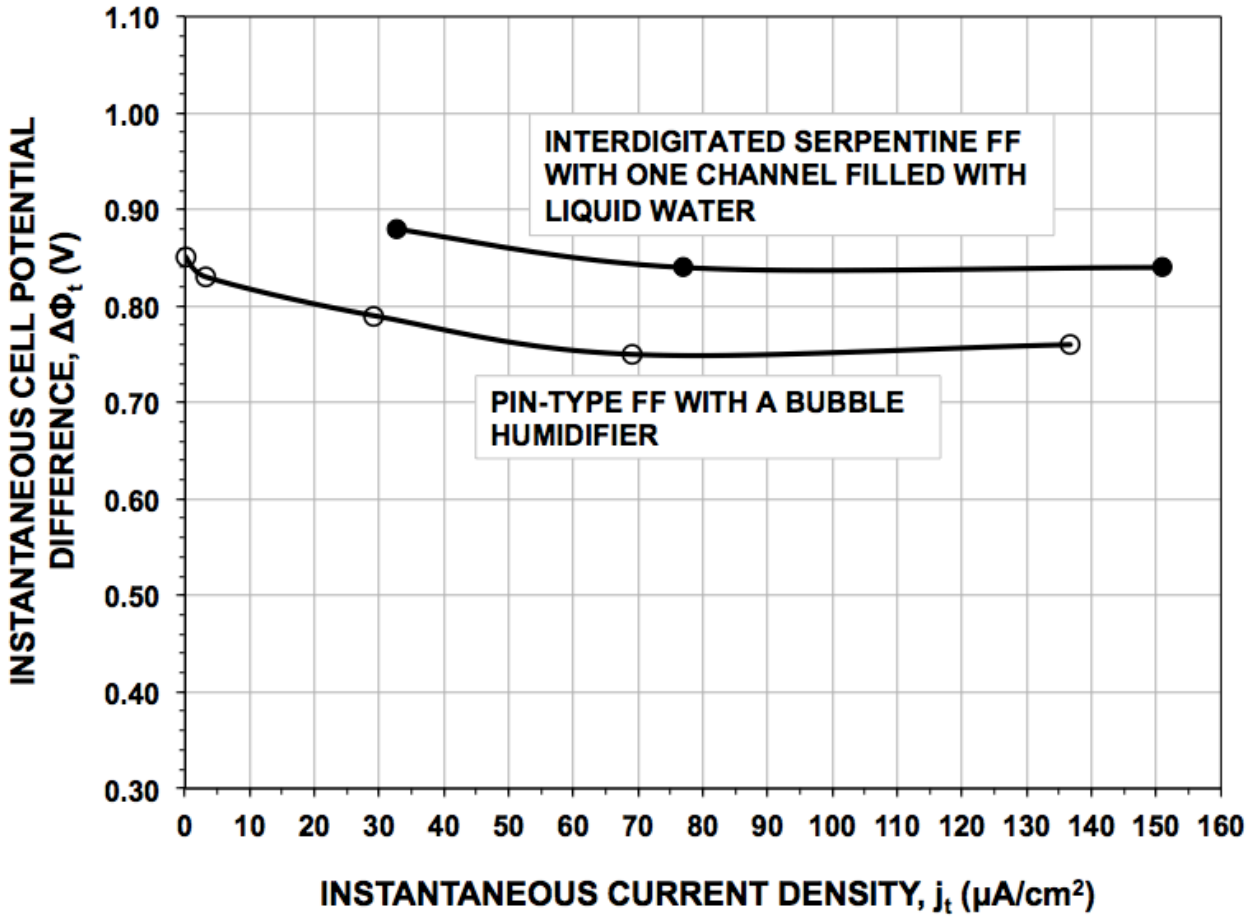


Figure 4.8 Polarization curve of a DPFC with 100% propane, different anode flow fields along with different humidification systems, Pt-Ru anode catalyst, 65°C, 1 atm, and using different fixed resistors. The anode flow field for the above two cases were represented by the following symbols: (i) solid circle: interdigitated serpentine FF (flow field) with one channel filled with liquid water, and (ii) open circle: pin-type FF (flow field) with a bubble humidifier.

the amount of water present in the flow fields. More water was present when liquid water filled one of the channels in the serpentine interdigitated flow field. Less water was present when water in the vapour phase fills all of the channels in a pin-type flow field.

Substantially, different amounts of water were observed leaving the fuel cell in the gas exit streams. These observations were based on the amount of additional water that accumulated in the water-filled open jars through which the exit gases bubbled. In the case of interdigitated flow field, liquid water was fed continuously at a rate of 23 ml/min (1.25 mol/min) in comparison to the water vapour feed rate of 89 ml/min (0.001 mol/min) for a pin-type flow field. The liquid-filled serpentine channel covered a face area of approximately 2 cm^2 in comparison to an approximate value of 24 cm^2 for a water vapour-filled pin-type flow field. These water flow measurements indicated that much more water was present per unit of channel face area with an interdigitated flow field than with a pin-type flow field. An insignificant amount of additional water was observed to accumulate in the anode gas stream leaving from the pin-type flow field. In contrast, a substantial amount of additional water was observed to accumulate in the anode gas stream leaving from the interdigitated flow field. For the interdigitated flow fields, water would have to flow through several fuel cell components in order to leave the fuel cell in the anode exit gas stream. It would have to enter through one of the channels in the flow field. Then, it would have to flow through the gas diffusion layer. Some of it might also flow through the catalyst layer in parallel to the gas diffusion layer. Finally, it would have to enter the other flow field channel that carries the propane feed gas, in order to leave in the anode exit gas stream.

In summary, the liquid-filled interdigitated flow fields produced a better performance than the water vapour-filled pin-type flow fields in propane fuel cells. More water flowed through the gas diffusion layer and possibly the anode catalyst layer of the interdigitated flow field than the pin-type flow field. These observations suggest that water may have inhibited the deactivation of the anode catalyst in propane fuel cells. This hypothesis would be consistent with water dissociating to form OH groups that react with CO to form CO_2.

4.3.5 Hydrogen fuel at a Platinum-Ruthenium anode catalyst with a pin-type anode flow field at 65°C

With one exception, the data in Figure 4.9 were obtained using exactly the same conditions as the data in Figure 4.8. The one exception was that for the data in Figure 4.9 hydrogen was the fuel used at the anode with a power-supply unit (in a galvanostatic mode) to measure the fuel cell performance. In contrast, propane was the fuel used at the anode with different fixed resistors for the data in Figure 4.8.

The fuel cell performance results with hydrogen fuel in Figure 4.9 were substantially different from those with propane fuel in Figure 4.8. With hydrogen fuel in Figure 4.9, both types of flow field had open-circuit potentials greater than 0.9 V. In contrast with propane fuel in Figure 4.8, both types of flow field had open-circuit potentials that were less than 0.9 V. When hydrogen was the fuel the current densities were almost three-orders of magnitude greater than those when propane was the fuel. At all current densities in Figure 4.9, the fuel cell performance, as measured by the potential difference ($\Delta\Phi_{cell}$) across the fuel cell, with the pin-type flow field was superior to that obtained with the interdigitated flow field. The ranking of the flow field type with hydrogen fuel in Figure 4.9 is exactly opposite to their ranking with propane fuel in Figure 4.8.

Some explanations can be suggested for the difference in performance when the fuel changed. Firstly, there should be no deactivation caused by CO or by hydrocarbon reaction intermediates when hydrogen is the fuel. In contrast, this work has shown that substantial deactivation occurs when propane is the fuel. Rapid deactivation might explain the almost three-order of magnitude difference in the current densities. Secondly, the amount of water present might have had some impact. Previously, it suggested that water might have inhibited the deactivation that occurred when propane was the fuel. That would not be a factor with a hydrogen fuel since no deactivation is anticipated with a hydrogen fuel. So, when large amounts

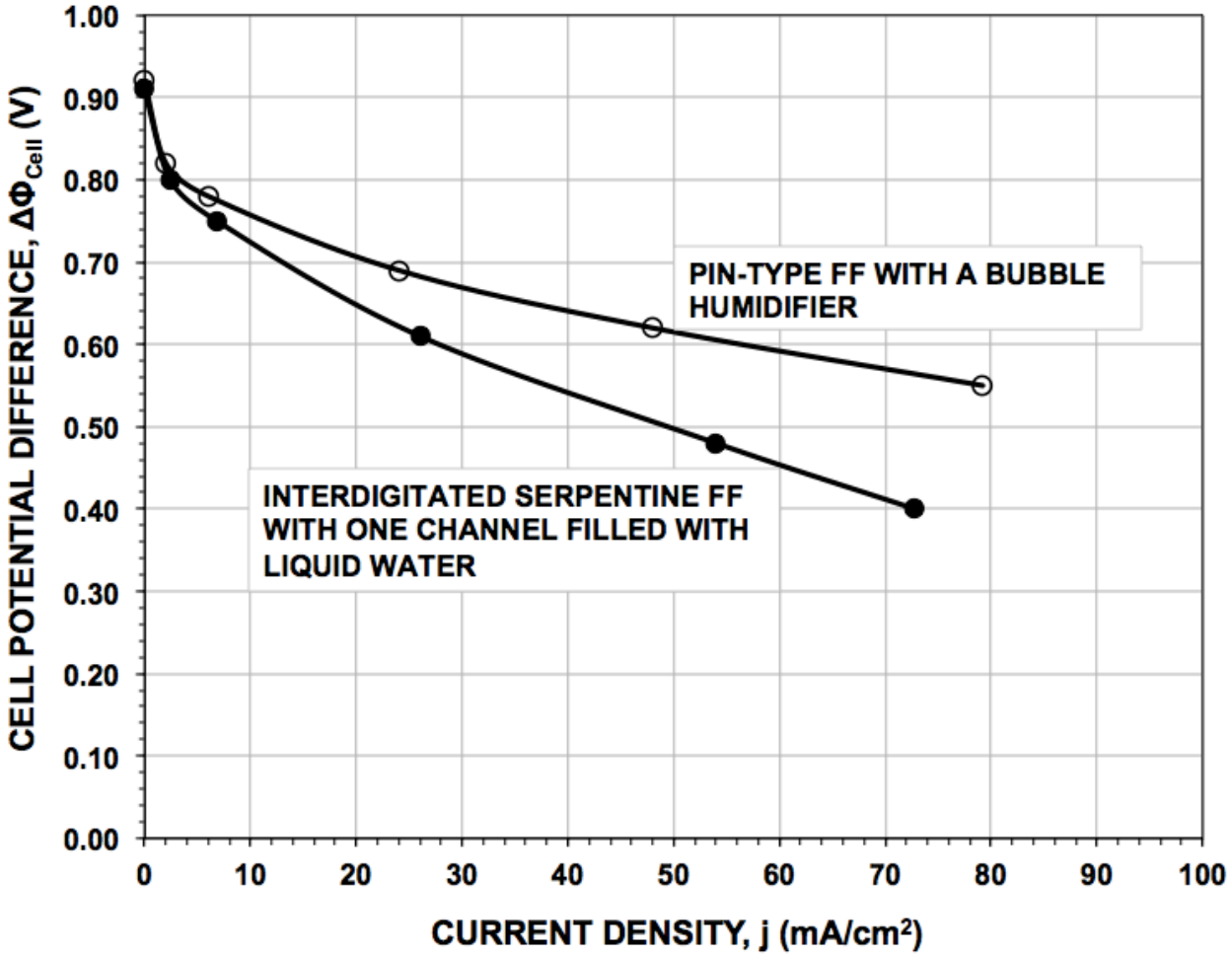


Figure 4.9 Polarization curve of a hydrogen fuel cell (after propane-air operation) with different anode flow fields along with different humidification systems, Pt-Ru anode catalyst, 65°C, 1 atm, and using the power-supply unit at a galvanostatic mode. The anode flow field for the above two cases were represented by the following symbols: (i) solid circle: interdigitated serpentine FF (flow field) with one channel filled with liquid water, and (ii) open circle: pin-type FF (flow field) with a bubble humidifier.

of water are present with a hydrogen fuel, the hydrogen would have to compete with the water for reaction sites. The water flow measurements indicated that much more water was present with an interdigitated flow field than with a pin-type flow field for the same face area. Therefore,

hydrogen might have had less access to the reaction sites (possible partial flooding) with the interdigitated flow field than with the pin-type flow field.

4.3.6 The effect of temperature on oscillations

Oscillations in the fuel cell performance, as measured by the potential difference ($\Delta\Phi_t$) across the fuel cell, were sometimes observed. For example, in Figure 4.10 fluctuations in the potential difference across the fuel cell can be seen at time-on-stream near 16 minutes when the fuel cell temperature was 65°C. No fluctuations were seen at 23°C. As explained in the discussion of Figure 4.6, with the exception of the temperature, identical experimental conditions were used to obtain both of the curves shown in Figure 4.10.

A frequent explanation for oscillations is that they result from the cyclical formation of a deactivating species via one reaction and removal of the deactivating species by a different reaction. On the basis of that explanation a deactivating species seems to have been both formed and removed when the fuel cell temperature was 65°C. It is suggested that CO might have been one of the deactivating species formed from the hydrocarbons.

In addition, it was suggested that when water was present the removal of the deactivating species occurred. In contrast, the absence of oscillations at 23°C suggests that a deactivating species was being formed but not being removed by a different reaction. Instead, it seems that at 23°C it may have been possible for a long residence time reaction intermediate to form on the catalyst surface and eventually be converted to another species that subsequently desorbed from the surface. This hypothesis was supported by a comparatively faster regeneration rate, of the fouled catalyst reaction sites, observed for the DPFC at 23°C (i.e. 23 minutes; Figures B.11, B.12, and B.13, Appendix B) than at 65°C (i.e. 33 minutes; Figures B.14, B.15, and B.16, Appendix B) when more current was passed through the fuel cell system using a 330 Ω resistor.

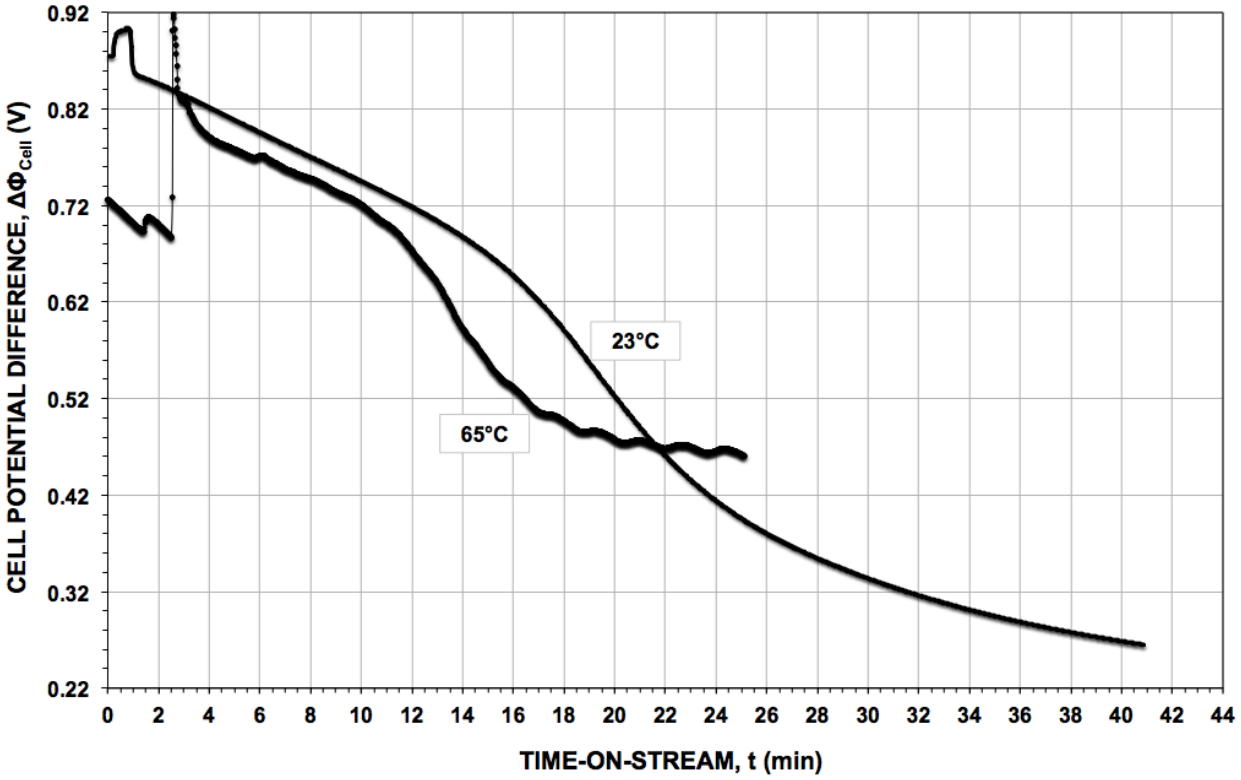


Figure 4.10 Cell potential difference, $\Delta\Phi_{cell}$ (V) versus time-on-stream, t (min) for a DPFC with 100% propane, IDFF anode humidified with liquid water, Pt anode catalyst, 1 atm, a 118 Ω fixed resistor, and different fuel cell operating temperatures.

4.3.7 The effect of anode catalyst composition on oscillations

The plot for the Pt anode catalyst at 65°C in Figure 4.10 is also shown in Figure 4.11. There it is compared with a Pt-Ru anode catalyst. As explained in the discussion of Figure 4.7, with the exception of the catalyst composition and membrane thickness, identical experimental conditions were used to obtain both of the curves shown in Figure 4.11.

Oscillations were observed with both the Pt anode catalyst and the Pt-Ru anode catalyst. Though, it would appear that the frequency of the Pt-Ru anode catalyst oscillations is more than that of the Pt anode catalyst oscillations. But, the amplitudes appear to be similar (i.e. 0.02 V). As was discussed in reference to Figure 4.7, the Ru component of the Pt-Ru anode catalyst enhanced the water dissociation mechanism. That made OH groups available to react

with CO adsorbed on Pt atoms to form CO_2, which can desorb from the catalyst surface more readily than CO. Steady-states were not observed for either catalyst. Even though oscillations occurred in both catalysts, both of them continued to deactivate with increasing time-on-stream.

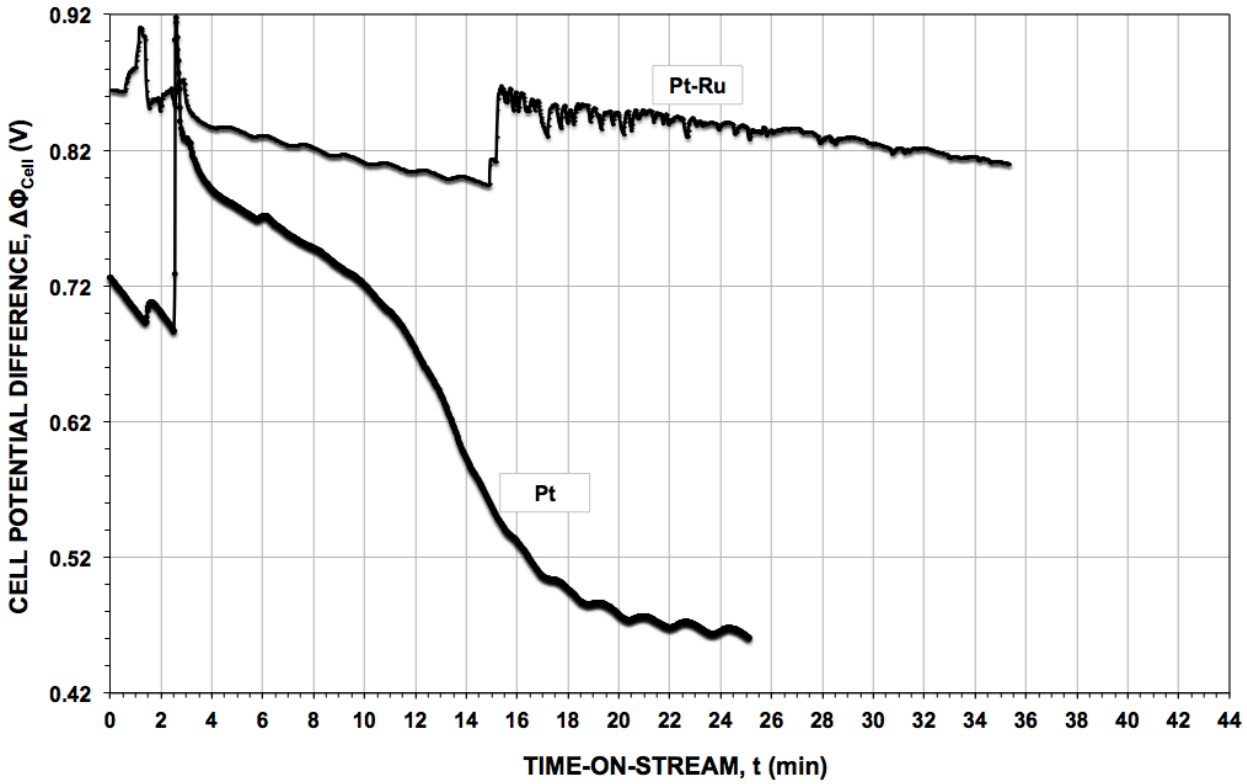


Figure 4.11 Cell potential difference, $\Delta\Phi_{cell}$ (V) versus time-on-stream, t (min) for a DPFC with 100% propane, IDFF anode humidified with liquid water, different anode catalysts, 65°C, 1 atm, and using a 118 Ω fixed resistor.

4.3.8 The effect of flow field type on oscillations

The plot for the Pt-Ru anode catalyst with an interdigitated flow field, having one serpentine channel filled with liquid water, that was shown in Figure 4.11 is also shown in Figure 4.12. There it is compared with a Pt-Ru anode catalyst with a pin-type flow field, having a bubble humidifier. As explained in the discussion of Figure 4.8, with the exception of the flow field and humidifying system, identical experimental conditions were used to obtain both of the curves shown in Figure 4.12.

The flow field / humidifier combination has a substantial effect on oscillations. The potential difference measured with the pin-type flow field with the bubble humidifier does not have oscillations. However, the one with the interdigitated flow field having a channel filled with liquid water does have oscillations. The amount of water available is quite different in the two cases. The larger quantity of water available with the interdigitated flow fields can be associated with the oscillations. In the presence of Pt-Ru catalyst, water dissociation can occur, which generates OH groups. The OH groups can then be available to react with CO adsorbed on Pt atoms to form CO_2, which can desorb from the catalyst surface more readily than CO. Steady-states were not observed for either catalyst and both of them continued to deactivate with increasing time-on-stream.

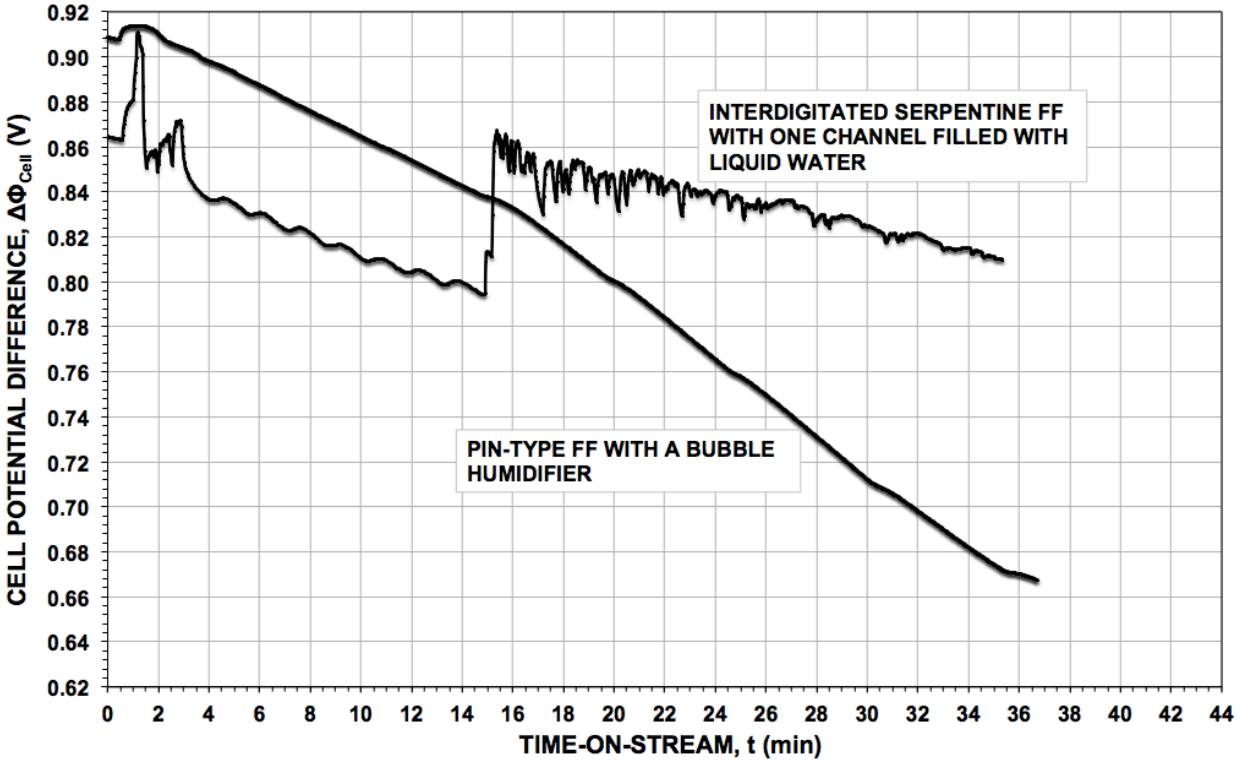


Figure 4.12 Cell potential difference, $\Delta\Phi_{cell}$ (V) versus time-on-stream, t (min) for a DPFC with 100% propane, different anode flow fields along with different humidification systems, Pt-Ru anode catalyst, 65°C, 1 atm, and using a 118 Ω fixed resistor.

4.3.9 DPFC with platinum-ruthenium anode catalyst, propane inlet mole fraction = 1.0, and without electrical connections to measure current (therefore, only thermo-chemical reaction is possible)

The time-on-stream plot of the cell potential difference, $\Delta\Phi_{cell}$ (V) versus the fuel cell time-on-stream, t (min) is shown in Figure 4.13. The plot in Figure 4.13 was obtained for the propane-air operation at 65°C and 1 atm using 100% propane at the anode inlet.

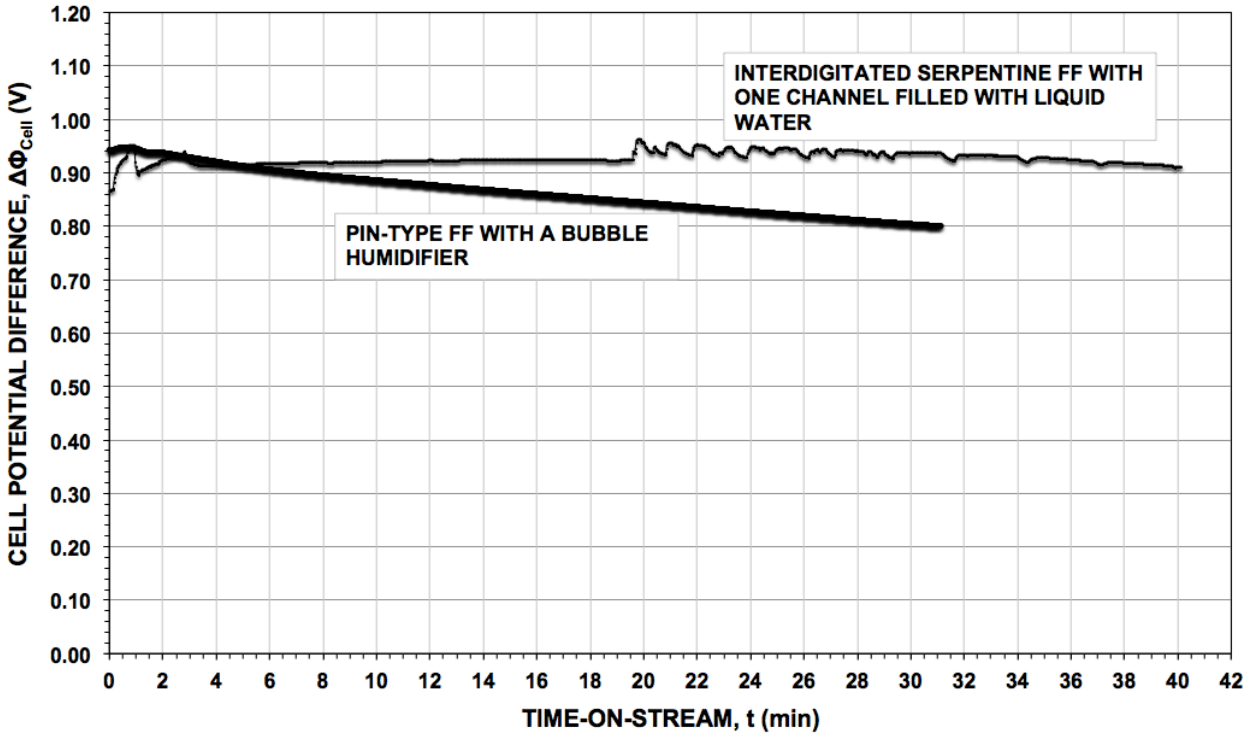


Figure 4.13 Cell potential difference, $\Delta\Phi_{cell}$ (V) versus time-on-stream, t (min) for a DPFC with 100% propane, different anode flow fields along with different humidification systems, Pt-Ru anode catalyst, 65°C, 1 atm, and no electrical connections to measure current (i.e. only thermo-chemical reaction possible).

During the time-on-stream measurement of $\Delta\Phi_{cell}$, the power-supply unit was disconnected from the DPFC and the fuel cell circuit was left open. As mentioned in section 4.2, the DPFC was stabilized with the hydrogen-air operation before feeding propane at the anode.

In one of the plots shown in Figure 4.13, the DPFC consisted of an IDFF anode and a Nafion 117 MEA with Pt-Ru anode catalyst. The experimental set-up is described in Figure 4.1C. The anode humidification was achieved by feeding liquid water through one of the interdigitated serpentine channels of the anode flow field by using a peristaltic pump. In this experiment, the propane-air thermo-chemical reaction began from an open-circuit potential (OCP) of 0.92 V. Initially the cell potential difference, $\Delta\Phi_{cell}$ in volt (V) was approximately 0.87 V when no gas was fed to the fuel cell system. The $\Delta\Phi_{cell}$ remained at 0.87 V when the air was introduced at the cathode. When the propane was fed at the anode, the $\Delta\Phi_{cell}$ gradually increased to 0.94 V. This increase in the $\Delta\Phi_{cell}$ was due to the occurrence of temporary hydrogen-air reaction from the hydrogen that remained within the fuel cell system. However, within 0.5 minutes the $\Delta\Phi_{cell}$ dropped from 0.94 V to the propane OCP of 0.92 V. Up to 19.5 minutes, an almost steady state condition was observed at the $\Delta\Phi_{cell}$ of 0.92 V. This was followed by autonomous oscillations and later V-shaped deactivations.

For the other plot shown in Figure 4.13, all the operating conditions remained same as the previous plot except for the anode flow field and humidification system. The DPFC consisted of a pin-type anode flow field and a bubble humidifier was employed for the anode humidification. The experimental set-up is described in Figure 4.1F. In this case, the propane-air thermo-chemical reaction began from an open-circuit potential (OCP) of 0.94 V. Initially the cell potential difference, $\Delta\Phi_{cell}$ in volt (V) was approximately 0.94 V when no gas was fed to the fuel cell system. The $\Delta\Phi_{cell}$ remained at 0.94 V when the air was introduced at the cathode. When the propane was fed at the anode, the $\Delta\Phi_{cell}$ gradually increased to 0.95 V. This increase in the $\Delta\Phi_{cell}$ was due to the occurrence of temporary hydrogen-air reaction from the hydrogen that remained within the fuel cell system. However, within 0.5 minutes the $\Delta\Phi_{cell}$ dropped from 0.95 V to the propane OCP of 0.94 V. After that, the $\Delta\Phi_{cell}$ gradually deactivated at the rate of 0.005 V/min. Hence, in the case of a DPFC, the quantity of liquid water at the anode affects the rate of

deactivation and eventually the fuel cell performance at a constant reaction rate.

4.4 Summary

1. Deactivation, as indicated by the curves for potential difference (Figure 4.2) versus time-on-stream, has a similar shape for all resistances from 118 Ω to 1 MΩ. The corresponding electrical current densities at those resistances varies from 140 $\mu A/cm^2$ to 1.4 $\mu A/cm^2$ / 70 = 0.02 $\mu A/cm^2$ (Figure 4.3), a variation of almost three orders of magnitude. The electrochemical reaction is proportional to the electrical current density. The combination of large change in the electrochemical reaction with minimal change in the shape of the initial deactivation curve suggests that much of the initial deactivation is not caused by an electrochemical reaction.
2. The mole fraction of propane in the gas phase (Figure 4.5) does not change the initial polarization curve (14 minutes time-on-stream). The similarity in polarization curves suggests that the adsorption of propane from the gas phase is not the rate-limiting step in the reaction mechanism.
3. The 23°C fuel cell temperature resulted in a superior initial polarization curve (Figure 4.6) than the 65°C fuel cell temperature. Normally, reaction kinetic rates increase with increasing temperature. In this case, two reaction rates should be considered. One is the rate of the electrochemical reaction that produces electrons. The other is the rate of deactivation. The superiority of the 23°C fuel cell temperature result suggests that the increase in the rate of initial deactivation when going from 23 to 65°C had a greater impact than the increase in the electrochemical reaction when going from 23 to 65°C.
4. The addition of Ru to a Pt catalyst (Figure 4.7) caused a significant improvement in the initial polarization curve. The Ru may have contributed to diminished deactivation caused by CO. The desired overall reaction is the conversion of propane to CO_2. CO is a reaction intermediate in the overall reaction. Many research investigations have reported that Ru

enhances the dissociation of H_2O to OH and H. The OH has been shown to react with CO that is adsorbed on Pt catalysts. The beneficial effect of Ru (Figure 4.7) suggests that CO may be one of the deactivating species.

5. When propane was the fuel, an interdigitated flow field that transported liquid water to the MEA produced a better initial polarization curve than a pin-type flow field with which only water in the vapour phase was transported to the MEA (Figure 4.8). The quantity of water in the MEA with the interdigitated flow field would be substantially greater than that limited to the water partial pressure in the vapour phase. This result suggests that water may have been reacting with deactivating species to clean some of the reaction sites on the catalyst surface.
6. When hydrogen was the fuel, the result was the opposite of that in point 5 above (Figure 4.9). When hydrogen was the fuel, a pin-type flow field with which only water in the vapour phase was transported to the MEA produced a better initial polarization curve than an interdigitated flow field that transported liquid water to the MEA. No deactivation occurred when hydrogen was the fuel, because there were no impurities in the hydrogen. In this case water may have competed with hydrogen for reaction sites on the catalyst surface. If more water were present on the catalyst surface, fewer reaction sites would have been available on which hydrogen could react.
7. Oscillations in the potential difference across the fuel cell and in the current were measured in many, but not all, of the experiments reported here. At 65°C oscillations were observed, but not at 23°C (Figure 4.10). The conventional explanation for oscillations when deactivation occurs is a combination of two reactions. One reaction causes deactivation and is dominant for some time periods. The other reaction causes regeneration and is dominant for other time periods. One possible explanation for the results in Figure 4.10 might be that a temperature of 23°C might be too cold for the water regeneration reaction to occur.

Current density data for the 65°C curve in Figure 4.10 is shown in Figure 4.3 as the 118 Ω curve. It is seen that the oscillation occurred near a current density of 85 $\mu A/cm^2$. Furthermore the 1 MΩ curve in Figure 4.3 also showed oscillations. In that case, the current density was 1.4 $\mu A/cm^2$ / 70 = 0.02 $\mu A/cm^2$, or 20 nA/cm^2. When these current densities are compared to the current densities of the hydrogen polarization curve in Figure 4.9 it is seen that oscillations in the nano-Ampere range are essentially at the open-circuit potential. This appears to be the first report of oscillations at open-circuit potential since no such reports could be found in the literature.

8. Oscillations were measured for both a Pt catalyst and a Pt-Ru catalyst (Figure 4.11). However, oscillations were observed at a potential difference across the fuel cell of 0.84 V for the Pt-Ru catalyst, and not until 0.48 V for the Pt catalyst. These potential differences are the same as those reported when the fuel is hydrogen that contains CO impurities. Also, these potential differences are consistent with the conventional explanation in the literature that water is being dissociated to form OH groups that convert CO to CO_2 at potentials near 0.84 V for Pt-Ru catalysts and 0.48 V for Pt catalysts.
9. Distinct oscillations were measured with an interdigitated flow field that transported liquid water to the MEA whereas the oscillations measured with a pin-type flow field with which only water in the vapour phase was transported to the MEA were barely perceptible (Figure 4.12). This difference suggests that the quantity of water in the MEA may be a factor that influences regeneration.
10. A thermo-chemical experiment in the absence of electrochemical reactions was attempted (Figure 4.13) at almost “open-circuit potential”. The circuit having both the resistor and the ammeter was removed. The only circuit connecting the anode and cathode was the one used to measure the fuel cell potential difference. Very large resistors are used when electrical potential is measured. Nevertheless, a very small current would have flowed

through that circuit. At almost “open-circuit potential”, oscillations were still measured with an interdigitated flow field that transported liquid water to the MEA. In contrast, no oscillations measured with a pin-type flow field with which only water in the vapour phase was transported to the MEA. Again, this suggests that a reaction involving water is connected with oscillations.

11. Experimental DPFC data on the following parameters were chosen to analyze and compare the trend with the model predictions of the previous chapter: (i) Anodic exchange current density, (ii) Inlet propane mole fraction, and (iii) Fuel cell operating temperature. Small current densities ($\mu A/cm^2$) were consistently observed when experiments were performed with propane as the fuel for the fuel cell. In contrast, much larger current densities (mA/cm^2) were observed in experiments with hydrogen as the fuel for the fuel cell. Time-on-stream experiments showed that extensive deactivation occurred when propane was the fuel. Even though the reason for the deactivation is unknown at the present time, there are at least two possibilities. CO poisoning of the metal atoms on the catalyst surface is one possibility. The other possibility is the deposition of coke or carbon on the reaction surface. Finally, the catalyst surface took a longer time to regenerate after its exposure to the propane than after its exposure to hydrogen. In general, the trend shown by the experimental results did not match the model predictions, except in the case for the anodic exchange current density. One of the reasons is that the model did not attempt to represent deactivation mathematically.

4.5 Conclusions

1. Extensive deactivation occurred after a few minutes of operating time with propane fuel at all conditions examined in this investigation.
2. CO may be one of the species causing deactivation.

3. The water involved in oscillations may be water that dissociates to form OH groups that react with CO that is adsorbed on some of the reaction sites.
4. At least part of the deactivation may be caused by reactions that are not electrochemical reactions.
5. When propane is the fuel, oscillations can be observed as the current density approaches open-circuit potential, even at current densities in the nano-Ampere region.
6. The trend shown by the experimental results did not match the model predictions, except in the case for the anodic exchange current density.

4.6 References

[1] H. A. Liebhafsky and L. W. Niedrach, "Fuel cells," *Journal of The Franklin Institute*, vol. 269, no. 4, pp. 257-267, 1960.

[2] Johnson Matthey PLC 2016, "Fuel cell applications," 2016. [Online]. Available: http://www.fuelcelltoday.com/applications.

[3] K. A. Adamson, “The fuel cell and hydrogen: Annual review, 2016,” *4th Energy Wave*, 2016.

[4] T. G. Services, *‘2004 fuel cell handbook: Advanced technology for generating electricity; series on renewable energy, Biofuels, Bioenergy, and Biobased products, 7th edition’*, 7th ed. Morgantown, WV: U.S. Department of Energy, Office of Fossil Energy, National Energy Technology Laboratory, 2004.

[5] G. J. K. Acres, "Recent advances in fuel cell technology and its applications," *Journal of Power Sources*, vol. 100, no. 1-2, pp. 60-66, 2001.

[6] G. Hoogers, “Introduction,” in *Fuel Cell Technology Handbook,* CRC Press, Boca Raton, 2003, pp. 2-37.

[7] H. G. Oswin, A. J. Hartner, and F. Malaspina, "A direct hydrocarbon/air fuel cell," *Nature*, vol. 200, no. 4903, pp. 256-257, 1963.

[8] W. T. Grubb, "Catalysis, electrocatalysis, and hydrocarbon fuel cells," *Nature*, vol. 198, no. 4883, pp. 883-884, 1963.

[9] W. T. Grubb and C. J. Michalske, "A high performance propane fuel cell operating in the temperature range of 150°C-200°C," *Journal of The Electrochemical Society*, vol. 111, no. 9, pp. 1015-1019, 1964.

[10] O. Savadogo and F. J. Rodriguez Varela, "Low-temperature direct propane polymer electrolyte membranes fuel cell (DPFC)," *Journal of New Materials for Electrochemical Systems*, vol. 4, no. 2, pp. 93-97, 2001.

[11] C. K. Cheng, J. L. Luo, K. T. Chuang, and A. R. Sanger, "Propane fuel cells using phosphoric-acid-doped polybenzimidazole membranes," *The Journal of Physical Chemistry B*, vol. 109, no. 26, pp. 13036-13042, 2005.

[12] F. J. Rodriguez Varela and O. Savadogo, "The effect of anode catalysts on the behavior of low temperature direct propane polymer electrolyte fuel cells (DPFC)," *Journal of New Materials for Electrochemical Systems,* vol. 9, no. 2, pp. 127-137, 2006.

[13] F. N. Büchi and S. Srinivasan, "Operating proton exchange membrane fuel cells without external humidification of the reactant gases fundamental aspects," *Journal of the Electrochemical Society*, vol. 144, no. 8, pp. 2767-2772, 1997.

[14] K. Ramya, J. Sreenivas, and K. S. Dhathathreyan, "Study of a porous membrane humidification method in polymer electrolyte fuel cells," *International Journal of Hydrogen Energy*, vol. 36, no. 22, pp. 14866-14872, 2011.

[15] D. G. Sanchez, T. Ruiu, K. A. Friedrich, J. Sanchez-Monreal, and M. Vera, "Analysis of the influence of temperature and gas humidity on the performance stability of polymer electrolyte membrane fuel cells," *Journal of The Electrochemical Society*, vol. 163, no. 3, pp. F150-F159, 2016.

[16] D. L. Wood, J. S. Yi, and T. V. Nguyen, "Effect of direct liquid water injection and interdigitated flow field on the performance of proton exchange membrane fuel cells," *Electrochimica Acta*, vol. 43, no. 24, pp. 3795-3809, 1998.

[17] L. W. Niedrach and M. Tochner, "Studies of hydrocarbon fuel cell anodes by the multipulse potentiodynamic method III. Behavior of saturated hydrocarbons on conducting porous teflon electrodes with a phosphoric acid electrolyte," *Journal of The Electrochemical Society*, vol. 114, no.1, pp. 17-22, 1967.

[18] M. C. Deibert and D. L. Williams, "Voltage oscillations of the H_2-CO system," *Journal of The Electrochemical Society*, vol. 116, no. 9, pp. 1290-1292, 1969.

[19] S. Balasubramanian and J. W. Weidner, "Analysis of an electrochemical filter for removing carbon monoxide from reformate hydrogen," *Journal of The Electrochemical Society*, vol. 162, no. 10, pp. E231-E236, 2015.

[20] Q. Li, R. He, J. Gao, J. O. Jensen, and N. J. Bjerrum, "The CO poisoning effect in PEMFCs operational at temperatures up to 200°C," *Journal of the Electrochemical Society*, vol. 150, no. 12, pp. A1599-A1605, 2003.

[21] B. W. Wojciechowski, "A theoretical treatment of catalyst decay," *The Canadian Journal of Chemical Engineering*, vol. 46, no. 1, pp. 48-52, 1968.

[22] H. Fukumoto, H. Maeda, and K. Mitsuda, "Oscillation phenomena on the cell voltage of PEFCs during CO poisoning," *Electrochemistry*, vol. 68, no. 10, pp. 794-800, 2000.

[23] H. Lu, L. Rihko-Struckmanna, R. Hanke-Rauschenbach, and K. Sundmacher, "Improved electrochemical CO removal via potential oscillations in serially connected PEM fuel cells with PtRu anodes," *Electrochimica Acta*, vol. 54, no. 4, pp. 1184-1191, 2009.

[24] H. Lu, L. Rihko-Struckmanna, and K. Sundmacher, "Spontaneous oscillations of cell voltage, power density, and anode exit CO concentration in a PEM fuel cell," *Physical Chemistry Chemical Physics*, vol. 13, no. 40, pp. 18179-18185, 2011.

[25] J. Lee, C. Eickes, M. Eiswirth, and G. Ertl, "Electrochemical oscillations in the methanol oxidation on Pt," *Electrochimica Acta*, vol. 47, no. 13, pp. 2297-2301, 2002.

[26] J. Zhang, J. D. Fehribach, and R. Datta, "Mechanistic and bifurcation analysis of anode potential oscillations in PEMFCs with CO in anode feed," *Journal of The Electrochemical Society*, vol. 151, no. 5, pp. A689-A697, 2004.

[27] P. P. Lopes, E. A. Ticianelli, and H. Varela, "Potential oscillations in a proton exchange membrane fuel cell with a Pd-Pt/C anode," *Journal of Power Sources*, vol. 196, no. 1, pp. 84-89, 2011.

[28] T. Kadyk, S. Kirsch, R. Hanke-Rauschenbach, and K. Sundmacher, "Autonomous potential oscillations at the Pt anode of a polymer electrolyte membrane fuel cell under CO poisoning," *Electrochimica Acta*, vol. 56, no. 28, pp. 10593-10602, 2011.

[29] H. A. Gasteiger, N. Marković, P. N. Ross, Jr., and E. J. Cairns, "Carbon monoxide electrooxidation on well-characterized platinum-ruthenium alloys," *The Journal of Physical Chemistry*, vol. 98, no. 2, pp. 617-625, 1994.

[30] Y. Si, R. Jiang, J. Lin, H. R. Kunz, and J. M. Fenton, "CO tolerance of carbon-supported platinum-ruthenium catalyst at elevated temperature and atmospheric pressure in a PEM fuel cell," *Journal of The Electrochemical Society*, vol. 151, no. 11, pp. A1820-A1824, 2004.

[31] Y. Zhu, A. Y. Tremblay, G. A. Facey, and M. Ternan, "Petroleum diesel and biodiesel fuels used in a direct hydrocarbon phosphoric acid fuel cell," *Journal of Fuels*, vol. 2015, pp. 1-9, 2015.

[32] P. Polverino, A. Esposito, and C. Pianese, "Experimental validation of a lumped model of single droplet deformation, oscillation and detachment on the GDL surface of a PEM fuel cell," *International Journal of Hydrogen Energy*, vol. 38, no. 21, pp. 8934-8953, 2013.

[33] Y. Zhai, J. St-Pierre, and M. S. Angelo, "The impact of operating conditions on the performance effect of selected airborne PEMFC contaminants," *ECS Transactions*, vol. 50, no. 2, pp. 635-647, 2013.

[34] J. A. Nogueira, I. K. Peña Arias, R. Hanke-Rauschenbach, T. Vidakovic-Koch, H. Varela, and K. Sundmacher, "Autonomous voltage oscillations in a direct methanol fuel cell," *Electrochimica Acta*, vol. 212, pp. 545-552, 2016.

Chapter 5: Linkages

5.1 Results and discussion

This section provides a link between the computational results of Chapter 3 and the experimental results of Chapter 4. Chapter 3 identified the following key parameters that had greatest effect on the overall performance of a direct propane fuel cell (DPFC): (i) Anodic exchange current density, (ii) Cathode exchange current density, (iii) Inlet propane mole fraction, (iv) Inlet propane molar flow rate, (v) Fuel cell operating pressure, and (vi) Fuel cell operating temperature. These key parameters mainly affected the catalyst i.e. the surface reaction rate. Chapter 4 described experimental work on a DPFC that was performed in our laboratory to assess the model predictions. Experimental DPFC data on the following parameters were chosen to analyze the trend: (i) Anodic exchange current density, (ii) Inlet propane mole fraction, and (iii) Fuel cell operating temperature. Small current densities ($\mu A/cm^2$) were consistently observed when experiments were performed with propane as the fuel for the fuel cell than those obtained from the computational results (mA/cm^2). Time-on-stream experiments showed that extensive deactivation occurred when propane was the fuel. In general, the trend shown by the experimental results did not match the model predictions, except in the case for the anodic exchange current density. One of the reasons is that the model did not attempt to represent deactivation mathematically.

Experimental work was also conducted for the parameter, type of anode flow field / humidifier, with both hydrogen and hydrocarbon (propane) fuels. This work indicated the effect of water, in the liquid phase, at the anode on the electrochemical reaction in the presence and absence of the deactivation phenomena. Apart from that, the effects of various parameters (i.e. fuel cell operating temperature, anode catalyst composition, and anode flow field / humidifier) on oscillations in DPFC were also studied. The oscillation phenomena were not included in the

modeling work to reproduce similar trends in the two works. In addition, following possible reasons might have also contributed for the difference in the two results.

1. Fuel cell operating temperature: To avoid the 80°C temperature limitation of commercial Nafion-based MEAs [1], the fuel cell experiments were conducted at 65°C. In contrast, the operating temperature used in the model was 150°C.
2. Anode humidification: Humidification with liquid water at 65°C using an interdigitated flow field (IDFF) allowed longer water residence times within the fuel cell. In contrast, the modeling was performed at 150°C with water in the vapour phase, which caused shorter water residence times.

Furthermore, the computational results consistently showed that the overall performance of the DPFC was primarily influenced by the electrochemical reaction over the entire computed polarization curve. In contrast, the experimental results showed that some portion of the polarization curve was influenced by the deactivation phenomena and not the electrochemical reaction.

5.2 Recommendations

1. The oscillation and deactivation phenomena should be included in the DPFC model to investigate their effect on the fuel cell performance.
2. The DPFC experiments should be conducted using lab prepared modified zirconium phosphate (m-ZrP) MEA to eliminate the fuel cell temperature constraints with Nafion-based MEAs. The experimental data would provide more insight into the oscillating phenomena of the DPFC and also on the fuel cell performance. The lab m-ZrP MEAs are capable of withstanding temperatures greater than 120°C [2]. However, further development of these MEAs is required before performing these DPFC experiments.

5.3 References

[1] J. O. Bockris and S. Srinivasan, “Fuel cells: Their electrochemistry,” in *Electrochemical Combustion of Organic Substances*, McGraw-Hill, New York, 1969, pp. 357-411.

[2] A. Al-Othman, A. Y. Tremblay, W. Pell, S. Letaief, T. J. Burchell, B. A. Peppley, and M. Ternan, "Zirconium phosphate as the proton conducting material in direct hydrocarbon polymer electrolyte membrane fuel cells operating above the boiling point of water," *Journal of Power Sources*, vol. 195, no. 9, pp. 2520-2525, 2010.

Chapter 6: Conclusions

6.1 Summary

This section is summarising the computational results of Chapter 3 and the experimental results of Chapter 4. Chapter 3 presents the simulation work, which is based on computational fluid dynamics (CFD), specifically on FreeFem++ software. The code describing a direct propane fuel cell (DPFC) [1] was modified and then a parametric study was performed. The parametric study successfully identified key parameters that could enhance the overall performance of a DPFC. The key parameters were: (i) Anodic exchange current density, (ii) Cathode exchange current density, (iii) Inlet propane mole fraction, (iv) Inlet propane molar flow rate, (v) Fuel cell operating pressure, and (vi) Fuel cell operating temperature. Chapter 4 describes the results of DPFC experiments, using commercial Nafion-Pt MEA, that were performed to investigate some of the key parameters. Time-on-stream plots of cell potential difference and current density were also generated. Overall performance of the DPFC was determined based on the polarization curve data extracted from the time-on-stream plots. Effect of anode flow field / humidifier type on a fuel cell fueled by hydrogen and propane was also investigated. Apart from that, the effects of various parameters (i.e. fuel cell operating temperature, anode catalyst composition, and anode flow field / humidifier) on oscillations in DPFC were also studied.

6.2 Conclusions

1. The computational work identified key parameters that affected the catalyst (the surface reaction rate) and had greatest effect on the overall performance of a direct propane fuel cell (DPFC).

2. In the computational work, the overall performance over the entirety of the computed polarization curve was influenced primarily by the electrochemical reaction rate (overpotential).
3. Extensive deactivation and oscillations were seen in most of the DPFC experiments.
4. The quantity of water in the liquid phase at the anode was connected with the occurrence of oscillations in the DPFC.
5. The DPFC experiments generated smaller current densities in the nanoscale.
6. The trend shown by the experimental results did not match the model predictions, except in the case for the anodic exchange current density.

6.3 Contribution to knowledge

1. It is the first low temperature direct hydrocarbon fuel cell (DHFC) model, which showed that the electrochemical reaction rate was the rate controlling mechanism over the entirety of the computed polarization curve.
2. It is the first study that reported rapid deactivation of a DHFC fueled with propane.
3. It is the first study that reported oscillations in a DHFC at nanoscale current densities approaching open-circuit potential (OCP).
4. The studies reported here showed that the performance of the direct propane fuel cell (DPFC) with an interdigitated flow field at the anode, humidified with water in the liquid phase, was better than a pin-type anode flow field, humidified with water in the vapour phase.

6.4 References

[1] H. Khakdaman, Y. Bourgault, and M. Ternan, "A Mathematical model of a direct propane fuel cell," *Journal of Chemistry*, vol. 2015, pp. 1-13, 2015.

Appendix A: Description of Equipment

Two cases were considered for the experimental work with a single cell direct propane fuel cell (DPFC) using a commercial Nafion membrane. The two cases were based on the two separate anode humidification methods and its effect on the overall performance of the DPFC. The experiments performed under case (a) used liquid water for anode humidification, while case (b) considered a DPFC with a bubble humidifier to humidify the fuel cell anode.

In general, the DPFC was operated under the galvanostatic mode at temperatures of 23 and 65°C, and at a pressure of 1 atm. The case (a) DPFC was operated at both the temperatures. But, the case (b) DPFC was performed only at a temperature of 65°C.

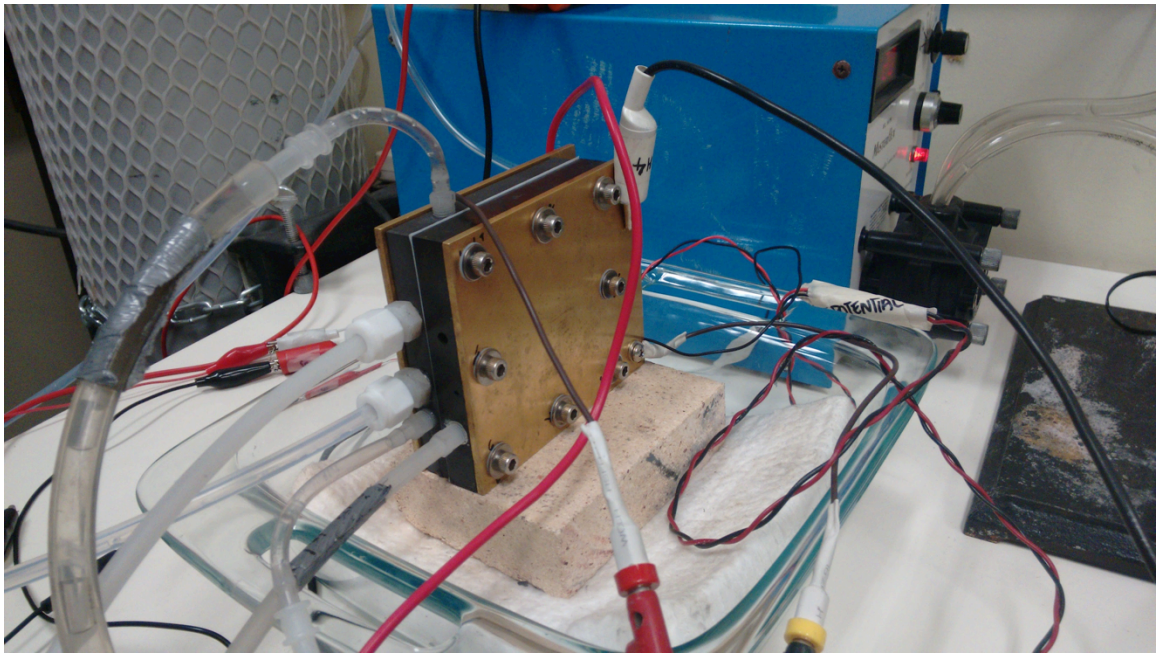


Figure A.1 DPFC at 23°C using liquid water for anode humidification.

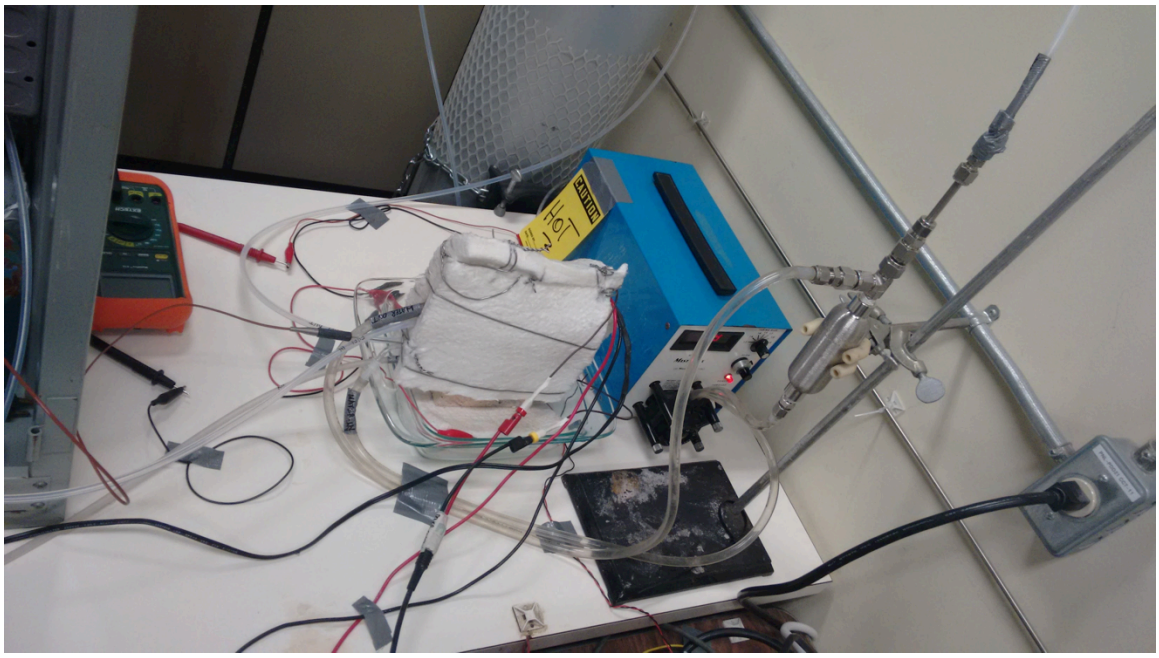


Figure A.2 DPFC at 65°C with peristaltic pump for water circulation through IDFF anode.

The DPFC operation carried out at 23 and 65°C, is shown in Figure A.1 and Figure A.2 respectively. Two different Nafion Pt-based MEAs were used with an effective area of 25 cm^2. Experiments were conducted using a Nafion 212 MEA, which had a Pt (platinum) catalyst loading of 1 mg/cm^2 at both the electrodes. While the other set of experiments were performed using a Nafion 117 MEA that had a catalyst loading of 4 mg/cm^2 for both Pt-Ru (platinum-ruthenium) catalyst at the anode and Pt catalyst at the cathode. The case (a) DPFC was operated with both the MEAs. But, the case (b) DPFC was operated only with the Nafion 117 MEA. The DPFC anode was fed continuously with fuels such as propane gas (~100% pure, 2.5 grade) or hydrogen gas. At the cathode, compressed air (21% oxygen, medical grade) was fed continuously. A mixture of pure propane and nitrogen gas stream was considered for some experiments of case (a) DPFC. The purpose of using nitrogen was to vary the inlet propane concentration at the DPFC anode. The feed gas inlet lines to the DPFC were installed with a rotameter for the flow measurements, which is shown in Figure A.3. The exit lines from the fuel

cell anode, and the cathode were bubbled through their respective water-filled open jars, which were placed in the fume hood (as shown in Figure A.7 and A.8).



Figure A.3 Temperature-controlling and flow measurement unit of DPFC.

The temperature-controlling unit of the DPFC system is shown in Figure A.3. The temperature-controlling unit of the fuel cell system consisted of a PID controller, a thermocouple (i.e. J-type for the fuel cell and T-type for the bubble humidifier), and a heating element. As a standard operating procedure (SOP), the DPFC was operated with hydrogen-air after every propane-air operation to regenerate the catalyst reaction sites. In the case of the hydrogen-air operation, the galvanostatic mode was achieved by using the power-supply unit shown in Figure A.4. The power-supply unit produces currents that ranged from -10 to 10 A. The electrical connections of the hydrogen-air operation of the DPFC are shown in Figure A.5. The deactivation process of the DPFC was sufficiently fast that a polarization curve could not be

generated at currents above 10^4 μA. Therefore, the propane-air operation was carried out at a μA current range by putting a fixed resistor and an ammeter in the fuel cell circuit instead of a power controller. The electrical circuit of the DPFC with a fixed resistor is represented in Figure A.6.

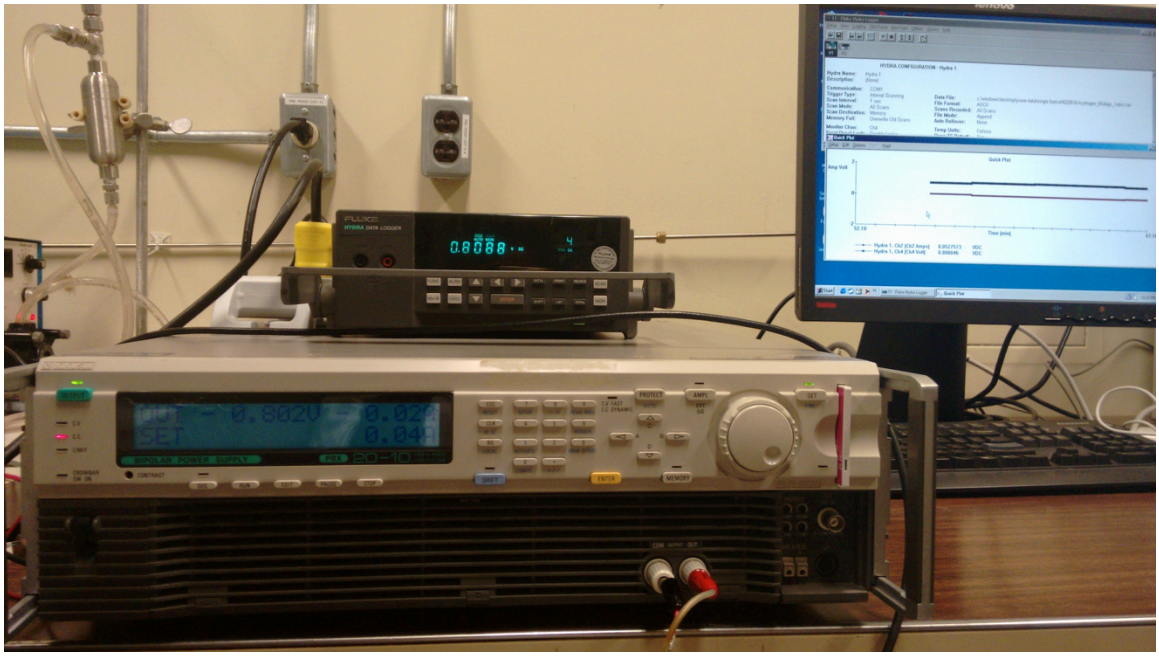


Figure A.4 Power-supply unit (below) and data logger (above) of DPFC.

The time-on-stream measurement of cell potential was obtained by measuring the potential difference between the DPFC electrodes. The time-on-stream measurement of current density was achieved by measuring the potential difference across the fixed resistor. The time-on-stream measurements were done and recorded by using a data logger shown in Figure A.4. The performance of the DPFC was analyzed by using the time-on-stream measurements of cell potential difference and current density that was obtained for the following five resistors i.e. 1 MΩ, 10 kΩ, 980 Ω, 330 Ω, and 118 Ω. For the DPFC system, the current range provided by the following five resistors were (a) 1 MΩ: 0 to 1 μA, (b) 10 kΩ: 1 to 100 μA, (c) 980 Ω: 100 to 1000 μA, (d) 330 Ω: 1000 to 2000 μA, and (e) 118 Ω: 2000 to 4000 μA.

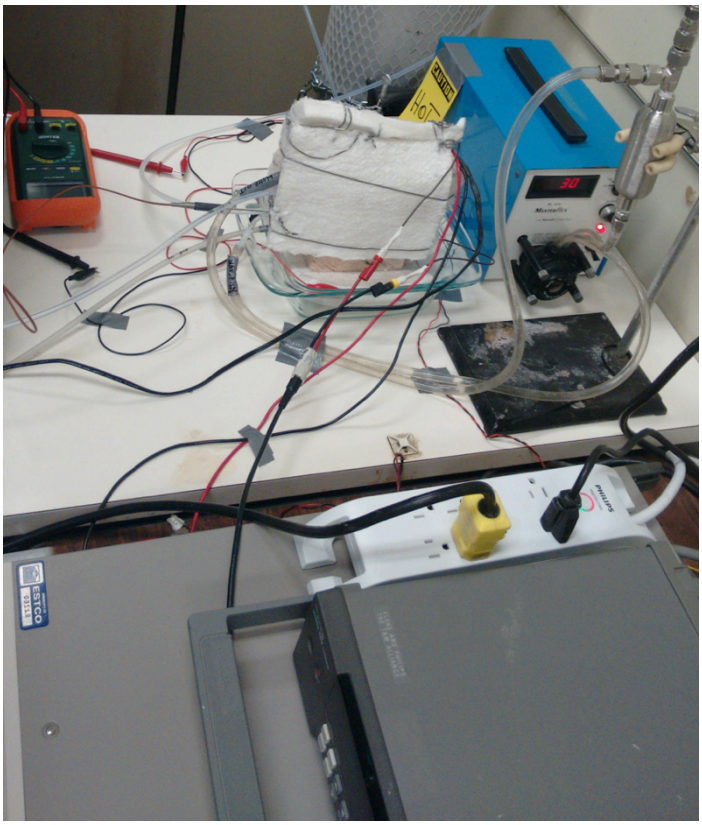


Figure A.5 Hydrogen-air/ propane-air operation of DPFC using power-supply unit.

Case (a): A single cell-DPFC with liquid water for anode humidification

The experimental set-up used for case (a) is shown in Figure A.7. The DPFC shown in Figure A.7 consisted of a Nafion Pt-based MEA, an interdigitated flow field (IDFF) for feed distribution at the anode, and a pin-type flow field at the cathode. At the anode, the propane or the hydrogen gas was fed continuously at a higher flow rate through one of the flow channels of the IDFF, which is shown in Figure A.9. The other flow channel was continuously fed with the liquid water at a lower flow rate through a peristaltic pump, which is shown in Figure A.2. As shown in the figure, the peristaltic pump consisted of a 75 ml vessel for feeding and recirculating water. The flow rate range of the peristaltic pump was 8 to 38 ml/min, which maintained a minuscule flow through the fuel cell. The frequency of refilling the vessel was once in every 3 to 4 h for the continuous operation of the DPFC at 23°C and once in every 1 to 2 h for the DPFC

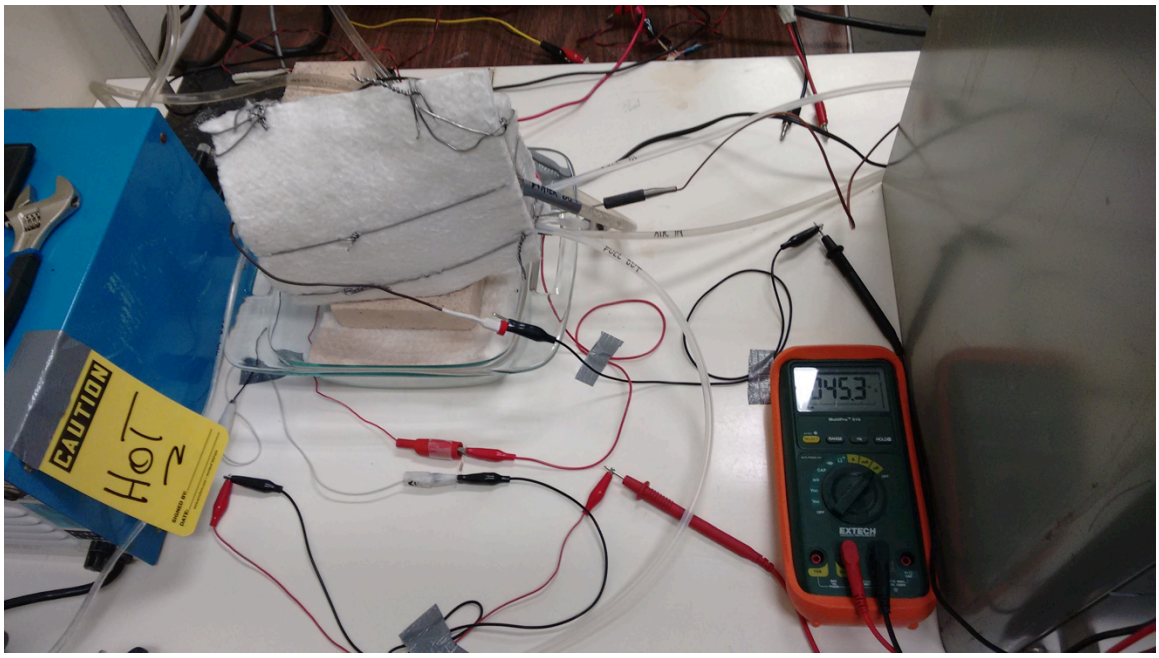


Figure A.6 Propane-air operation of DPFC using a fixed resistor and an ammeter in the fuel cell circuit.

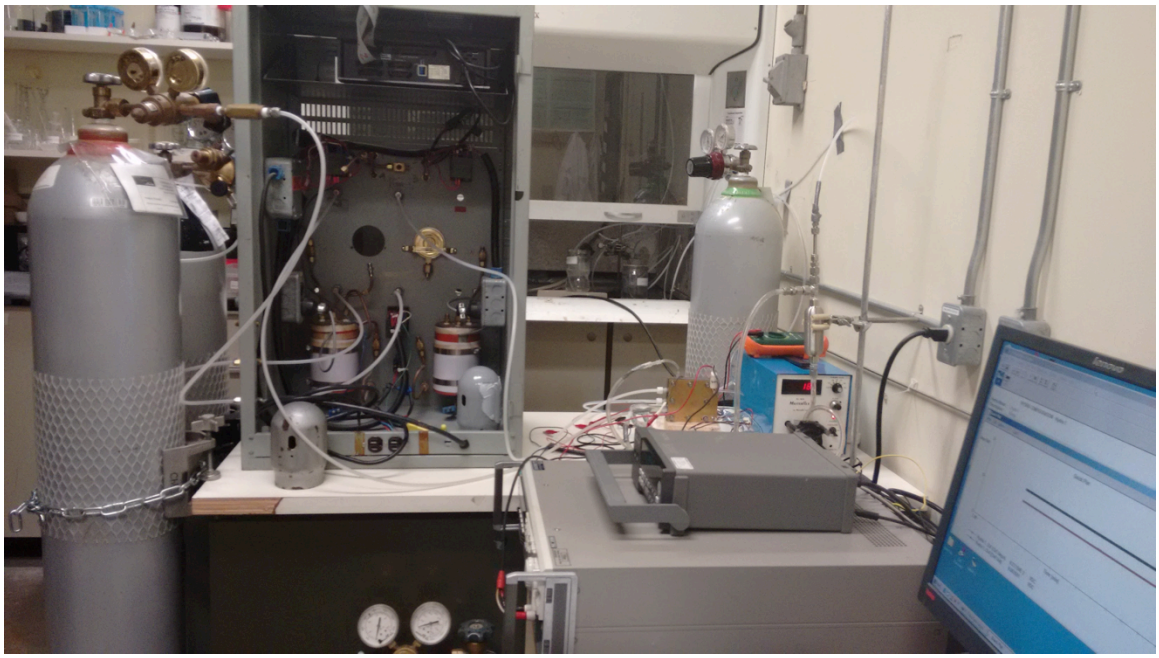


Figure A.7 Experimental set-up of DPFC with IDFF anode and liquid water for anode humidification.

continuous operation at 65°C. At the cathode, the compressed air was fed continuously through the pin-type flow channels shown in Figure A.9.



Figure A.8 DPFC exit lines with water-filled open jars placed within the fume hood. Water-filled open jar for anode (left) and for cathode (right).

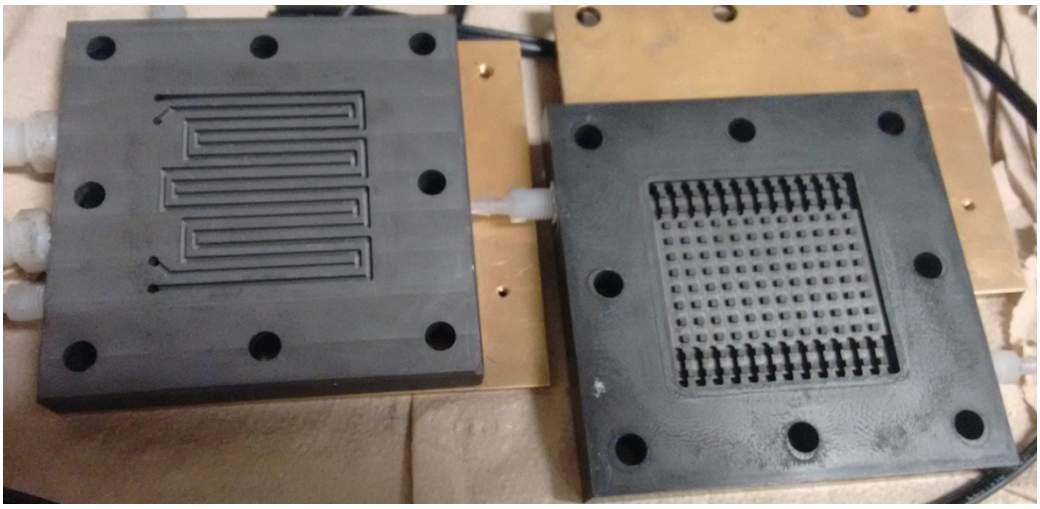


Figure A.9 Flow fields of DPFC using liquid water for anode humidification. IDFF anode (left) and pin-type cathode flow field (right).

The following sequence of operation was followed after turning on the data logger: (a) first, the

air was fed at the fuel cell cathode, (b) then, the hydrogen/ the propane was fed at the fuel cell anode inlet-1 (topmost inlet on the left-hand side of IDFF anode shown in Figure A.9), and (c) finally, the liquid water was fed at the fuel cell anode inlet-2 (bottommost inlet on the left-hand side of IDFF anode shown in Figure A.9).

For 100% propane inlet concentration, the rotameter reading for propane was 5 mm (178 Scm^3/min). For 74% propane inlet concentration, the rotameter readings were 3 mm (131 Scm^3/min) for propane and 34 mm (47 Scm^3/min) for nitrogen. For 34% propane inlet concentration, the rotameter readings were 0 mm (60 Scm^3/min) for propane and 85 mm (119 Scm^3/min) for nitrogen. For all the experiments, the rotameter reading for compressed air was maintained at 100 mm (2451 Scm^3/min). The above float positions of the rotameter provided an approximately same exit gas bubbling flow rate.

Case (b): A single cell-DPFC with a bubble humidifier

The experimental set-up used for case (b) is shown in Figure A.10. The DPFC shown in Figure A.10 consisted of a Nafion Pt-based MEA and a pin-type flow field for feed distribution at the electrodes.

Figure A.10 shows two 1100 ml bubble humidifiers, but only one humidifier (i.e. the leftmost shown in Figure A.10) was used for the case (b) DPFC. At the start of the experiment, approximately a quarter of the humidifier was filled with the liquid water. After which the humidifier was heated up to its set temperature. A steady and continuous operation of the fuel cell at 65°C was achieved by maintaining the bubble humidifier at 85°C and the fuel cell inlet line from the humidifier at 115°C.

The following sequence of operation was followed after turning on the data logger: (a) first, the air was fed at the fuel cell cathode and (b) then, the hydrogen/ the propane was fed at the fuel cell anode through the bubble humidifier (as seen in Figure A.10). The flow measurement of the fuel was done before passing through the bubble humidifier. For 100%

propane inlet concentration, the rotameter reading for propane was 10 mm (296 Scm^3/min) and 105 mm (2494 Scm^3/min) for compressed air. The above float positions of the rotameter achieved an approximately same exit gas bubbling flow rate.

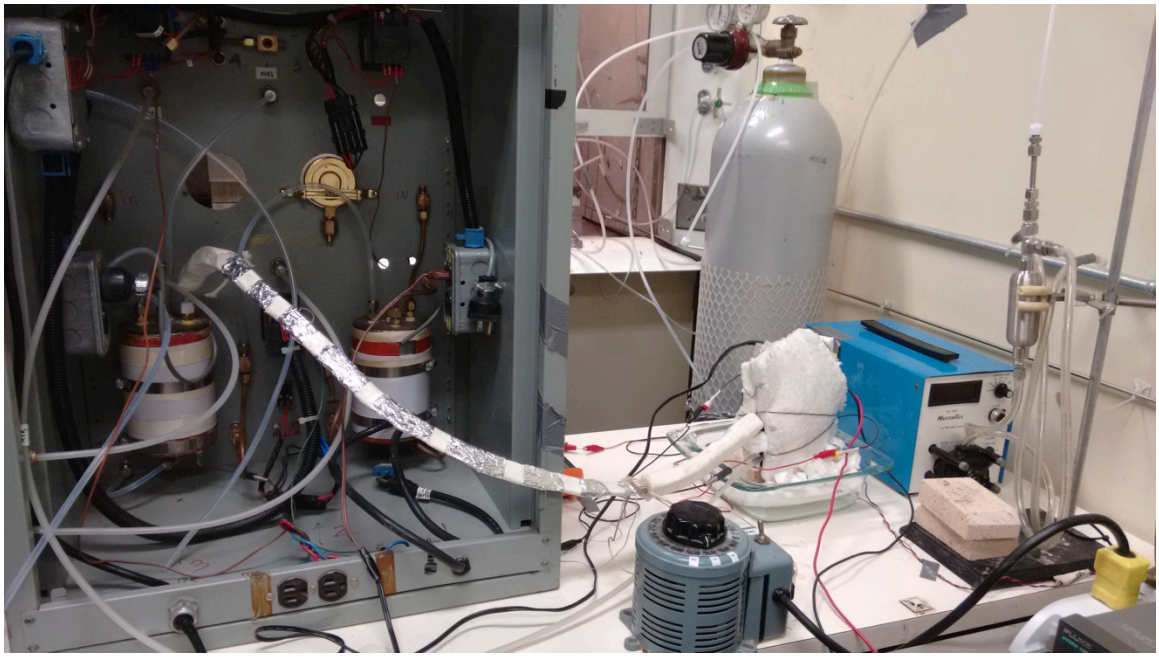


Figure A.10 Experimental set-up of DPFC with pin-type anode FF and a bubble humidifier.

Figure A.11 represents the flow field arrangement of the case (b) DPFC. At the anode, the propane or the hydrogen gas was fed continuously through the pin-type flow channels. And, at the cathode, the pin-type flow channels were fed continuously with the compressed air.

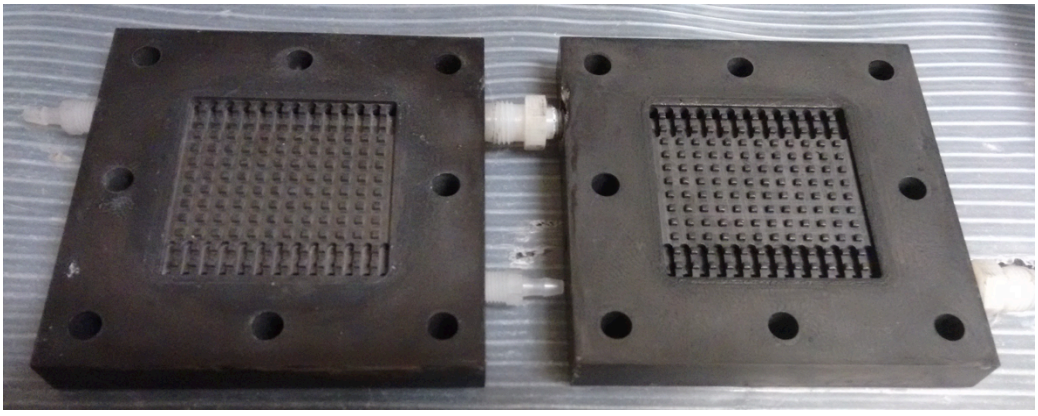


Figure A.11 Flow fields of DPFC using a bubble humidifier for anode humidification; pin-type flow field for both anode (right) and cathode (left).

Appendix B: Time-on-stream graphs of cell potential difference and current density

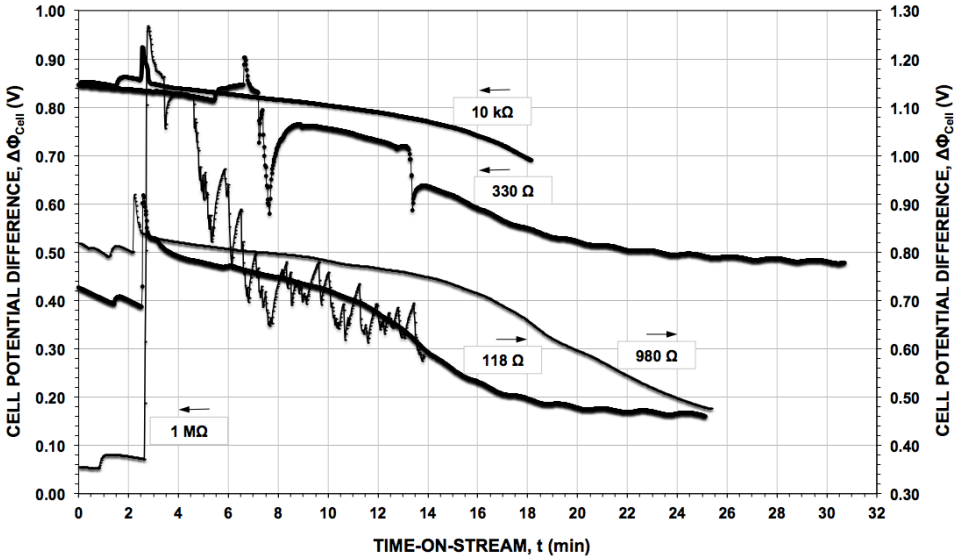


Figure B.1 Cell potential difference, $\Delta\Phi_{cell}$ (V) versus time-on-stream, t (min) for a DPFC with 100% propane, IDFF anode humidified with liquid water, Pt anode catalyst, 65°C, 1 atm, and using fixed resistors of 1 MΩ, 10 kΩ, 980 Ω, 330 Ω, and 118 Ω.

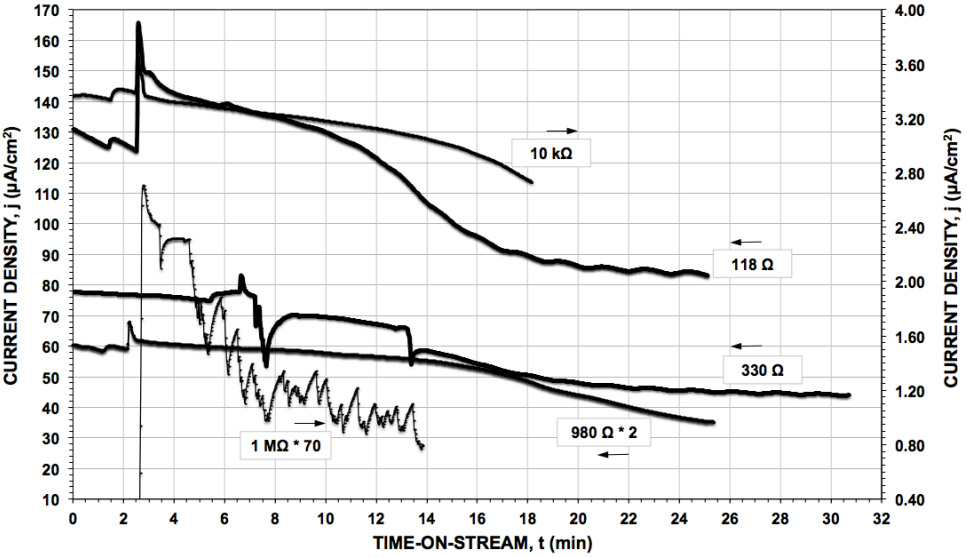


Figure B.2 Current density, j ($\mu A/cm^2$) versus time-on-stream, t (min) for a DPFC with 100% propane, IDFF anode humidified with liquid water, Pt anode catalyst, 65°C, 1 atm, and using fixed resistors of 1 MΩ, 10 kΩ, 980 Ω, 330 Ω, and 118 Ω. A factor of 2 and 70 has been multiplied to the curve data of 980 Ω and 1 MΩ respectively.

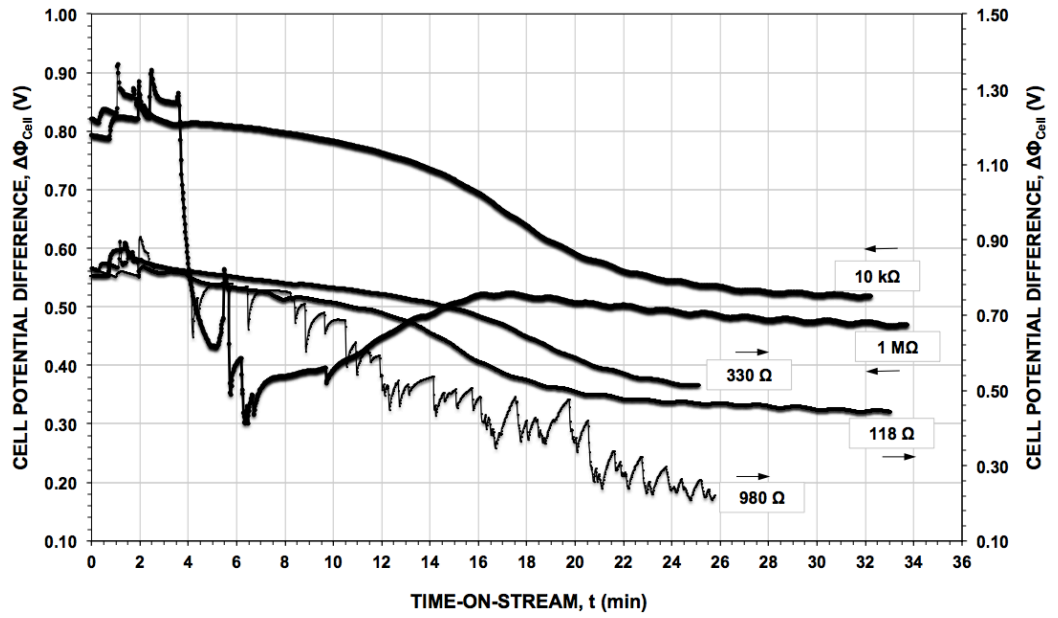


Figure B.3 Cell potential difference, $\Delta\Phi_{cell}$ (V) versus time-on-stream, t (min) for a DPFC with 74% propane, IDFF anode humidified with liquid water, Pt anode catalyst, 65°C, 1 atm, and using fixed resistors of 1 MΩ, 10 kΩ, 980 Ω, 330 Ω, and 118 Ω.

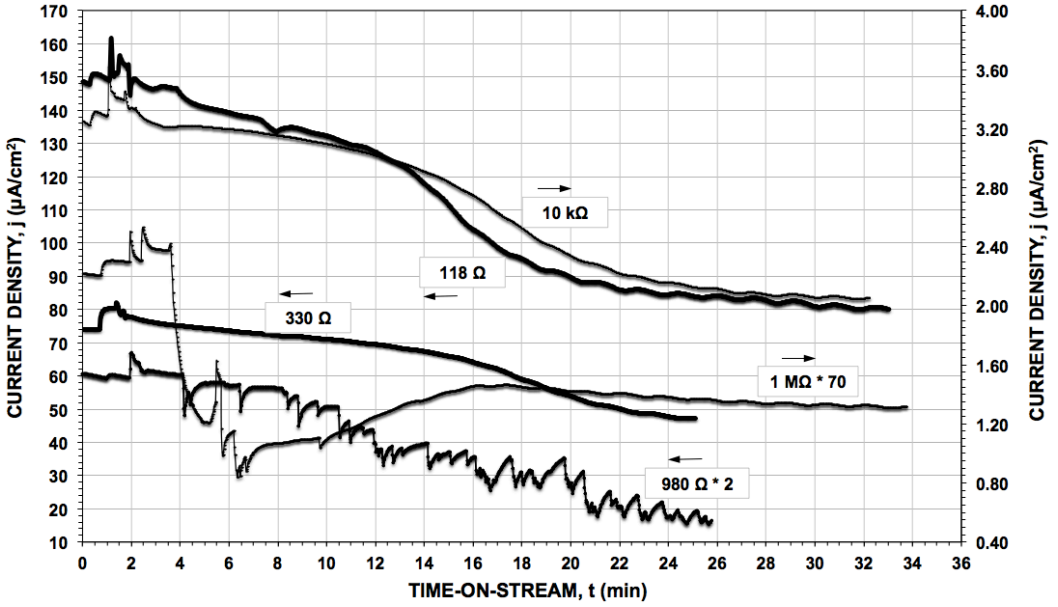


Figure B.4 Current density, j ($\mu A/cm^2$) versus time-on-stream, t (min) for a DPFC with 74% propane, IDFF anode humidified with liquid water, Pt anode catalyst, 65°C, 1 atm, and using fixed resistors of 1 MΩ, 10 kΩ, 980 Ω, 330 Ω, and 118 Ω. A factor of 2 and 70 has been multiplied to the curve data of 980 Ω and 1 MΩ respectively.

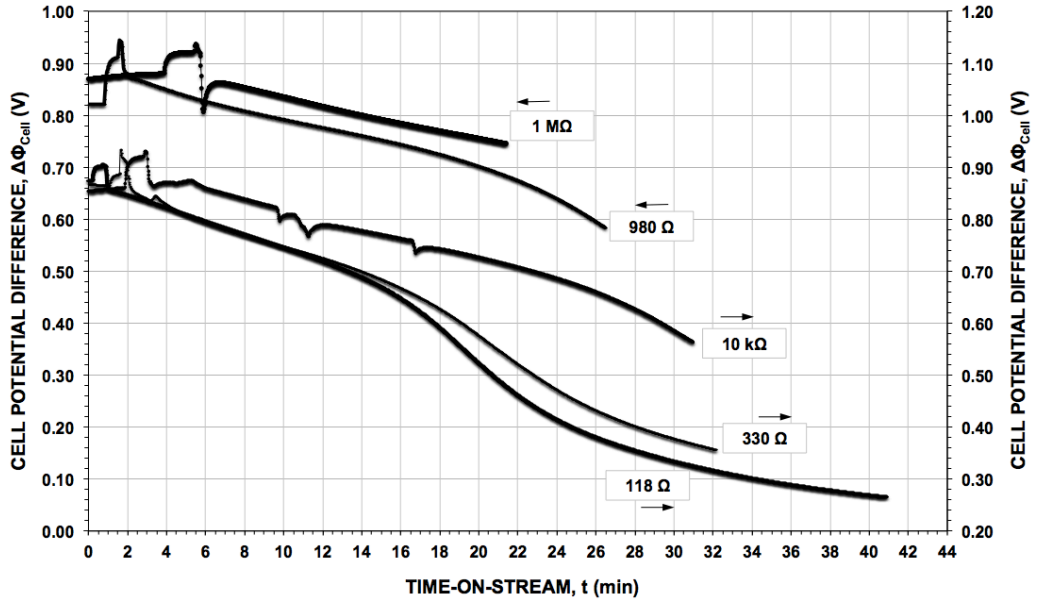


Figure B.5 Cell potential difference, $\Delta\Phi_{cell}$ (V) versus time-on-stream, t (min) for a DPFC with 100% propane, IDFF anode humidified with liquid water, Pt anode catalyst, 23°C, 1 atm, and using fixed resistors of 1 MΩ, 10 kΩ, 980 Ω, 330 Ω, and 118 Ω.

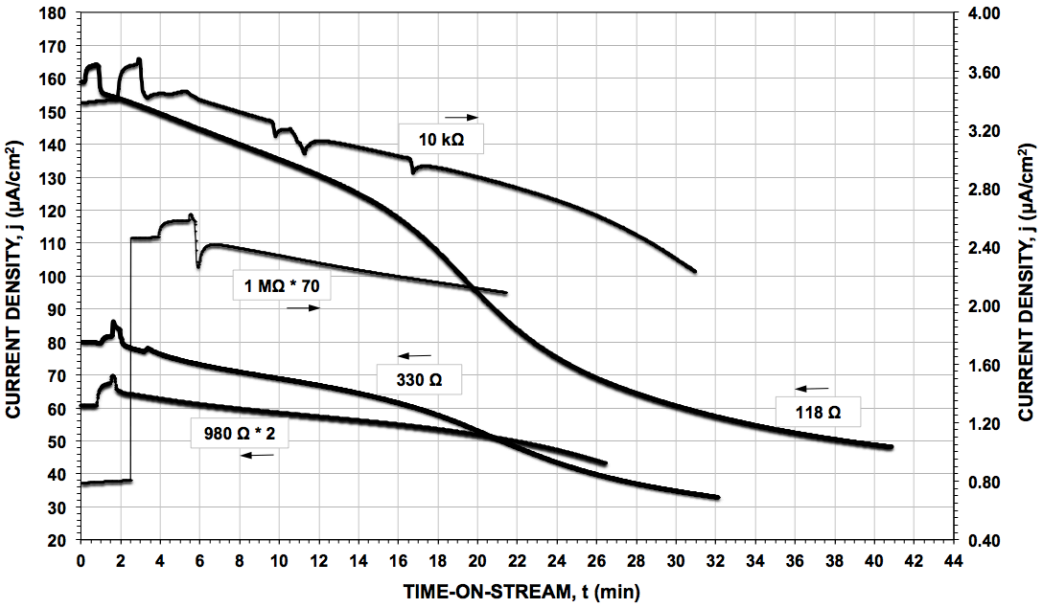


Figure B.6 Current density, j ($\mu A/cm^2$) versus time-on-stream, t (min) for a DPFC with 100% propane, IDFF anode humidified with liquid water, Pt anode catalyst, 23°C, 1 atm, and using fixed resistors of 1 MΩ, 10 kΩ, 980 Ω, 330 Ω, and 118 Ω. A factor of 2 and 70 has been multiplied to the curve data of 980 Ω and 1 MΩ respectively.

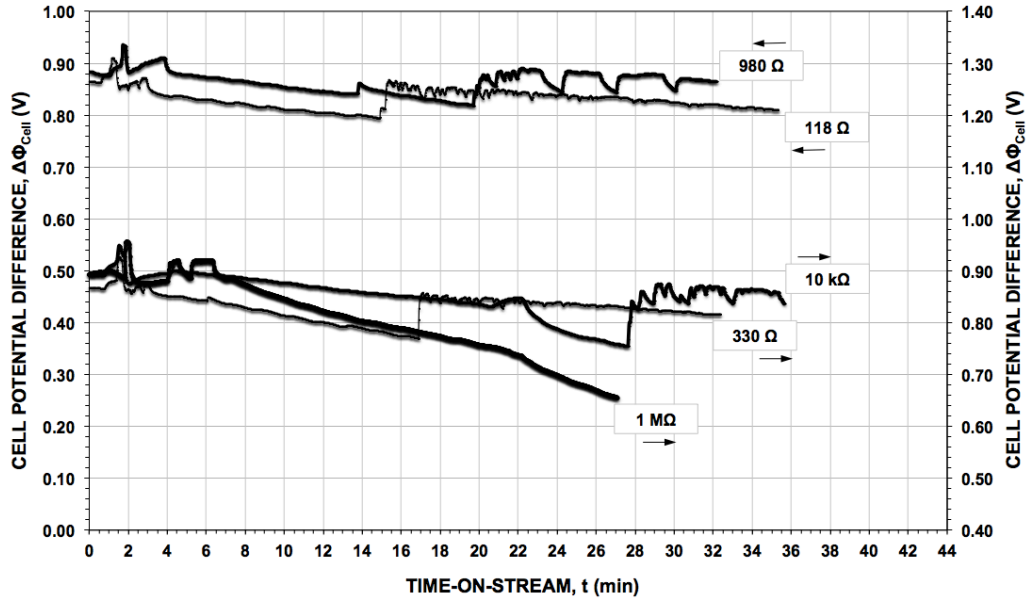


Figure B.7 Cell potential difference, $\Delta\Phi_{cell}$ (V) versus time-on-stream, t (min) for a DPFC with 100% propane, IDFF anode humidified with liquid water, Pt-Ru anode catalyst, 65°C, 1 atm, and using fixed resistors of 1 MΩ, 10 kΩ, 980 Ω, 330 Ω, and 118 Ω.

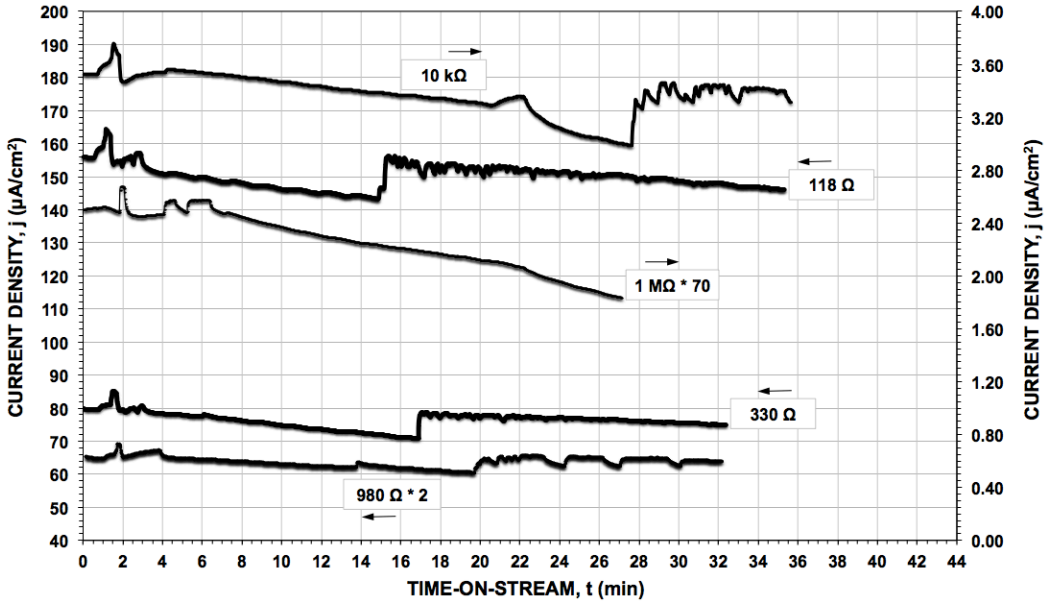


Figure B.8 Current density, j ($\mu A/cm^2$) versus time-on-stream, t (min) for a DPFC with 100% propane, IDFF anode humidified with liquid water, Pt-Ru anode catalyst, 65°C, 1 atm, and using fixed resistors of 1 MΩ, 10 kΩ, 980 Ω, 330 Ω, and 118 Ω. A factor of 2 and 70 has been multiplied to the curve data of 980 Ω and 1 MΩ respectively.

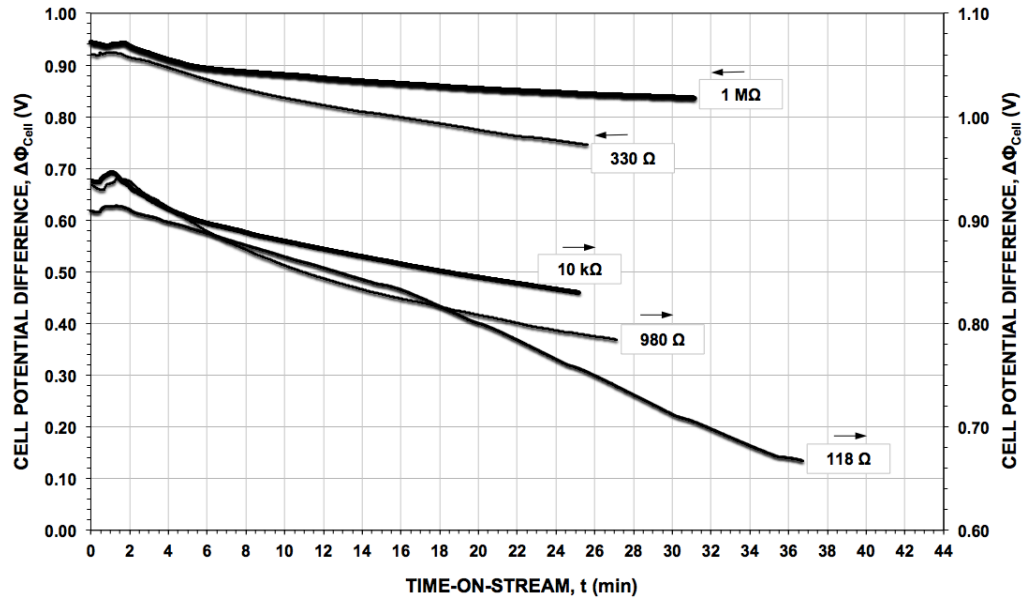


Figure B.9 Cell potential difference, $\Delta\Phi_{cell}$ (V) versus time-on-stream, t (min) for a DPFC with 100% propane, pin-type anode flow field humidified with a bubble humidifier, Pt-Ru anode catalyst, 65°C, 1 atm, and using fixed resistors of 1 MΩ, 10 kΩ, 980 Ω, 330 Ω, and 118 Ω.

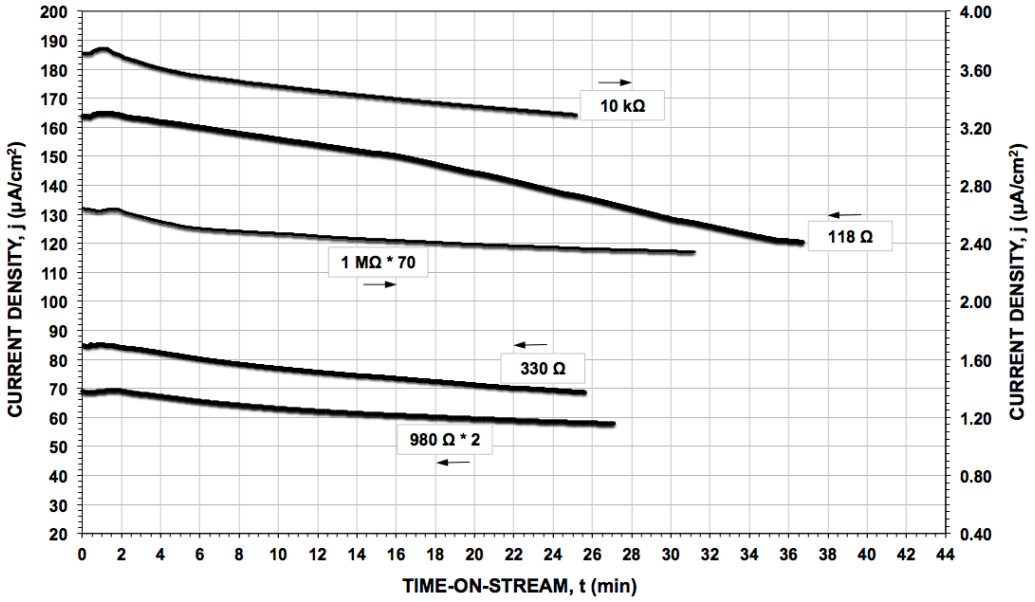


Figure B.10 Current density, j ($\mu A/cm^2$) versus time-on-stream, t (min) for a DPFC with 100% propane, pin-type anode flow field humidified with a bubble humidifier, Pt-Ru anode catalyst, 65°C, 1 atm, and using fixed resistors of 1 MΩ, 10 kΩ, 980 Ω, 330 Ω, and 118 Ω. A factor of 2 and 70 has been multiplied to the curve data of 980 Ω and 1 MΩ respectively.

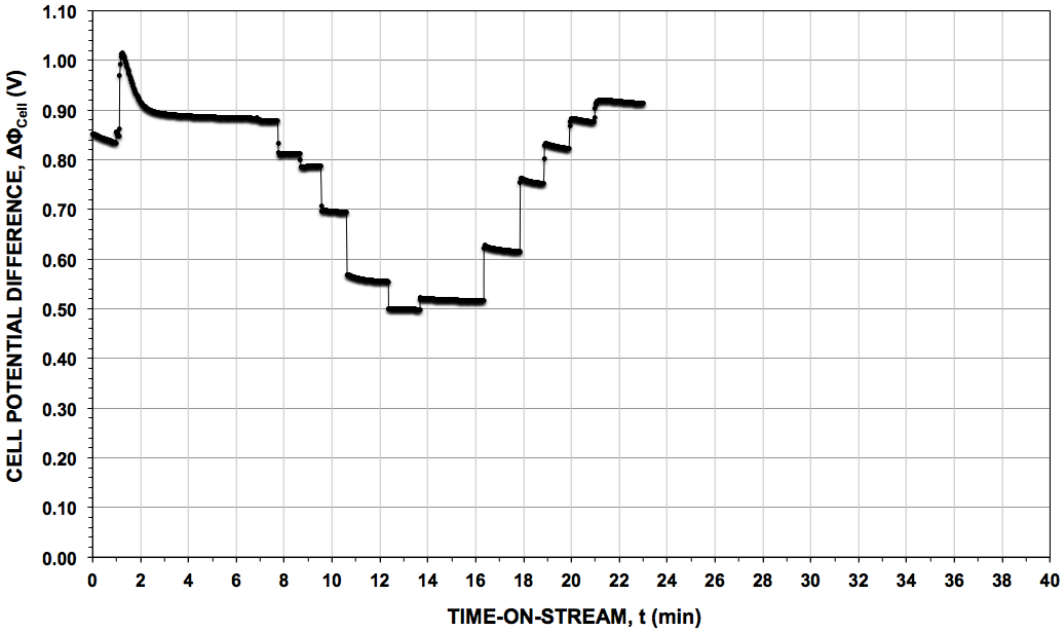


Figure B.11 Cell potential difference, $\Delta\Phi_{cell}$ (V) versus time-on-stream, t (min) for a hydrogen-air operation after a DPFC operation with 100% propane, IDFF anode humidified with liquid water, Pt anode catalyst, 23°C, 1 atm, and using a 330 Ω fixed resistor.

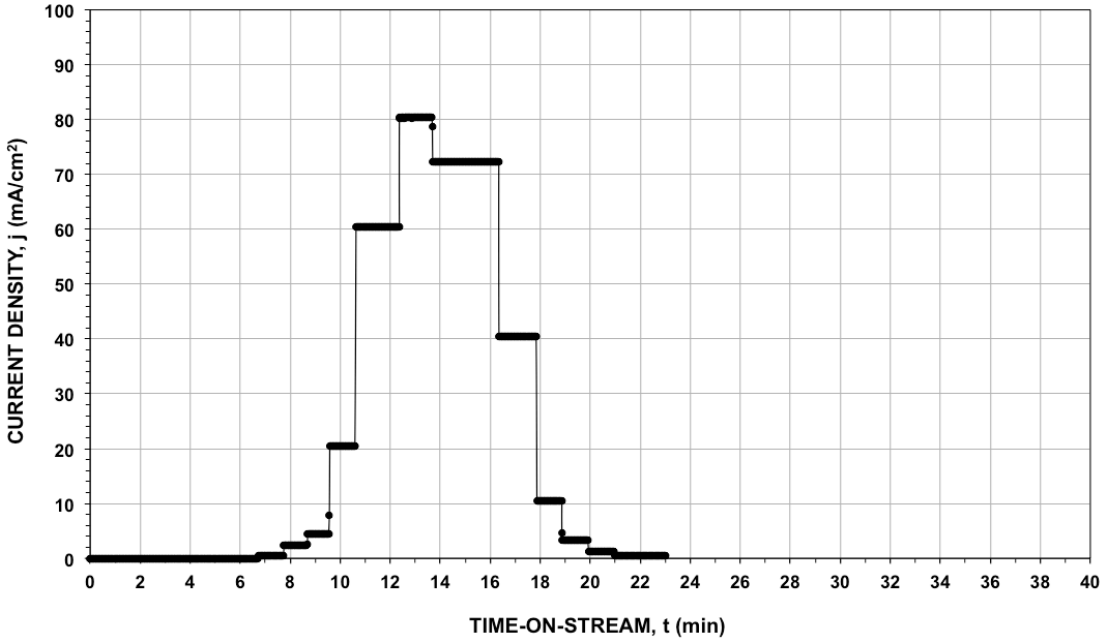


Figure B.12 Current density, j ($\mu A/cm^2$) versus time-on-stream, t (min) for a hydrogen-air operation after a DPFC operation with 100% propane, IDFF anode humidified with liquid water, Pt anode catalyst, 23°C, 1 atm, and using a 330 Ω fixed resistor.

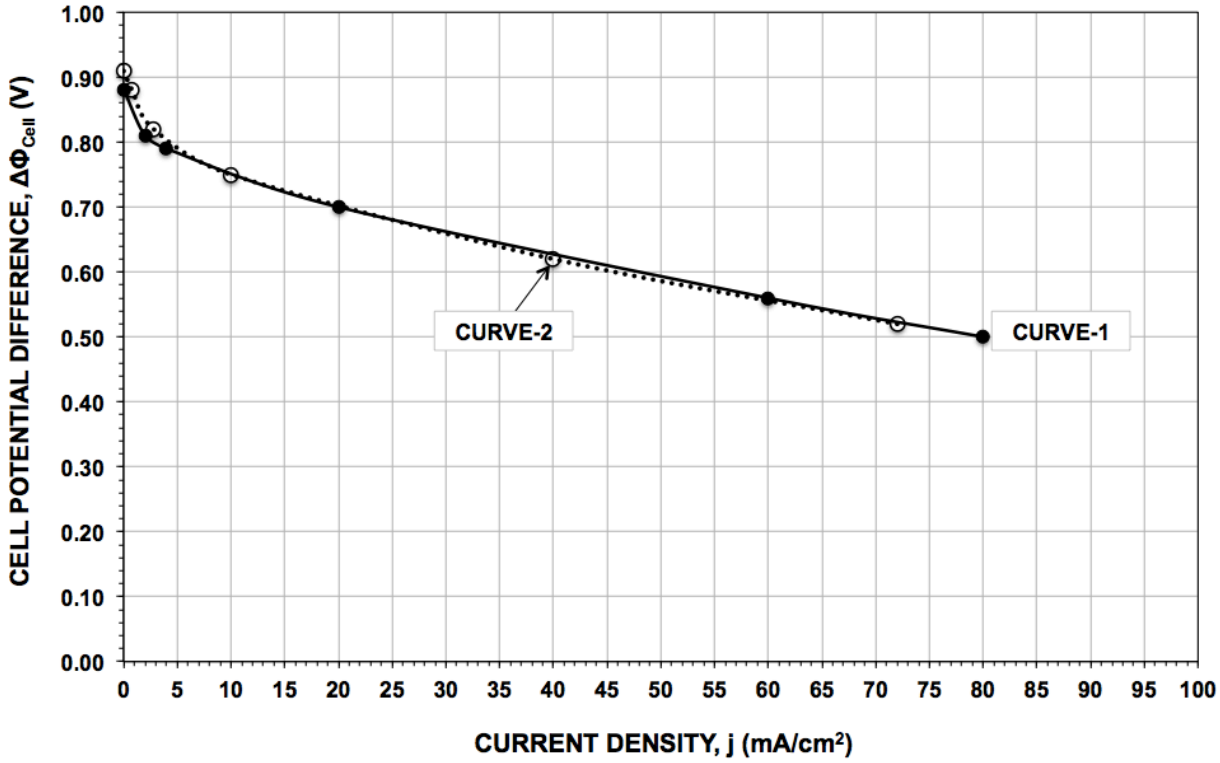


Figure B.13 Polarization curve of a hydrogen fuel cell (after propane-air operation) with IDFF anode humidified with liquid water, Pt anode catalyst, 23°C, 1 atm, and using the power-supply unit at a galvanostatic mode. The above two polarization curves were represented by the following symbols: (i) solid circle: fuel cell operation from time, t = 0 to 12 minutes, and (ii) open circle: fuel cell operation from time, t = 12 to 24 minutes.

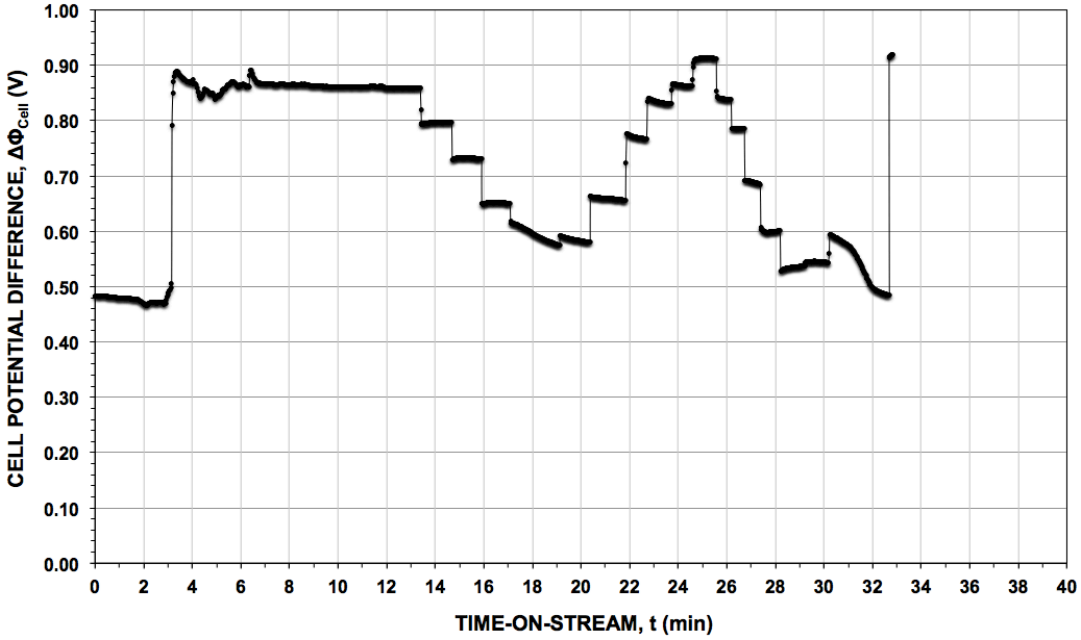


Figure B.14 Cell potential difference, $\Delta\Phi_{cell}$ (V) versus time-on-stream, t (min) for a hydrogen-air operation after a DPFC operation with 100% propane, IDFF anode humidified with liquid water, Pt anode catalyst, 65°C, 1 atm, and using a 330 Ω fixed resistor.

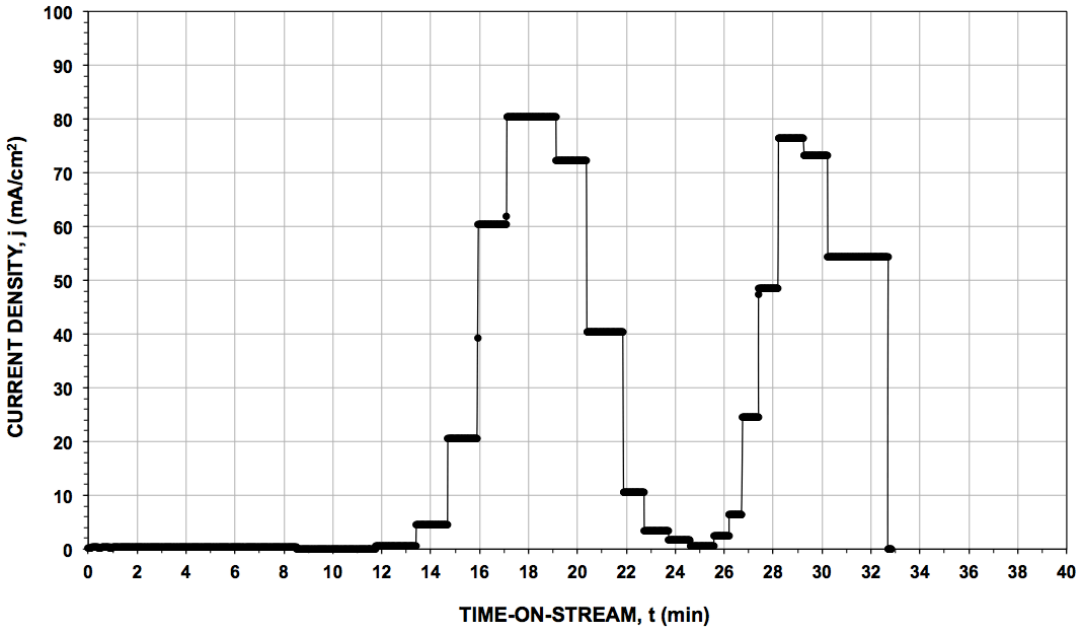


Figure B.15 Current density, j ($\mu A/cm^2$) versus time-on-stream, t (min) for a hydrogen-air operation after a DPFC operation with 100% propane, IDFF anode humidified with liquid water, Pt anode catalyst, 65°C, 1 atm, and using a 330 Ω fixed resistor.

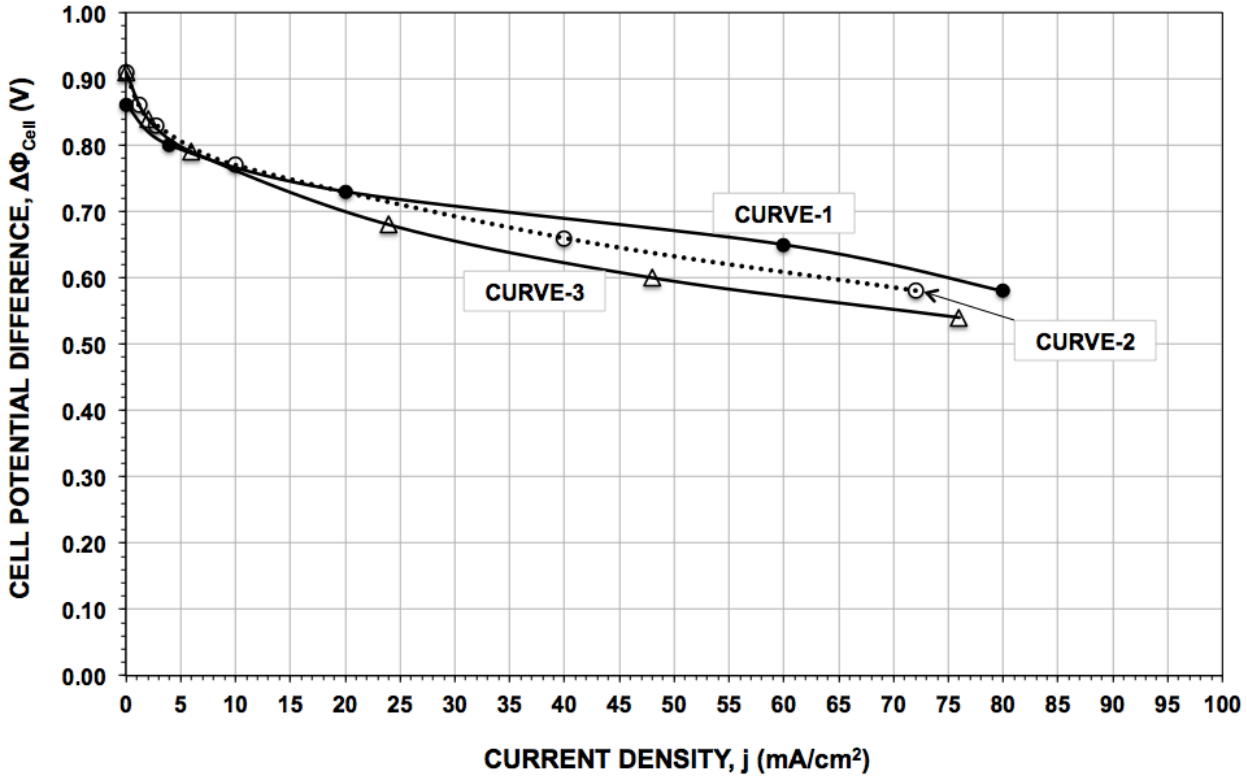


Figure B.16 Polarization curve of a hydrogen fuel cell (after propane-air operation) with IDFF anode humidified with liquid water, Pt anode catalyst, 65°C, 1 atm, and using the power-supply unit at a galvanostatic mode. The above three polarization curves were represented by the following symbols: (i) solid circle: fuel cell operation from time, t = 0 to 10 minutes, (ii) open circle: fuel cell operation from time, t = 10 to 22 minutes, and (iii) open triangle: fuel cell operation from time, t = 22 to 34 minutes.

.

Appendix C: Thermodynamic calculations

C.1 Thermodynamic fuel cell efficiency (η_{th})

Overall reaction in a H_2-PEMFC:

$$H_{2\,(g)} + \tfrac{1}{2}O_{2\,(g)} \longrightarrow H_2O_{\,(l)}$$

Standard Gibbs free energy change of reaction (ΔG°_{298}) for a H_2-PEMFC:

$$\Delta G^\circ_{298} = \Delta G^\circ_{f,298\,(H2O)} - [\Delta G^\circ_{f,298\,(H2)} + \tfrac{1}{2}\,\Delta G^\circ_{f,298\,(O2)}]$$

$$= [-237.13 \text{ kJ/mol}] - [0 + \tfrac{1}{2} * 0]$$

$$= -237.13 \text{ kJ/mol}$$

Standard enthalpy change of reaction (ΔH°_{298}) for a H_2-PEMFC:

$$\Delta H^\circ_{298} = \Delta H^\circ_{f,298\,(H2O)} - [\Delta H^\circ_{f,298\,(H2)} + \tfrac{1}{2}\,\Delta H^\circ_{f,298\,(O2)}]$$

$$= [-285.83 \text{ kJ/mol}] - [0 + \tfrac{1}{2} * 0]$$

$$= -285.83 \text{ kJ/mol}$$

$$T\Delta S^\circ_{298} = \Delta H^\circ_{298} - \Delta G^\circ_{298} = -285.83 \text{ kJ/mol} - [-237.13 \text{ kJ/mol}] = -48.70 \text{ kJ/mol}$$

$$\eta_{th} = \frac{\Delta G^\circ_{298}}{\Delta H^\circ_{298}} = [-237.13 \text{ kJ/mol}] / [-285.83 \text{ kJ/mol}] = 83\%$$

Note that there is a 17% energy loss ($T\Delta S$) caused by the reversible change in entropy (ΔS), (100 - 83), that occurs when hydrogen is transformed into water.

Overall reaction in a DPFC:

$$C_3H_{8\,(g)} + 5O_{2\,(g)} \longrightarrow 3CO_{2\,(g)} + 4H_2O_{\,(l)}$$

Standard Gibbs free energy change of reaction (ΔG°_{298}) for a DPFC:

$$\Delta G^\circ_{298} = [3\,\Delta G^\circ_{f,298\,(CO2)} + 4\,\Delta G^\circ_{f,298\,(H2O)}] - [\Delta G^\circ_{f,298\,(C3H8)} + 5\,\Delta G^\circ_{f,298\,(O2)}]$$

$$= [\{3 * (-394.36 \text{ kJ/mol})\} + \{4 * (-237.13 \text{ kJ/mol})\}] - [(-24.29 \text{ kJ/mol}) + (5 * 0)]$$

$$= -2107.31 \text{ kJ/mol}$$

Standard enthalpy change of reaction ($\Delta H°_{298}$) for a DPFC:

$\Delta H°_{298} = [3\ \Delta H°_{f,298\ (CO2)} + 4\ \Delta H°_{f,298\ (H2O)}] - [\Delta H°_{f,298\ (C3H8)} + 5\ \Delta H°_{f,298\ (O2)}]$

$= [\{3 * (-393.51\ kJ/mol)\} + \{4 * (-285.83\ kJ/mol)\}] - [(-104.68\ kJ/mol) + (5 * 0)]$

$= -2219.17\ kJ/mol$

$T\Delta S°_{298} = \Delta H°_{298} - \Delta G°_{298} = -2219.17\ kJ/mol - [-2107.31\ kJ/mol] = \underline{-111.86\ kJ/mol}$

$\eta_{th} = \dfrac{\Delta G°_{298}}{\Delta H°_{298}} = [-2107.31\ kJ/mol] / [-2219.17\ kJ/mol] = \underline{95\%}$

Note that the reversible energy loss ($T\Delta S$) when propane is transformed into CO_2 and water vapour is only 5% (100 - 95).

Temperature limitations of materials

The energy efficiencies of thermal power cycles and heat engines are limited by the maximum temperature (900 K) of the materials used in their construction. The most efficient cycle is the Carnot cycle having an efficiency, $\eta = [(1 - T_{out} / T_{in} = 1 - 298 / 900) * 100\ \% =] 67\%$. In contrast fuel cells are capable of operating at moderate temperatures and therefore, their efficiencies would not increase if their operating temperatures were increased.

C.2 Pressure effect on overall fuel cell efficiency (η_{FC})

As per the Nernst equation (under equilibrium condition):

$\Delta\Phi_{cell} = E° + [(RT/n_EF) * \ln \{(P_{C3H8} * P_{O2}^5)/(P_{CO2}^3 * P_{H2O}^4)\}]$ ---------- (C.1)

or, $E° = \Delta\Phi_{cell} - [(RT/n_EF) * \ln \{(P_{C3H8} * P_{O2}^5)/(P_{CO2}^3 * P_{H2O}^4)\}]$ ---------- (C.2)

$\Delta G° = -n_EF\ E°$ ---------- (C.3)

Substitute Eq. C.2 in Eq. C.3, to obtain the following:

$\Delta G° = -n_EF * (\Delta\Phi_{cell} - [(RT/n_EF) * \ln \{(P_{C3H8} * P_{O2}^5)/(P_{CO2}^3 * P_{H2O}^4)\}])$

or, $\Delta G° = -n_EF\ \Delta\Phi_{cell} + [(RT/n_EF) * \ln \{(P_{C3H8} * P_{O2}^5)/(P_{CO2}^3 * P_{H2O}^4)\}])$ ---------- (C.4)

Also, Propane partial pressure, $P_{C3H8} = y_{C3H8} * P$

where, P is the anode pressure (bar)

y_{C3H8} is the propane inlet mole fraction

Overall fuel cell efficiency, $\eta_{FC} = \eta_{th} * \eta_{el} * \eta_c$ ---------- (C.5)

where,

η_{th} is the thermodynamic efficiency = $\Delta G° / \Delta H°$

η_{el} is the electrochemical efficiency = $\Delta\Phi_{cell} / \Delta\Phi_{OCP}$

$\Delta\Phi_{OCP}$ is the open-circuit potential (V)

η_c is the conversion efficiency, considered = 1

Now the above Eq. C.5 can be written as, $\eta_{FC} = \eta_{th} * \eta_{el} = \{\Delta G° / \Delta H°\} * \{\Delta\Phi_{cell} / \Delta\Phi_{OCP}\}$

As per Eq. C.4 and Eq. C.1, if P_{C3H8} ↑ then $\Delta G°$ ↑, $\Delta\Phi_{cell}$ ↑ and therefore, η_{FC} ↑.